INFORMATION TO USERS

This manuscript has been reproduced from the microfilm master. UMI films the text directly from the original or copy submitted. Thus, some thesis and dissertation copies are in typewriter face, while others may be from any type of computer printer.

The quality of this reproduction is dependent upon the quality of the copy submitted. Broken or indistinct print, colored or poor quality illustrations and photographs, print bleedthrough, substandard margins, and improper alignment can adversely affect reproduction.

In the unlikely event that the author did not send UMI a complete manuscript and there are missing pages, these will be noted. Also, if unauthorized copyright material had to be removed, a note will indicate the deletion.

Oversize materials (e.g., maps, drawings, charts) are reproduced by sectioning the original, beginning at the upper left-hand corner and continuing from left to right in equal sections with small overlaps.

Photographs included in the original manuscript have been reproduced xerographically in this copy. Higher quality 6" x 9" black and white photographic prints are available for any photographs or illustrations appearing in this copy for an additional charge. Contact UMI directly to order.

Bell & Howell Information and Learning
300 North Zeeb Road, Ann Arbor, MI 48106-1346 USA
800-521-0600

UNIVERSITY OF OKLAHOMA

GRADUATE COLLEGE

Abundances of Sulfur in the Milky Way Disk from Peimbert Type II Planetary Nebulae

A Dissertation

SUBMITTED TO THE GRADUATE FACULTY

in partial fulfillment of the requirements for the

degree of

Doctor of Philosophy

By

Jacquelynne B. Milingo
Norman, Oklahoma
2000

Abundances of Sulfur in the Milky Way Disk from Peimbert Type II Planetary Nebulae

A Dissertation APPROVED FOR
THE DEPARTMENT OF PHYSICS AND ASTRONOMY

BY

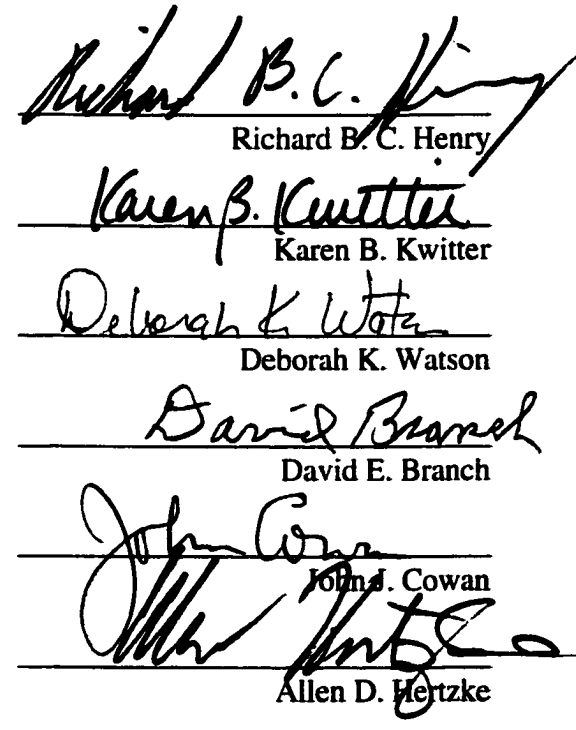

Richard B. C. Henry

Karen B. Kwitter

Deborah K. Watson

David E. Branch

John J. Cowan

Allen D. Hertzke

Acknowledgments

I'll never forget the first time I looked through Becky Sullivan's 2" refractor. Standing speechless in her rather large backyard, I was stunned that I had lived so many years and never thought to look up and notice an entire universe waiting to be recognized. The siren song of Saturn that called to me on that summer night did much more than briefly engage an insignificantly small girl from Kansas; it sparked a paradigm shift that would change the rest of my life. The starry skies have given me much more than something to do with my time. I see the value in learning for the sake of learning, working hard for little tangible gain, realizing that my vantage point is one of many, and recognizing that however humble my contribution may be it fits into a much larger, more meaningful context.

One million pages couldn't begin to convey my gratitude to the following people, so I will attempt to do it in just a few. Becky, wherever you are, thank you for opening up this entire world and beyond to me. Thanks to the Lake Afton Public Observatory (Greg, Dave A., Mark, Nancy, and Dave G.) for existing and investing in my potential. Janie Clark, your ability to keep a remarkably tidy house is matched only by your friendship, loyalty, and integrity. Thank you Jennifer and Tyler; your Tigger-like spirit inspires this V.S.A. to occasionally take off her shoes and socks. To Katie and Neil for many years of crunchy taco bake and seeing past the blue hair to all that is beneath my skin. To Kirsten, Dean, and Jimmy for being an invariable source of friendship and support, and for giving me a small place in this universe where I know I belong. I want to thank Kirsten in particular for being my own personal lighthouse. On my best days I can only try to be as patient, warm, and accepting as you've been for the past seven years. Thank you Debra for being an example of raw strength and fierce independence, and for teaching me that if there must be a balance of power, it's up to me to move the fulcrum so that my tiny voice weighs in. Thank you Louanna for your nurturing voice and for being my cheering section and waving

my flag. Why you decided to invest your time and kindness in me many years ago I will never know, but I'm awfully glad you did. Thanks to Dick Henry, Karen Kwitter, John Cowan, Deborah Watson, David Branch, and Allen Hertzke - for your time, patience, and input. I still have a lot to learn but you have given me the best start that anyone could ask for. Thanks to my fellow grad students that have celebrated and commiserated with me over the years (you know who you are). Friendships wrought by our common experience, I will keep you with me always (especially during episodes of PTSD). Thank you Scott and Scott for your friendship, warmth, humor, creativity, and time spent doing ANYTHING BUT science. I owe an incalculable debt to the entire Twarog family including Walker and Kitty. Bruce and Barb I could never thank you enough for everything that you've given me. You have been my instructors, my mentors, and my friends. You both taught me to think, to be prepared for what I find outside of Lawrence (good and bad), to use no more than one overhead/minute, and the most valuable lesson of all - you taught me the lost art of being reasonable. I may never be the best astrophysicist in the world, but you have contributed more than you'll ever know in teaching me how to be the best person that I can possibly be. Last but certainly not least I want to thank my small family Mark, Fred, and Benji. As my roommates you've endured frustration, busy days, long nights, bursts of glee, bits of sorrow, and everything that comes along with achieving a hard-earned, long-term goal. I'm not sure what brings people together but I must be quite charmed and extremely lucky to have found you. As my best friend and full-time personal superhero I hope you know Mark how much I appreciate your love and support. This is a small victory but it's OURS!

Contents

Chapter 1

Introduction

1.1 Galactic Chemical Evolution and the Impetus for this Dissertation

Galactic chemical evolution (or GCE) is the study of the origin, evolution, and distribution of all nuclear species that exist in the gas, dust and stars of galaxies. Determining how these nuclear species came into being and evolved chemically and dynamically into what we observe today requires synthesizing information from practically every branch of astrophysics.

To say that this subject is interesting as a motivation for its study doesn't do justice to its breadth as an area of astronomical research and as a secular search for the beginnings from which everything we know to exist was ultimately derived. From the vantage point of an astrophysicist the empirical question of our origins begins with this study of the evolution of our most rudimentary building blocks – the chemical elements.

The existence of all the elements that make up our universe is due to nuclear processes that occur primarily in Big Bang nucleosynthesis, stellar fusion processes, and nuclear processes that take place during the deaths of massive stars. Therefore understanding how and where these elements were formed, subsequently distributed throughout the interstellar medium (ISM), and swept up in the formation of later generations of stars, is fundamental to understanding the chemical history of any galaxy. Essentially this is a study of the ecology of galaxies.

Considering we have such a temporally and spatially limited scope of data-taking opportunities, experiment and theory must work together carefully in this investigation.

Observational information about the chemical abundances, kinematics, and dynamics of stars and gas in galaxies must be used to constrain theoretical models of stellar nucleosynthesis and evolution, parameters of star formation and death, and the chemical and dynamic evolution of all galactic components.

This dissertation will not address the kinematic or dynamic studies of galactic evolution except where necessary. But it is important to note that striking correlations between morphology and stellar populations and the spatial dependence of metallicity in galaxies clearly tell us that the dynamic evolution of a galaxy controls the initial deposition and subsequent distribution of chemically evolved material. The stars are responsible for the nucleosynthesis of the elements but the dynamics of the host galaxy and its surrounding environment ultimately define the location of the material.

To recreate the chemical history of any galaxy one needs to establish the initial conditions of its chemical state and the spatial distribution and physical form of the material within it (gas, dust, stars, stellar remnants). In addition we must have a reliable picture of these physical properties presently and a reasonable idea of how they evolved in time. We can obtain snapshots of the chemical history of a galaxy that allow us to observationally constrain theoretical models. These snapshots in time come from stars and gas that "freeze out" their natal composition which reflects the chemical epoch of their formation. In the case of stars and objects that evolve from stars care must be taken to account for any nucleosynthesis, convective mixing, etc. that occurs during the lifespan that may alter the chemical abundances we measure.

The impetus of this dissertation is to improve our knowledge of the chemical composition of the ISM of our Galaxy at a particular epoch, specifically that of sulfur,

but oxygen, neon, and argon will also be investigated. Our particular approach to this problem is to find chemical abundances throughout the disk of our Galaxy using Peimbert type II planetary nebulae (PNe). This information can be used to observationally constrain GCE parameters such as stellar yields that tell us the relative amounts of particular elements that are produced by stars in various mass ranges, and radial abundance gradients that indicate the chemical enrichment that has occurred at different locations in the galaxy. Abundance gradients depict the temporal and spatial distribution of synthesized elements which can be used to infer how the chemical enrichment of the Milky Way disk has progressed over time. Heavy element ratios such as S/O are useful as a means of measuring the differential production of both elements, sulfur and oxygen in this case, and how it may vary with time, metallicity of the progenitor star, and perhaps location within the Galaxy.

Chapter 4 will discuss the theoretical origins of sulfur, argon, neon, and oxygen and how our data set can be used to constrain and reinforce ideas of stellar nucleosynthesis and evolution. We are looking specifically at type II PNe because they have a rather narrow progenitor mass range of ~1.2 – 2.4 solar masses (Maciel, 1992). The homogeneity of our sample is helpful because it focuses the chemical, kinematic, and evolutionary history of the progenitor stars that we must understand in order to gain insight into what the PNe gas is presently telling us. It is also very important to point out that compiling a homogeneous set of objects that have been consistently observed, reduced, and analyzed will eliminate any scatter associated with systematic effects from hybrid data samples. Our observations provide abundances for the empirical construction

of the aforementioned radial abundance gradients and heavy element ratios. Both of these quantities will also be discussed in greater detail in chapter 4.

Our investigation of the chemical abundances of this sample of PNe involves taking a somewhat novel approach to the determination of sulfur abundances. We have observed our objects over an unusually extended wavelength range of 3500 – 9600 Å in order to include the near-IR emission lines of the S^{+2} ion. Chapter 3 will discuss this topic in much greater detail.

The remainder of this chapter will focus on the origin of planetary nebulae, how our choice of progenitor mass range allows us to investigate the S, Ar, Ne, and O in type II PNe, and finally how these abundances can be used to characterize the natal interstellar medium out of which the progenitor stars for our PNe formed. Hopefully throughout these pages I will be able to convey the integral connections between the abundances of our data set, the past chemical evolution of the galaxy ,and contributions from previous generations of stars.

1.2 Planetary Nebulae; Physical Description and Origin

Before we go any further we should define exactly what a planetary nebula is and illuminate the connections between the progenitor star, its natal ISM, and the abundances that we are measuring in these objects. A planetary nebula is a visibly luminous low density gaseous "shell" that is actually the expelled envelope of an intermediate mass star. An intermediate mass star is typically defined as having an initial mass between .8 and 8 solar masses. The morphology of PNe and the physical origins behind their various shapes is an interesting subject alone. I loosely use the term shell here but it is important to note that PNe are rarely perfectly spherical shells; they often have complex shapes and

filamentary structure the explanation for which is an entirely different subject of study. Stars in this intermediate mass range have generally similar paths through the HR diagram. The production of a planetary nebula essentially defines whether a star falls into this intermediate mass category. This is because a PN will only form from stars that are massive enough to allow for helium shell burning but not so massive that degenerate carbon can be ignited in the core. The formation of a planetary nebula occurs during the end of the asymptotic giant branch phase of evolution. After the exhaustion of core helium burning an intermediate mass star (IMS) ascends the asymptotic giant branch with two shell burning sources, a hydrogen shell and a helium shell. Due to the thinness of the helium shell and the very temperature-sensitive nature of helium fusion, instabilities arise that cause He shell fusion to turn "on" and "off" over a relatively short period of time. The cyclic "on and off" phases of helium shell burning are referred to as thermal pulses or helium shell flashes. During the periodic flashes when the helium shell is "on" the hydrogen rich envelope of the star is driven to an increasingly large distance from the core. The thermal pulses continue until the envelope becomes distended enough that the gas is able to escape from the star. At this point the material travels outward at approximately 20-30 km/sec and is physically dissociated from the core of the star. The ejected envelope continues to expand and initially has the form of a cool molecular dusty gas envelope. The remaining core of the star is degenerate and depending on the mass of the progenitor, primarily made of carbon and oxygen. The remaining core no longer has an available fusion source so it will eventually cool until it becomes a degenerate compact object known as a white dwarf.

In the meantime the slowly expanding envelope officially becomes a planetary nebula when the now exposed and very hot (50,000 to 150,000 K) stellar core begins to photoionize the expelled material, which is becoming increasingly less dense as the "shell" continues to expand. PNe have relatively short lives, on the order of tens of thousands of years, before they are so distended that they are no longer luminous. Eventually this material blends in with the neighboring ISM making PNe equal in importance to SNe in the recycling of stellar material. PNe, SNe, and stellar winds all play a role in re-seeding the ISM with processed material from stars. Subsequent generations of stars will form out of this recycled material and they will in turn return a portion of that back into the ISM, hence our analogy to an environmental ecology. So on a large scale we see PNe as photoionized expelled stellar envelopes that fluoresce due to short wavelength radiation coming from what was previously the core of the star. On a smaller scale there are just a few specific atomic processes that take place in order to produce the rather striking visual radiation we see in these magnificent objects. Understanding these physical processes is they key to inferring chemical abundances from PNe.

When examined spectroscopically this low-density gas that we refer to as a planetary nebula yields an emission line spectrum. The emission spectra in PNe are due primarily to recombination lines of hydrogen and helium and collisionally excited forbidden lines of metals. Please note that in the field of astrophysics the term "metal" is used loosely to refer to any nuclear species that isn't hydrogen or helium. As was stated before the emission lines in PNe occur as a result of fluorescence, the initial source of energy being the copious amount of UV radiation that comes from the very hot central

star of each PN. The photons with wavelengths short of the Lyman limit have enough energy to photoionize the abundant hydrogen in the gas. Subsequent recombinations give us the strong series of hydrogen lines that are so familiar in these objects. The characteristic red color that can be seen in many direct images of PNe is due to the very strong Hα emission from the Balmer series. The ongoing process of photoionization and recombination makes available a distribution of free electrons that can collisionally excite the much less abundant metals in the gas. PNe provide the favorable physical conditions of low matter density and low radiation density that allow some ions to exist in metastable states until they can radiatively de-excite and produce the very familiar nebular forbidden lines. Typical sources of these forbidden lines are ions of oxygen, sulfur, neon, and argon. Historically emission nebulae such as PNe, HII regions (diffuse ionized hydrogen), and supernovae remnants (SNR, material violently expelled during the deaths of massive stars) were easily recognized by their very strong forbidden lines at wavelengths of 4959 and 5007 Å. Figure 1.a is a typical spectrum of a PN illustrating the strength of these particular emission lines. We refer to forbidden lines as "forbidden" because of their low transition probabilities in typical laboratory matter densities where collisions cause non-radiative de-excitations. The very visible and strong λ4959 and λ5007 Å lines of [O III] are a perfect example of this because they are not usually observed under terrestrial conditions. When they were first seen in astrophysical sources they were attributed to the mysterious element "nebulium" – thought to exist only in extra-terrestrial conditions. In 1928 Ira Bowen correctly identified the "nebulium" lines as due to electronic transitions within the O^{+2} ion. PNe, HII regions, and SNR all have

these very strong [O III] lines because the matter density within these objects is low enough to allow the forbidden transitions to occur.

As will be explained in more detail in chapter 3, it is the strength of these forbidden lines that allows us to determine the physical conditions inside of PNe (and other emission nebulae) such as temperature, density, and chemical abundance.

1.3 Why Sulfur Determined from Type II PNe is Useful to GCE

As we narrow in on the specifics of this study it is important to explain exactly why PNe are recognized as being important conveyors of information about the chemical evolution of galaxies. Our ultimate goal is to find the chemical abundances of S, Ar, Ne, and O at different locations in the disk of our Galaxy. There are different ways to approach this problem of finding chemical abundances. Galaxies in general are made up of gas, dust, and stars. Any one of these physical manifestations can give us information about their chemical makeup but the different temperature and density regimes that allow gas, dust, and stars to exist dictate the physical processes that allow us to infer their chemical abundances. I will not address the expanse of work that has been done on characterizing interstellar dust and the chemical abundances of stars. It should be sufficient to say that there is a myriad of information that exists on these subjects and it is complementary to the work done investigating interstellar gas. It is worthwhile to note that all of these forms of material in galaxies are inextricably linked just as organisms are related to each other and their environment in any ecosystem. The concern of this dissertation is the validity and use of PNe as tracers of chemical abundances in the gaseous form of interstellar material. Interstellar gas makes up approximately 20% of

the mass of our Galaxy. This gas can exist as cold molecular clouds, dense pre-cursors to stars, or rarefied emission nebulae like H II regions, supernovae remnants, and planetary nebulae. All of these are very different beasts and each yields information about their chemical history and present physical conditions. What epoch of the Galaxy those chemical abundances reflect depends on when the object (or progenitor of the object) was formed. H II regions, as their name implies, are diffuse nebulae of ionized hydrogen. The source of photoionization for H II regions is a young hot star (or group of stars) that is rich in UV photons. They are our most direct view into the chemical abundance of the interstellar medium because the previously dark gas that makes up an H II region literally is the gas between the stars and the gas that present generations of stars are being formed out of. In other words, chemical abundances from H II regions indicate the present chemical state of the interstellar medium. It follows that chemical abundances from young hot stars that have recently formed out of this gas should show similar abundance patterns and in fact they do (Henry & Worthey, 1999). Planetary nebulae require a bit more thought when trying to use them as abundance tracers for the ISM. Since PNe occur during the dying stages of a wide range of intermediate mass stars one must carefully consider how much of the abundance pattern in a PN reflects the conditions of the ISM during the formation of the progenitor star and how much it reflects the chemical evolution that has occurred during the life of the progenitor star itself. It is clear that in a range of .8 to 8 solar masses a wide range of stellar lifetimes will occur. The length of a star's life (loosely defined to be the time it spends fusing hydrogen in it's core) which depends on its progenitor mass, will tell us the amount of time that has elapsed between the formation of the star and its presently observed PN phase. Planetary nebulae are

often referred to by their Peimbert "type" which essentially groups them by narrow mass ranges of their progenitor stars (Peimbert, 1978; Maciel, 1989). As was stated previously, Peimbert type II PNe have a progenitor mass range of about 1.2 – 2.4 solar masses. A sample of type II PNe was chosen for this study specifically because their progenitor masses dictate their lifespan, nuclear fusion history, and kinematic history. All of these factors need to be considered when trying to nail down a time and a place for the abundance patterns we see in these objects. The mass range of type II PNe also indicate that their progenitor stars do not undergo self-enrichment or depletion of their metals. An important aspect of this study is incorporating our present knowledge of how mass dictates the core and shell nuclear burning stages that will occur in a star. The primary element of interest in this dissertation is sulfur, which is not synthesized in intermediate mass stars. Sulfur (and argon, neon, and oxygen for that matter) is produced in massive stars (> 8 solar masses) so we know that any sulfur that we detect in our PNe has not been altered by the evolution of its intermediate mass progenitor. Thus the S abundances we find should reflect the composition of the interstellar material from which the PN progenitor star formed. Given the finite life span of such an intermediate mass progenitor (approximately 4-6 Gyrs for type II PNe; Maciel & Koppen, 1994), these abundances will then tell us the chemical composition at a particular location in the Galaxy at a particular time.

Subsequent chapters of this dissertation will examine our observing program, the data set, the impetus behind our choice to re-examine sulfur, our reduction and calibration methods, abundance determinations, and the physical analysis of the data.

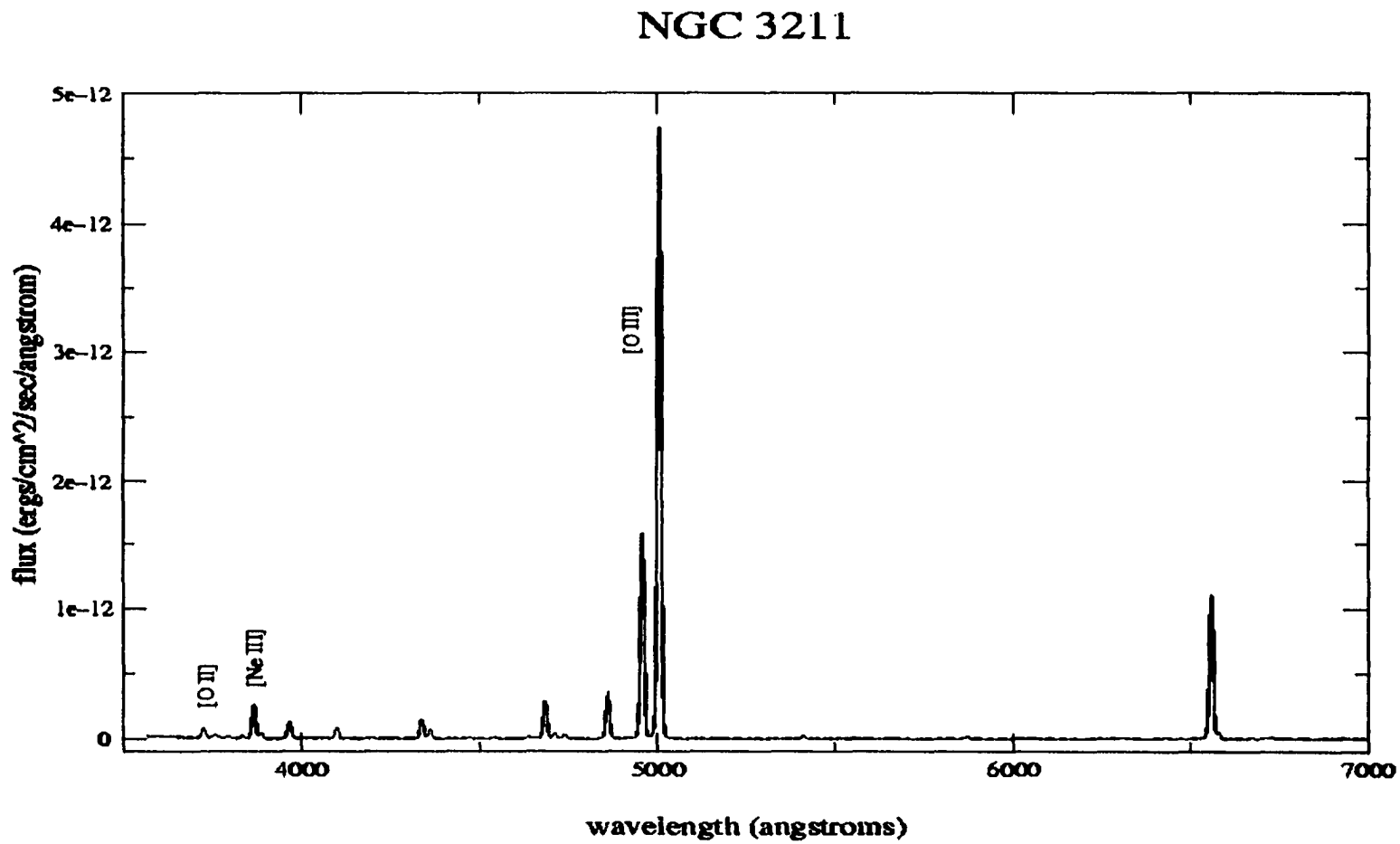

Figure 1.a - Typical spectrum of a PN illustrating the strength of the 4959 and 5007 Å lines.

Chapter 2

Data Set, Observations, and Data Reduction

2.1 Description of the Sample

Our sample of objects for this study consists of 48 southern hemisphere planetary nebulae. These are type II PNe in the Milky Way so by definition they are confined to the disk of our Galaxy. These objects have been observed before but their sulfur abundances have not been measured using the very strong [S III] lines that we are using in this study. Forethought was given in selecting these PNe to insure a large range in galactocentric distance (R_g) for use in constructing abundance gradients. Our sample ranges from approximately 4 to 13 kiloparsecs (kpc) in R_g (distance from the center of the galaxy). Again, it should be noted that these objects have been observed before in other studies but not with the extended spectral coverage that was applied in this work. Given the impetus for this dissertation it was interesting to find that very few sulfur abundances in the literature for either PNe or H II regions, have been determined using the strong λ9069 and λ9532 Å lines of [S III]. Nearly all S abundances found utilize the [S II] λ6724 doublet and/or the [S III] λ6312 line.

It is important to emphasize again that type II PNe were chosen for this sample specifically for their low progenitor mass range and restricted height above the Galactic plane. As was discussed before in the introduction, a low progenitor mass precludes type II PNe from being subject to self-contamination via the processing and/or production of O, Ne, S, and Ar. In addition to low self-contamination, a low progenitor mass dictates stellar lifetime and kinematic history (Dutra and Maciel, 1990) which allows the

star and eventually its PN to remain near its birthplace. Thus the importance of type II PNe in this study – they tell us that the levels of S, Ar, Ne, and O we measure are those of the progenitor star and hence characterize abundance patterns in the ISM at the time of their formation.

2.2 Observations

2.2.1 Instrumentation

The data for our sample were acquired at CTIO during a six night observing run in the spring of 1997. The spectra were obtained using the 1.5 meter telescope and cassegrain spectrograph with Loral 1K CCD. Each object was observed from 3600-9600 Å which enabled us to detect the emission lines needed to determine the desired relative abundances. Two diffraction gratings were used to enable us to observe each object over this spectral range, #22 for the "red" nights and #09 for the "blue" nights. The six nights were split in half so that the first three could be used to observe in the red end of the spectrum from 3600 – 7000 Å, and the last three were used to observe each object again in the blue from 6500 – 9600 Å. The choice of gratings allowed for coverage of the near-IR [S III] lines and a sufficient overlap of ~1000 Å in the region of Hα. This overlap is crucial to the subsequent process of merging the red and blue spectra of each object. Merging the two spectral regions allows for a seamless flux-calibrated, sensitivity-corrected spectrum for each object in the sample.

It should be additionally noted that the acquired observations are long-slit spectra. The term "long-slit" refers to the shape of the mask that is used to confine the area of observable sky that enters the telescope and is eventually transmitted through the diffraction grating and onto the CCD. As the name long-slit implies the mask allows a

long rectangular area with dimensions of 5" wide and ~320" long (in our case) to be projected onto the CCD. This is quite important when observing angularly large and extended objects. Our sample contained very few angularly large objects but it was crucial that with each observation we obtained a considerable amount of surrounding sky signal which was possible using the extended slit mask.

2.2.2 Integration Times and Object Frames

Each object was observed at least twice and usually three times to assure adequate signal to noise without saturation of the stronger lines such as Hα and the [O III] λ4959 and λ5007 Å lines. If more than one usable frame was left after the reduction process for a given object, these frames were combined to increase the signal. Object frames that were saturated in the strongest lines (Hα and the [O III] 4959 & 5007 lines) were kept with the intention of eventually utilizing the weak lines with an alternate merging and de-reddening scheme. Most of the objects in our sample were angularly small enough to fit entirely into the slit mask. Those PNe that did not fit entirely into the slit were observed at a chosen offset from the central star.

2.2.3 Calibration Frames

Each night appropriate calibration frames were acquired for the removal of instrumental signature and wavelength and flux calibration of the data. For our observing program appropriate calibration frames consisted of bias frames, dome flats, twilight sky flats, comparison lamp exposures, and standard star frames. A significant number of projector flats (exposures of a quartz lamp illuminating the spectrograph slit) were taken with the intention of using them to remove fringing at long wavelengths due to the thinness of the CCD. It was later decided to forego this step as it would have

introduced as much error as was removed. The bias frames are zero second integration exposures and as their name implies they are used to remove any pedestal level of counts that exist across the CCD. Dome flats are exposures of an illuminated white spot on the interior of the dome that are used to "flatten" the response of the CCD. Flat frames remove pixel to pixel gain variations and larger scale spatial response variations due to the innate character of the CCD. The sky flats are exposures taken of the sky at twilight. In our case they were obtained to correct for any uneven illumination along the slit – this can be a problem when doing long slit work when one needs to utilize information that is far from the center of the slit. Comparison lamp frames are two dimensional exposures of a given emission tube source such as HeNeAr or in our case a HeAr lamp. The comparison frames are used to calibrate the wavelength scale of the data. Finally exposures of known southern hemisphere standard stars were taken in order to flux calibrate the data and convert the emission line strengths from instrumental counts to actual physical flux units.

2.3 Calibration and Removal of Instrumental Signature

2.3.1 IRAF Steps

The reduction of our CTIO data was done using available software packages within IRAF. IRAF (Image Reduction and Analysis Facility) is a rather hearty application designed by the National Optical Astronomical Observatories (NOAO) to provide tools for general image processing and specific software "packages" for the reduction and analysis of optical astronomical data in the form of direct images or spectra. Data was transferred from the observing site as FITS (Flexible Image Transport System) files via 8 mm exabyte tapes to be read onto any machine running IRAF. The

FITS files can then be read and split into a pixel file that holds an array of information about the counts received across the CCD, and a "header" file that holds text information about the frame itself (observation location, exposure time, RA & DEC, what reduction steps have been done, etc ...). IRAF operates using a command language so each task requires a set of input parameters that dictate exactly how the program at hand will manipulate the given set of CCD frames. Data coming from national observing sites such as CTIO and KPNO can be (somewhat) easily reduced by existing packages in IRAF that were specifically written for that purpose.

Given the breadth of this project (the observations and reduction methods being just one part of finding the final abundances) I will only include an outline of the general reduction steps that were used for our object and calibration frames.

a.) A dome flat exposure is used to determine the area of the good response and usable data on the CCD chip. The overscan area is also identified (figure 2.a) to characterize any changes in bias signal along the columns of the chip. This step allows me to literally trim off the unusable sections on each CCD frame.

b.) The task CCDPROC was used (in the CCDRED package) to perform a number of tasks on our data including :

i.) characterizing the overscan region of each dome flat

ii.) trimming the raw frames to smaller arrays of usable data information

iii.) subtracting bias signal using the combined bias (or zero) frames

iv.) dividing each frame by a flat field (created with the combined dome flats)

v.) finally, applying any illumination correction created with the sky flats

The reduction steps described above basically remove any effects that the combined instrumentation has on the actual physical signal. After this instrumental signature has been removed the next step is to wavelength and flux calibrate the object spectra using the standard star and comparison lamp frames. The last step is to extract a one dimensional spectrum from the fully reduced and calibrated two dimensional object frames. Between the extraction and flux calibration any signal that comes from the Earth's atmosphere (often referred to as "sky") needs to be removed from the actual PN signal. These steps will be explained in the remainder of the outline.

c.) The wavelength calibration of object spectra and standard star frames involves mapping the dispersion of these observations to column locations along the CCD. In other words we must calibrate where specific wavelengths fall at a particular location along the dispersion axis on the CCD (figure 2.a). The reference for this dispersion calibration comes from the identification of known lines in the observed HeAr comparison spectra. The minimally interactive task DOSLIT can be used to do both dispersion and flux calibration steps and also extract the final spectra, but I chose to do each step in a more direct way with separate tasks outside of DOSLIT. DOSLIT incorporates and applies these individual tasks in a semi-automatic fashion but it should be noted that they can and should be applied to the object frames separately in the case where a reasonable amount of interaction with the data frames is required.

d.) Due to the fact that the objects in our sample are PNe, their emission line spectra have very little continuum in the visible portion of the spectrum. This is significant because when a one-dimensional spectrum is extracted from a two-dimensional frame, a swath many lines wide is cut along the dispersion axis (in this case rows) that contains emission from the object. To avoid an automated trace "losing track" of the PNe emission, the two dimensional frames were first "straightened out" using the TRANSFORM task. The nebular continuum is extremely faint compared to the emission lines, so it cannot be reliably used to track the location of the spectrum across the entire width of the CCD frame. The TRANSFORM task transforms longslit images to user coordinates – in other words it forces the slit length to align with the CCD columns and the dispersion axis to align with the CCD rows. In the process of fitting user coordinates (columns and rows) to image feature coordinates (slit axis and dispersion axis) the transformed two dimensional spectra are wavelength calibrated and the dispersion of features along the slit are forced to remain in a given set of rows across the entire length of the chip.

e.) Once the TRANSFORM task has been applied the object and standard star spectra can then be extracted. In the extraction process a swath many lines wide containing the desired spectrum is cut from each two dimensional frame. At the same time sky samples are taken at different locations along the slit length (figure 2.b). Any signal due the sky is then subtracted from the extracted object spectrum

and we are left with a wavelength calibrated, sky subtracted, one-dimensional spectrum of instrumental counts versus wavelength.

f.) Once the observatory location is identified (longitude, latitude, and altitude) and airmass is calculated for each frame, the one dimensional spectra are then corrected for attenuation due to atmospheric extinction.

g.) The final step in the reduction and calibration process is the flux calibration of the emission line strengths. Flux calibration is the conversion of instrumental counts to physical units of flux. This is done using the extracted standard star spectra. The standard stars have judiciously tabulated fluxes over a wide wavelength range. The standard stars we used were chosen for their location (visible from the southern hemisphere) and similar spectral coverage to our observing program (3600 to 9700 Å). Our observed standard star fluxes are compared against the tabulated values available in IRAF for the same stars. The ratios of the observed flux over some bandpass to the "accepted" flux over the same bandpass are fit by a "sensitivity" function. This sensitivity function describes how the observed instrumental flux relates to the actual physical flux as a function of wavelength.

At this point our sample of PNe are represented by one-dimensional spectra (figure 2.c). The next step is to measure the flux of the relevant and needed emission lines for each object. Table 2.1 lists the emission lines that were measured. This was

done within the IRAF task SPLOT. SPLOT is an interactive plotting task that is used to display and analyze one-dimensional spectra. For lone emission lines the "e" function was used to integrate all full pixel intensities under the line profile between the two points specified at the continuum level. For blended lines the "d" function was used. The deblending command can use a Gaussian fit to characterize each line in a multiple profile and subtracts a linear continuum background. Again two points marking the extent of the blended feature and an educated guess at the centers of the individual line profiles are used for the Gaussian fits and subtraction of the continuum. A log file option was used to automatically record the wavelength and flux determinations for each feature. At this point each PN in our sample has a log file containing the observed wavelength and flux of all prominent emission lines in physically meaningful units of ergs/sec/cm^2.

2.4 Dereddening

We now need to account for any reddening that has occurred due to dust between the observer and the object. This is a particularly important step given that these PNe reside in our Galaxy's disk where most of the dust is found. Interstellar dust is responsible for the extinction and reddening of light coming from distant objects such as our PNe. Extinction is a general term that accounts for both the attenuation due to absorption and scattering. For observations in the optical region extinction is due largely to scattering. Due to the nature of interstellar dust and the strong wavelength dependence of scattering, shorter wavelengths are preferentially scattered thus the term "reddening." When interstellar dust preferentially scatters blue wavelengths out of the line of sight, light from an observed object appears redder than it should.

In general for two emission lines originating from the same source (same distance) the ratio of their observed intensities can be written as follows with the intrinsic intensity ratio being attenuated by some amount that is a function of the optical depth of the dust at the wavelength of the emission line.

$$\frac{I_{\lambda 1}}{I_{\lambda 2}} = \frac{I_{\lambda_0 1}}{I_{\lambda_0 2}} e^{-(\tau_{\lambda 1} - \tau_{\lambda 2})}$$

Here $I_{\lambda 1}/I_{\lambda 2}$ is the observed ratio of two emission line strengths from the same object, $I_{\lambda 1o}/I_{\lambda 2o}$ is the intrinsic value of the same ratio, and the τ_λ values are optical depths. In the optical portion of the spectrum the wavelength dependence of interstellar extinction is fairly universal (Osterbrock 203) so the optical depth can be expressed in terms of a function describing the wavelength dependence of interstellar extinction $\tau_\lambda = Cf_\lambda$ (Osterbrock 204). Given this and the functional form of the interstellar extinction curve we can express the relationship between intrinsic line strength, observed line strength, and the extinction constant as:

$$\frac{I_{\lambda 1}}{I_{\lambda 2}} = \frac{I_{\lambda_0 1}}{I_{\lambda_0 2}} e^{-C(f_{\lambda 1} - f_{\lambda 2})}$$

$$\frac{I_{\lambda 1}}{I_{\lambda 2}} = \frac{I_{\lambda_0 1}}{I_{\lambda_0 2}} 10^{-c(f_{\lambda 1} - f_{\lambda 2})} \qquad \text{where} \quad c = .434C$$

Here c is the extinction constant and f_λ is the aforementioned function that relates the optical properties of dust at the observed wavelengths. This is valid for any two lines in the spectrum but of course one must know the value for the extinction constant c in order to determine the intrinsic ratio $I_{\lambda_0 1}/I_{\lambda_0 2}$ of the two line strengths. Typically this is found

by using the known ratio of two Balmer lines such as Hα/Hβ. Given the low matter and radiation density of the PN gas we are investigating, we could ideally use two lines that originate from the same upper level. In this case the known intrinsic ratio of the two lines would be set by the ratio of their radiative de-excitation rates. In practice it is often not possible to observe two such lines that are far enough apart in wavelength space and have no contamination from other features or observational effects. Thus we settle for the easily observable ratio of two Balmer lines which is valid given the relative insensitivity of the Balmer decrement (Hα:Hβ:Hγ...) to the range in temperatures that exist in PNe. We find the extinction constant using the relationship $I_{H\alpha}/I_{H\beta} = (2.86)\cdot 10^{.36c}$ where we have used the intrinsic ratio of $I_{H\alpha_o}/I_{H\beta_o} = 2.86$ for all objects in our sample (Osterbrock 84). Extinction constants and dereddened line strength ratios were determined for each object in this manner.

2.5 Merging the Spectra

Once the observed line strengths are dereddened the blue and red spectra must be merged. Merging the blue and red spectra for each PN allows the two sets of data to represent a seamless spectrum across the entire spectral range that was observed. The overlap between the red and blue spectra purposely contains the strong H-alpha line. Any difference in the H-alpha flux between the two spectra is accounted for in this merging process. At this point in the raw data reduction the merging factor shouldn't be far from unity, any deviation being due to the observations taking place on different nights and slight variations in the removal of instrumental signature from night to night.

After this rather long process we now have a set of observed emission line strengths for each object in our sample of type II PNe. The spectral coverage ranges from about 3500 – 9600 Å and contains the needed information to characterize physical properties within the gaseous nebulae. This needed information is simply the fluxes of the recombination lines of hydrogen and a host of forbidden lines due to electronic transitions in ions of oxygen, neon, sulfur and argon. Of course there are other measurable emission lines in these objects but given the impetus for this study we will concentrate only on lines due to the above elements. The next section will discuss how we use these emission line strengths to determine relative elemental abundances. Table 2.2 is a compiled list of raw and dereddened-merged line strengths for our sample of objects. I have only included those emission lines that are relevant to the study at hand.

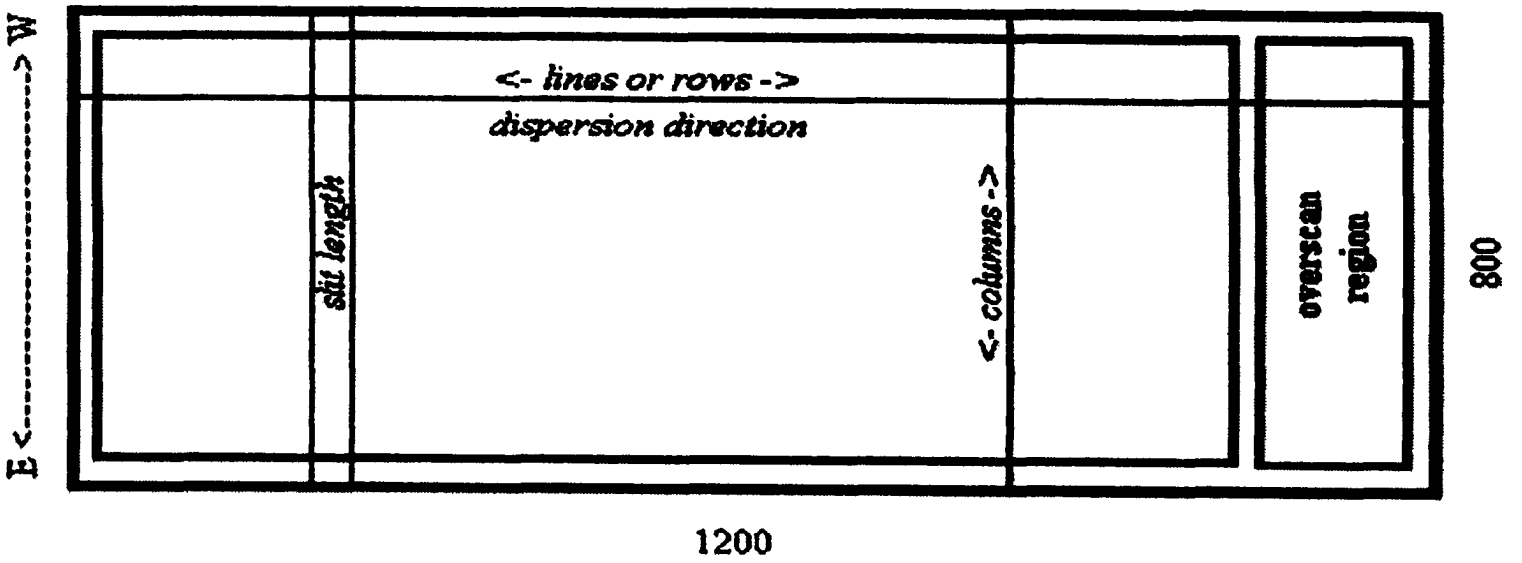

Figure 2.a - Schematic diagram of 1200 x 800 pixel CCD.

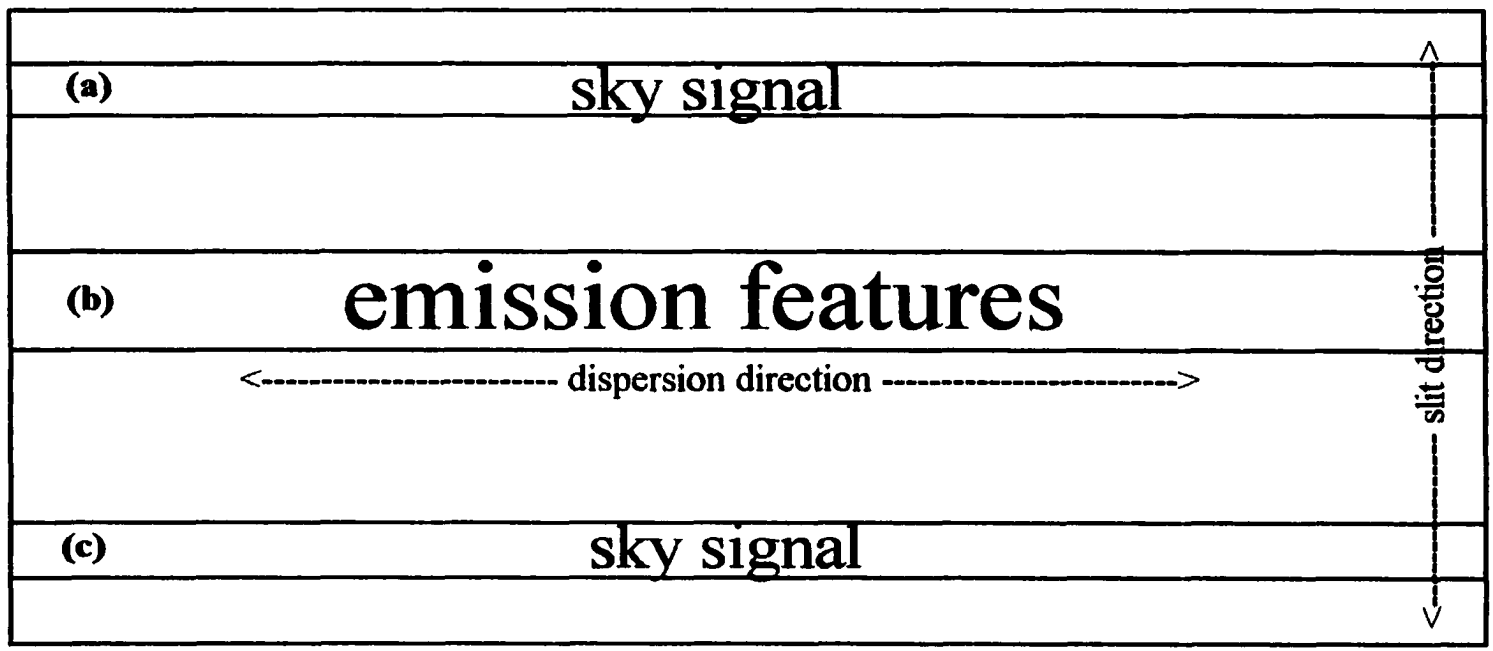

Figure 2.b - (b) marks the swath cut across the 2-dimensional image that contains the PN signal, (a) and (c) contain "sky" signal to subtract foreground emission.

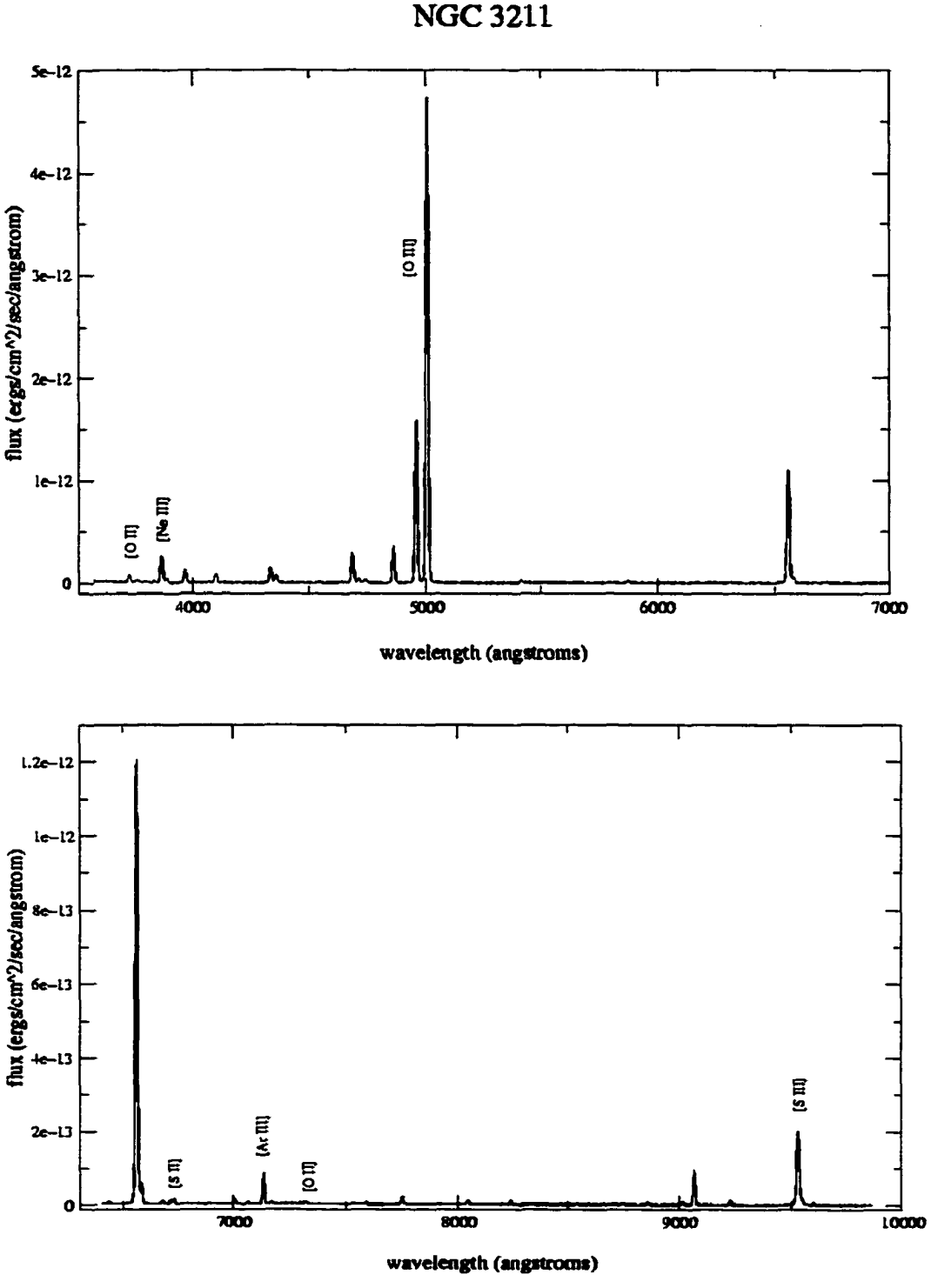

Figure 2.c - Reduced and calibrated spectrum before de-reddening and merging.

Table 2.1

Measured Emission Lines
(ion and λ in Å)

[O II] 3727
[Ne III] 3869
[S II] 4072
[O III] 4363
He II 4686
Hβ 4861
[O III] 4959
[O III] 5007
[N II] 5755
He I 5876
[N II] 6548
Hα 6563
[N II] 6584
[S II] 6716
[S II] 6731
[Ar III] 7135
[S III] 9069
[S III] 9532

Table 2.3
Optical Line Strengths

F_λ values are raw measured emission line strengths
I_λ are the final dereddened and merged line strengths that were used to determine abundance

	th2-A		pc 14		n6629		n6578		n6567		n6565	
	F_λ	I_λ	F_λ	I_λ	F_λ	I_λ	F_λ	I_λ	F_λ	I_λ	F_λ	I_λ
ion and λ												
[O II] 3727	73.95	140.70	42.53	67.10	21.24	37.60	7.22	16.60	16.42	28.90	294.20	379.90
[Ne III] 3869	112.30	195.80	81.66	121.10	27.10	44.37	30.02	61.61	51.11	80.31	108.00	134.70
[S II] 4072	...	...	1.97	2.69	0.08	.11	0.81	1.42	...	...	...	...
[O III] 4363	14.56	19.10	5.59	6.74	2.56	3.23	1.46	2.05	8.10	9.90	7.97	8.85
He II 4686	77.41	83.97	9.42	9.70	0.72	0.77	0.93	1.03	0.76	0.82	15.42	16.50
[O III] 4959	561.60	526.4	468.20	447.1	244.70	231.2	265.30	243.6	369.50	350.1	394.90	384.9
[O III] 5007	1764.00	1613.00	1426.00	1338.00	764.10	705.90	851.60	757.30	1154.00	1071.00	1213.00	1171.00
[N II] 5755	...	...	0.65	0.47	...	...	0.59	0.33	0.77	0.53	8.19	6.85
He I 5876	19.15	11.54	23.98	16.70	24.05	15.35	36.54	18.93	27.19	17.30	18.05	14.80
[N II] 6548	76.02	37.55	25.04	14.35	11.58	5.78	19.44	6.82	7.86	6.56	189.70	135
[N II] 6584	230.80	113.50	68.57	37.60	22.74	10.85	49.40	16.40	32.23	26.20	583.50	416.30
[S II] 6716	16.20	7.30	9.17	4.96	0.91	0.41	3.21	1.03	1.27	0.87	54.66	38.60
[S II] 6731	19.53	8.70	13.94	7.58	2.02	0.76	5.43	1.66	2.37	1.58	72.90	50.50
[Ar III] 7135	58.96	23.32	33.98	16.10	30.82	11.99	57.05	15.26	12.71	8.93	38.00	25.10
[S III] 9069	88.93	21.88	88.74	30.03	34.40	9.21	142.70	20.62	22.56	12.78	74.86	40.93
[S III] 9532	158.70	54.26	106.80	74.47	92.79	22.85	354.10	51.14	68.66	31.69	153.30	101.50

	n6439		n6309		n5882		n5307		n3918		n3242a	
	F_λ	I_λ	F_λ	I_λ	F_λ	I_λ	F_λ	I_λ	F_λ	I_λ	F_λ	I_λ
ion and λ												
[O II] 3727	28.14	55.90	12.88	17.21	10.63	13.89	5.08	6.31	63.31	78.00	8.73	9.60
[Ne III] 3869	69.63	126.20	65.73	84.70	71.79	90.40	90.99	109.75	108.10	128.40	114.80	125.00
[S II] 4072	3.47	5.51	1.18	1.43	0.70	.84	...	...	2.56	2.95	1.04	1.11
[O III] 4363	6.74	9.00	9.73	10.90	4.71	5.32	14.92	16.08	19.60	21.40	15.45	16.00
He II 4686	26.06	28.50	76.85	79.70	3.56	3.68	39.79	40.89	45.81	47.20	35.48	36.10
[O III] 4959	481.30	450.2	367.80	357.2	355.30	345.8	431.30		555.00	543.4	476.60	471.8
[O III] 5007	1404.00	1279.00	1130.00	1085.00	1107.00	1066.00	1293.00	1255.00	1697.00	1648.00	1462.00	1442.00
[N II] 5755	3.67	2.30	0.40	0.33	0.25	0.21	...	...	2.10	1.80	...	...
He I 5876	28.61	16.70	9.35	7.44	21.11	17.10	11.53	9.72	12.24	10.40	12.73	11.80
[N II] 6548	112.80	40.6	13.79	8.8	10.09	5.33	3.77	3.47	36.69	28.14	0.37	.82
[N II] 6584	352.70	126.90	42.24	21.43	20.68	12.34	6.59	3.76	104.20	79.70	3.03	3.63
[S II] 6716	21.70	7.23	4.56	2.41	1.58	1.09	0.49	0.41	3.61	2.87	0.15	0.32
[S II] 6731	36.42	11.98	7.32	3.70	2.67	1.73	0.86	0.62	6.34	4.84	0.18	0.26
[Ar III] 7135	98.52	28.40	30.11	15.38	24.25	15.39	8.27	5.33	28.01	20.00	3.59	7.70
[S III] 9069	252.70	43.82	70.85	28.8	28.97	18.84	11.98	6.39	25.92	17.08	2.17	5.16
[S III] 9532	493.50	108.67	70.90	71.42	90.88	46.72	28.61	15.85	69.85	42.35	6.45	12.79

	n3211		n3195		n2867		n2792		m3-6		m3-4	
	F_λ	I_λ	F_λ	I_λ	F_λ	I_λ	F_λ	I_λ	F_λ	I_λ	F_λ	I_λ
ion and λ												
[O II] 3727	21.59	22.80	241.90	285.40	80.68	102.20	5.75	9.21	11.62	13.55	278.00	366.20
[Ne III] 3869	82.40	86.50	74.36	85.78	91.24	111.90	48.43	72.75	38.65	44.15	124.00	155.40
[S II] 4072	1.61	1.67	6.57	7.34	1.98	2.32	0.92	1.27	0.66	.732	...	...
[O III] 4363	21.99	22.50	3.73	3.80	12.38	13.63	15.05	18.22	1.31	1.39	11.70	12.65
He II 4686	86.33	85.00	12.70	12.96	34.14	35.16	99.02	105.00	0.81	0.82	31.01	32.09
[O III] 4959	476.20	473.5	214.30	210.7	452.70	441.8	345.90	329.6	229.40	225.7	377.80	367.2
[O III] 5007	1450.00	1438.00	648.20	633.20	1397.00	1351.00	1085.00	1014.00	691.30	676.40	1156.00	1111.00
[N II] 5755	0.38	0.36	4.54	4.04	1.48	1.10	0.16	0.11	...	...	5.17	4.25
He I 5876	5.34	5.10	19.63	17.21	14.30	11.86	4.61	3.18	19.39	17.16	18.02	14.49
[N II] 6548	7.19	6.29	150.30	117.89	25.70	20	7.36	1.09	3.48	4.77	125.90	95.24
[N II] 6584	15.59	13.20	470.10	371.20	78.01	60.20	10.34	3.66	8.12	7.34	380.80	288.40
[S II] 6716	2.97	2.59	57.66	45.70	6.16	4.70	1.27	0.52	0.44	0.42	13.21	9.70
[S II] 6731	3.63	3.14	50.29	38.90	9.25	6.80	1.45	0.63	0.69	0.65	11.06	7.91
[Ar III] 7135	22.24	18.60	28.45	21.14	19.40	13.85	19.82	9.17	16.73	11.99	30.39	20.50
[S III] 9069	25.71	20.97	34.11	28.29	22.91	16.33	20.16	7.82	28.15	18.83	12.51	8.75
[S III] 9532	64.51	52.01	101.90	70.16	67.78	40.50	61.85	19.40	65.23	46.69	36.77	21.69

	m3-15		m1-57		m1-54		m1-50		m1-5		m1-34	
	F_λ	I_λ	F_λ	I_λ	F_λ	I_λ	F_λ	I_λ	F_λ	I_λ	F_λ	I_λ
ion and λ												
[O II] 3727	10.13	35.68	74.43	250.60	138.30	252.20	6.31	14.32	13.83	38.61	110.90	226.80
[Ne III] 3869	21.86	64.76	61.07	174.20	77.13	129.50	70.50	143.10	2.65	6.42	39.07	72.50
[S II] 4072	...	...	7.35	16.65	7.29	10.92	...	...	...	...	...	...
[O III] 4363	1.63	2.72	15.77	25.82	4.30	5.49	10.56	14.73	2.55	3.87	2.26	3.03
He II 4686	3.25	3.82	43.26	50.39	15.80	17.05	22.67	25.13	0.17	0.19	11.37	12.45
[O III] 4959	340.20	299.2	684.80	605.6	322.70	303.8	630.70	580.5	132.90	120.75	220.50	205.2
[O III] 5007	1097.00	919.20	2149.00	1813.00	994.20	914.50	1653.00	1474.00	438.40	379.40	692.50	626.70
[N II] 5755	2.31	0.95	24.45	10.40	13.95	9.15	0.40	0.23	6.21	3.01	11.35	6.86
He I 5876	49.37	18.30	28.78	11.05	30.03	18.72	28.67	15.03	39.00	17.33	30.91	17.59
[N II] 6548	76.01	15.7	635.80	133.87	507.40	229.55	16.54	8.20	138.50	30.88	498.70	197.98
[N II] 6584	223.70	45.60	1978.00	422.50	1574.00	705.48	18.30	8.21	366.90	89.78	1564.00	611.31
[S II] 6716	16.58	2.89	127.00	25.50	88.60	38.72	2.24	0.77	4.31	1.14	146.60	54.38
[S II] 6731	28.81	5.20	219.50	42.50	116.40	49.17	3.94	1.35	9.11	2.11	163.00	59.38
[Ar III] 7135	129.20	17.50	209.90	31.49	65.11	24.21	41.49	11.11	42.17	7.64	84.48	26.55
[S III] 9069	509.10	27.56	709.60	43.45	159.80	38.15	87.03	12.73	121.40	10.31	222.70	41.24
[S III] 9532	1287.00	68.35	1717.00	107.76	200.40	94.61	240.20	31.64	306.60	25.57	482.70	102.28

	m1-25		j320		ic 2621		ic 1297		he2-55		he2-48	
	F_λ	I_λ	F_λ	I_λ	F_λ	I_λ	F_λ	I_λ	F_λ	I_λ	F_λ	I_λ
ion and λ												
[O II] 3727	42.73	103.80	6.73	7.51	40.87	76.03	46.06	48.24	11.28	17.18	206.20	260.00
[Ne III] 3869	4.62	9.98	89.01	97.85	106.80	184.20	107.80	112.20	66.38	95.39	81.27	99.29
[S II] 4072	3.50	6.37	0.42	.46	6.15	9.34	2.13	2.19	1.02	1.35	...	...
[O III] 4363	0.66	1.24	15.00	15.50	20.25	25.80	9.16	9.30	9.34	11.07	8.33	9.30
He II 4686	5.98	6.20	3.42	3.47	44.44	47.65	37.11	35.80	105.60	111.30	17.31	17.82
[O III] 4959	167.60	152.9	410.80	399.6	649.00	609.3	446.60	444.6	292.90	280.6	336.90	329
[O III] 5007	530.20	467.10	1228.00	1206.50	2011.00	1843.00	1344.00	1335.00	906.70	854.40	1017.00	983.60
[N II] 5755	4.39	2.34	...	...	10.10	6.52	0.71	0.68	...	...	2.69	2.28
He I 5876	44.33	21.89	18.79	17.23	21.64	13.26	14.00	13.54	4.53	3.25	13.87	11.54
[N II] 6548	235.50	69.82	8.60	6.37	127.20	88.18	21.45	18.52	9.15	5.26	75.53	58.45
[N II] 6584	701.50	212.40	17.12	12.68	283.70	175.37	54.95	48.90	16.14	8.94	227.30	164.90
[S II] 6716	19.27	5.54	0.88	0.70	5.86	3.40	5.42	5.12	3.37	1.84	20.31	14.60
[S II] 6731	35.75	10.10	1.48	1.25	12.59	7.00	8.07	7.39	3.10	1.69	14.56	11.60
[Ar III] 7135	100.70	23.51	10.13	7.86	75.90	43.85	17.71	16.81	24.22	12.13	21.47	15.60
[S III] 9069	300.80	39.11	8.98	7.38	88.90	34.93	31.39	28.79	39.50	14.51	12.82	9.95
[S III] 9532	947.90	96.99	26.55	18.29	257.70	86.62	75.03	71.39	78.28	35.98	43.53	24.70

	he2-37		he2-21		he2-158		he2-141		fg1		cn2-1	
	F_λ	I_λ	F_λ	I_λ	F_λ	I_λ	F_λ	I_λ	F_λ	I_λ	F_λ	I_λ
ion and λ												
[O II] 3727	260.40	421.20	11.46	13.40	107.30	141.80	48.14	73.69	30.50	37.12	23.68	47.61
[Ne III] 3869	123.50	187.00	65.37	73.90	28.46	36.50	68.00	98.56	56.12	66.49	96.41	176.20
[S II] 4072	3.09	4.28	...	...	1.56	1.88	1.26	1.68	1.92	2.19	1.89	3.03
[O III] 4363	20.84	25.30	13.12	14.20	1.99	2.20	14.10	16.70	3.30	3.58	9.73	12.94
He II 4686	63.21	66.90	27.16	27.70	0.04	0.04	77.78	82.08	14.51	14.87	4.64	5.07
[O III] 4959	704.50	670.5	382.00	375.8	176.70	171.7	434.30	416.3	230.50	225.9	685.30	639.4
[O III] 5007	2173.00	2030.00	1156.00	1130.00	551.00	529.80	1338.00	1261.00	703.40	684.00	2108.00	1914.00
[N II] 5755	7.23	5.10	...	...	2.29	1.90	1.56	1.15	0.67	0.58	1.41	0.86
He I 5876	11.81	8.10	13.88	12.20	21.28	17.10	7.96	5.69	18.32	15.68	32.21	18.62
[N II] 6548	147.00	84.08	10.33	6.55	57.58	36.88	43.89	23.79	23.26	16.76	29.95	14.45
[N II] 6584	453.60	256.40	8.17	4.59	165.50	113.00	132.10	64.89	62.74	47.40	75.10	33.86
[S II] 6716	48.09	25.67	0.62	0.44	9.61	6.10	8.72	4.19	6.17	4.80	4.55	2.03
[S II] 6731	41.20	21.70	0.95	0.57	15.24	9.42	11.41	5.45	6.51	5.07	8.76	3.70
[Ar III] 7135	61.18	29.90	8.21	5.60	15.49	9.90	42.24	19.93	16.18	12.05	45.10	16.49
[S III] 9069	72.20	25.22	10.09	6.26	38.43	19.91	58.23	20.07	23.67	15.99	94.62	21.17
[S III] 9532	195.80	62.55	19.96	15.52	37.90	49.38	77.44	49.77	63.88	39.66	175.10	52.50

Chapter 3

Abundance Determinations

3.1 Deriving Abundances from Observed Emission Line Strengths

To understand how we can infer abundances from emission line strengths we need to understand what physical processes are taking place in the PN gas. If we understand these physical processes and the parameters they depend on then we can quantify relationships between these parameters and our only observable, the emission line strengths. The source of energy for these gaseous "shells" is ultimately radiation from the PN central star. How this radiation interacts with the surrounding PN depends on the geometry of the gas (extent and structure), the matter density and its chemical composition. Given that these are ground-based spectroscopic observations of angularly small PNe we are not in a position to discuss structure. It should be noted though that PNe can be very "clumpy" objects with extraordinary filamentary structure but we are addressing each nebula as a whole and making the simplifying assumption that whatever chemical composition these objects possess is sampled in our spectra and thus represents average abundances for each PNe.

The emission line spectra of PNe are due primarily to recombination lines of hydrogen and helium and collisionally excited forbidden lines from ions of metals such as C, N, O, Ne, S, and Ar (remember a metal is any nuclear species that isn't hydrogen or helium). The terms "forbidden" and "collisionally excited" are used interchangeably. Referring to an emission line as collisionally excited is more descriptive of its physical origin whereas the term forbidden has more of an historical charm.

Many elements in the PN gas can exist simultaneously in many stages of ionization. There is a stratification of ionization "zones" that is essentially a function of the ionization potentials of each neutral atom and ion and the distance of these "zones" from the central star. Transitions due to all of these ionization stages (from each element) can be observed across the electromagnetic spectrum. Considering that our observations are essentially in the visible portion of the spectrum we are limited to investigating ions that produce emission lines in this wavelength region. PN emission occurs as a result of fluorescence, the initial source of energy being the copious amount of UV radiation that comes from the very hot central star of each PN. The photons with wavelengths short of the Lyman limit (those shortward of 912 Å) have enough energy to photoionize the abundant hydrogen and less abundant helium in the gas given that the ionization potential is 13.5 eV for H and 24.6 eV for the removal of the first electron from He. Subsequent recombinations produce the very familiar sequence of Balmer lines that are so prominent in these objects. Helium lines are also produced by the mechanism of recombination and subsequent downward cascades of electrons. The actual physical extent of the PN is defined by a region of space containing the expelled former envelope of the progenitor star. Generally the chemical composition of the gas has universal demographics with hydrogen being about 90% of the nebula (by number), helium about 10%, and trace metals making up the rest of the gas.

The ongoing process of photoionization and recombination of hydrogen and helium makes available a source of free electrons that can collisionally excite the much less abundant metals that exist in the gas. This is integral to producing the forbidden lines in gaseous nebulae. The physical conditions of low matter and radiation density

that exist in PNe and other gaseous nebulae provide a unique environment that allows us to investigate elements such as oxygen, sulfur, neon, and argon (tracers of metallicity) – elements that lend themselves to these forbidden lines. We will now investigate the physical relationships between observed emission line intensities and the physical processes that allow the formation of the two types of lines that are primarily visible in PNe, recombination lines and forbidden lines.

It is useful to pause here and give the gist of our method for determining final elemental abundances from the relative ionic line strengths. Symbolically the final abundances will be found as follows:

$$N(x) = \sum_i N(x^i) \cdot icf(x) \cdot mcf(x)$$

Where the first factor in the equation is the sum of number densities $N(X^i)$, in other words the sum over all observed ionic abundances of the given element X, the second factor is a correction for the unseen ions of that element that contribute significantly to its abundance, and the third a model correction factor for more subtle physical corrections. The remainder of this chapter will explain in detail how we determine each factor of the above equation.

3.2 Ionic Abundance Ratios for Recombination and Forbidden Lines

Regardless of the nature of the emission line, recombination or forbidden, the strength of each line indirectly represents the abundance of the ion that produced that particular transition (for example: λ5007 Å for [O III]). This means that we can find a number abundance for each visible ionic species from the line strengths we so carefully reduced. Keeping in mind that each element can exist in many ionic stages throughout

the PN gas we must sum the contributions from all of the ions to find the total element abundance. This is the first term in the equation above :

$$N(X) = \sum_i N(X^i)$$

$$\text{where} \quad \sum_i N(X^i) = N(X^0) + N(X^1) + N(X^2) + N(X^3) + \ldots$$

N(X) is the abundance in number per unit volume and the index i refers to the ionization stage of the element X; i=0 refers to the neutral atom, i=1 the singly ionized atom, i=2 the doubly ionized stage and so on.

Ionic abundances from recombination lines and collisionally excited lines are found differently, and I will discuss each of them separately.

3.2.1 Recombination Lines

Recombination lines result from free electrons recombining with available ions of H and He. Generally these recombinations occur putting the electron in an excited state where it subsequently can radiatively cascade to lower energy levels. This radiative cascade produces emission line patterns such as the familiar Balmer decrement of hydrogen. The relative intensity of a generic recombination line depends functionally on the following :

$$\frac{I_\lambda(X^i)}{I_{H\beta}(H^+)} = \frac{N(X^i) N_e \alpha_\lambda^{eff} E_\lambda}{N(H^+) N_e \alpha_{H\beta}^{eff} E_{H\beta}}$$

I have explicitly written the intensity relative to the Hβ line because all of our final line strengths are scaled to Hβ=100. In the end we would like to have the number abundance of ion X^i relative to hydrogen. Given the time scales for the photoionization of hydrogen and subsequent recombinations, at a typical point of interest in a PN H is almost completely ionized. This means that $N_e=N_p=N_H$ and the number density of ionized

hydrogen, represented by the strength of the Hβ line, traces the abundance of total hydrogen. N_e is the number density of electrons, $N(X^i)$ the number density of ion X^i, E_λ the energy of the particular transition that creates the emission line, and α_λ^{eff} is the effective recombination coefficient that accounts for all recombinations and subsequent cascades that lead to the particular transition that creates the line at λ.

Solving for the number abundance of ion X^i relative to hydrogen we have the following functional form:

$$\frac{N(X^i)}{N(H^+)} = \frac{I_\lambda \alpha_{H\beta}^{eff} E_{H\beta}}{I_{H\beta} \alpha_\lambda^{eff} E_\lambda}$$

The left hand side of the equation represents the relative number density of ion X^i and on the right we have the relative intensity of the emission line to Hβ, the ratios of the energies of the two transitions, and the ratio of the effective recombination coefficients.

3.2.2 Collisionally Excited Lines

Forbidden lines, or more descriptively collisionally excited lines, occur in the much less abundant metals that exist in the gas. Among the more abundant metals that can be observed in PNe are C, N, O, Ne, Na, Mg, Al, Si, S, Ar, Ca, Fe, and Ni. The metals we are particularly concerned with in this study are O, Ne, S, and Ar not only because they are easily detected in PNe but also because they are tracers of the metallicity of the interstellar medium and indicative of the chemical history of both the progenitor star and previous generations of massive stars.

The origin of a forbidden line is due to the continuously available distribution of free electrons, the majority of which come from the photoionization of H. For typical PNe this distribution of free electrons has energies characteristic of the excitation

energies of the lower-lying fine-structure levels of the available metal ions. Thus the free electrons collisionally excite the available metal ions where they "sit" in metastable states until they spontaneously de-excite emitting a photon characteristic of the particular electronic transition that took place. The cross section for elastic scattering collisions between electrons is quite large (Oserbrock 15) compared to other interactions that take place in the nebulae. This large cross section allows the e-e collisions to set up a Maxwellian distribution of electron energies. This is fundamental to PN physics for many reasons, one of the most useful being that the ratios of carefully chosen forbidden lines can be strong indicators of both electron temperature and electron density of the PN gas. This will be discussed later in this section.

Just as we did before with the recombination lines we can quantify the abundance of some ion X^i relative to hydrogen in terms of measurable and theoretically determined quantities. For a collisionally excited line the intensity relative to Hβ is:

$$\frac{I_\lambda(X^i)}{I_{H\beta}} = \frac{N(X^i)\chi^i_{ul}A_\lambda E_\lambda}{N(H^+)N_e\alpha^{eff}_{H\beta}E_{H\beta}}$$

Solving for the number density ratio we have ... $$\frac{N(X^i)}{N(H^+)} = \frac{I_\lambda N_e \alpha^{eff}_{H\beta} E_{H\beta}}{I_{H\beta}\chi^i_{ul}A_\lambda E_\lambda}$$

The ratio of the line intensities comes from our reduced data (already in terms of Hβ = 100), the energies of the transitions, recombination coefficients, and Einstein A transition rates come from the atomic data sources collected in table 3.1. Here χ^i_{ul} is the fraction of the ions X^i that are excited to the appropriate upper level to have the potential to produce the specific line at λ. Symbolically χ^i_{ul} can be written as $\chi^i_{ul} = \frac{N(X^i_{ul})}{N(X^i)}$

All of the physics that occurs in the nebula to produce the forbidden lines is contained in this fraction χ^i_{ul}. It is important to note here that in general quantifying the intensity of any emission line will depend on being able to characterize the population of the excited states that give rise to the radiative downward transitions that create the emission lines we see. For both the recombination and forbidden lines we must determine the electron temperature of the gas (T_e), the electron density (N_e), and the level populations of each ion. Physical quantities such as electron temperature, electron density, level populations of the metal ions, transition rates from atomic data such as effective recombination coefficients and collisional excitation rates, and ionization correction factors are all calculated within the abundance determination code ABUN, written by R.B.C. Henry and described in Henry, Kwitter, & Dufour, (1999). As input ABUN requires relative line strengths $\frac{I_\lambda}{I_{H\beta}}$ from the ions of interest and uses these line strengths to calculate T_e, N_e, ionic abundances, ionization correction factors, and finally total element abundances of He, O, Ne, S, and Ar. ABUN has the ability to deal with other elements, such as carbon and nitrogen, depending on the available line strengths.

3.2.3 Electron Temperature and Density

The ABUN code determines T_e in two ways using the emission lines from the [O III] and [N II] ions. Nebular temperatures from the forbidden lines of these ions are possible because of the nature of the spacing of the five lowest energy levels (sublevels). For typical PNe temperatures, the free electrons do not have enough kinetic energy to collisionally excite the metal ions outside of the first five energy levels (typically within about 8 eV of the ground state). As a side note, this is why ABUN and most analytical studies of PNe and H II regions approximate each of the metal ions as only having

available the 5-lowest levels for transitions. This method of temperature determination via forbidden lines takes advantage of the wide spacing between the top two levels in the [O III] and [N II] ions. Figure 3.a illustrates the lowest five energy levels of these two ions. The rather large difference in energy between the singlet-S and singlet-D levels is useful because in a low density gas the population of these levels is dictated by collisional excitations and radiative de-excitations, so the relative population of the singlet-S and singlet-D levels is an indicator of temperature. Given the small contribution from collisional de-excitations, the relative intensities of a line originating from the D level to a line originating from the S level will be a function of temperature. In practice the [O III] and [N II] ions are used because they have rather strong lines in the optical portion of the spectrum.

$$\frac{^1D_2 \rightarrow ^3P_{0,1,2}}{^1S_0 \rightarrow ^1D_2} = f(T_e)$$

The specific lines used from O^{+2} ion are $\frac{I_{\lambda 4959} + I_{\lambda 5007}}{I_{\lambda 4363}}$

The lines used in this ratio from the N^{+} ion are $\frac{I_{\lambda 6584} + I_{\lambda 6548}}{I_{\lambda 5755}}$

In practice ABUN uses a 5^{th} order polynomial fit to the functional dependence of the temperature on the ratio of the above line strengths. Note that the temperatures found via the two methods will be slightly different. This is expected due to the fact that the ionization zones for [O III] and [N II] exist at different physical distances from the central star.

Once the electron temperature has been determined the density is found by using a similar method. For the electron density ABUN uses the optical lines from the [S II] ion. The first five levels of the S^+ ion are as follows:

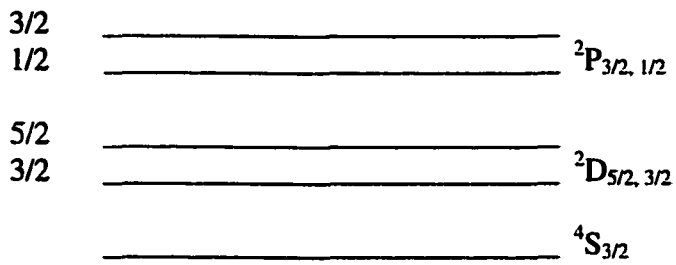

The spacing of the lowest five levels here is markedly different from that of the p^2 ions (referring to the configuration of the optically active electron). The small energy difference between the two J states of the D-level is used to exploit the electron density of the gas. Given the close spacing, collisional excitations to the two J states will not reflect changes in temperature very well. In the general case, depopulation of the two states can occur via radiative de-excitations or collisional de-excitations. The density of the gas will dictate which process, collisional or radiative de-excitations, will have more of an effect. Given that the emission from the lines at λ6717 and λ6731 Å only comes about from radiative de-excitations, the relative strengths of those two lines will characterize the electron density.

$$\frac{^2D_{5/2}\rightarrow{}^4S_{3/2}}{^2D_{3/2}\rightarrow{}^4S_{3/2}} = f(N_e) \quad \text{using the } S^+ \text{ ion this ratio would be } \frac{I_{\lambda 6716}}{I_{\lambda 6731}}$$

Once the temperature and density are found then the relative populations of the five levels in each metal ion can be found from the atomic data. It is the relative

populations of the levels that allow us to determine χ_{ul}^{i} for each radiative transition that we are considering and finally the ionic abundances. To find the relative populations of each level in a given ion first we must characterize all of the possible physical processes that bring electrons into and out of each level. This is referred to as level-balancing. For the low matter density and low radiation density found in gaseous nebulae (PNe included) only collisional excitations are considered for upward transitions and collisional and radiative de-excitations for downward transitions. A smaller scale example of level balancing is shown in Appendix B.

Once the level balancing accounts for all of the physical processes that bring electrons into and out of each level we are left with a system of five linear equations. The five unknown variables N_i in the system of equations represent the number density of ions that have the i^{th} level populated. The sum of all of the N_i values is the total number density of the ion. Once the level populations are determined, the χ_{ul}^{i} values can be calculated and the ionic abundances can be found. ABUN performs these calculations for each 5-level atom/ion. The ABUN code is listed in Appendix C.

3.3 Ionization Correction Factors

Once the ionic abundances are found they are summed together as noted in section 3.2. The next step is to apply an ionization correction factor to the summed ionic abundances. The ionization correction factor (icf) is, as its name implies, a correction that accounts for any ionization stages that cannot be measured in the available spectrum. A number of different factors such as central star temperature, chemical composition of the gas, and density of the gas, determine the ionization structure of each PN. Depending on the ionization potential for the successive removal of electrons from an atom the most

prominent ions of any given element may not exhibit emission lines in the wavelength region under study. Our sulfur study illustrates this concept quite well. Figure 3.b is a plot of the degree of ionization of sulfur versus ionization stage, extracted from photoionization models of PNe (Henry, Kwitter, & Howard, 1996).

The ionization structure of a PN is dictated by the spectrum of photons coming from the central star. Given the mass range for PNe progenitors the typical PN central star is hot enough to ionize available sulfur three or more times. In other words there are appreciable amounts of sulfur in the S^{+}, S^{++}, and S^{+++} stages of ionization all co-existing within the nebular gas. Each ion can have emission lines spread across the electromagnetic spectrum but to find the abundance one must observe a prominent (strong and high signal/noise) emission line for each ion. In the case of sulfur the strongest lines of S^{+} exist in the optical portion of the spectrum at λ6716 and λ6731 Å, while S^{++} is usually traced using the particularly weak and temperature sensitive line at λ6312 Å also in the typically observed optical portion of the spectrum (3500 to 7500 Å). Our study of sulfur uses the very strong forbidden lines of [S III] at λ9069 and λ9532 Å to determine the S^{+2} abundance. Given the strength of these lines compared to the typically used λ6312 Å line, this should provide a more reliable S^{+2} abundance and thus more reliable S abundances as a whole. To illustrate this concept, figure 3.c shows a typical PN spectrum from our sample.

To account for S IV (S^{+3}) and further ionized stages of sulfur one would have to observe the available lines in the infrared or ultraviolet since there are no prominent lines in the optical portion of the spectrum. Since we did not observe our sample of objects in

these other wavelength regions an ionization correction factor was applied to account for the fraction of sulfur that exists in the S^{+3} or higher stages.

Icfs are typically determined from model PNe. By specifying central star and gas characteristics, emission line strengths from all possible ionization stages can be examined. Using this output of model PNe spectra typical populations of the many ionization stages available for an element can be observed. A functional dependence can be fit to describe what fraction of some element is not being accounted for when only certain observed ions are found. For instance one could model a PN and see directly how much oxygen resides in the O^{+2} stage compared to O^{+1} or O^{+3} and also whether any appreciable neutral oxygen or O^{+4}, O^{+5}, etc. exists in the gas. In practice the functional form for an icf relies on exploiting similar ionization potentials of "seen" and "unseen" ionic species. For example the ionization potential of O^{+} (35.1 eV) is nearly identical to S^{+2} (34.8 eV). Knowing this if we can actually observe O^{+2} in a PN we know there must be S^{+3} present whether we can see it via lines in the optical region or not. Using sulfur again as an example, typical observations of PNe observe S^{+} and S^{+2} lines in the optical spectrum. Emission lines due to the S^{+3} ion (or higher stages) are not seen in the optical spectrum but O^{+2} lines most certainly are. I can directly measure the fraction of O^{+2} to total oxygen and by exploiting the nearly identical ionization potentials of S^{+2} and O^{+}. I can approximate fairly well the amount of S^{+3} to total sulfur. Symbolically the total sulfur abundance can then be written as follows:

$$N(S) = [N(S+) + N(S+2)]\ icf(S)$$

$N(S^{+})$ and $N(S^{+2})$ are the number densities of these ions and I can directly observe them from my optical spectra. The icf(S) is based on directly observed oxygen abundances

and the model-borne functional dependence of the population of the sulfur ionization stages to those of oxygen. The following icfs were used for O, Ne, S, and Ar where the ion symbol denotes the number abundance of that particular ion.

$$icf(O) = \frac{He^{+2} + He^{+}}{He^{+}}$$

$$icf(Ne) = \frac{O^{+2} + O^{+}}{O^{+2}} \cdot icf(O)$$

$$icf(S) = \left[1 - \left(1 - \left(\frac{O^{+2} + O^{+}}{O^{+}} \cdot icf(O)\right)\right)^{3}\right]^{-1/3}$$

$$icf(Ar) = 1.87$$

The oxygen icf within ABUN is originally from Torres-Peimbert & Peimbert, 1977 and the neon, sulfur, and argon icfs used are from Kingsburgh & Barlow, 1994.

3.4 Model Correction Factors

The last step in the abundance determination process is to apply what is uniquely referred to as a model correction factor (Henry, Kwitter, and Dufour, 1999). The purpose of the model correction factor is to account for any physics that is represented in CLOUDY (Ferland 1990) but not in ABUN. CLOUDY is a model nebular photoionization analysis code that produces an emission line spectrum from a small set of input parameters. The input to CLOUDY can be quite detailed including characteristics of the source spectrum and the density, structure, chemical composition, and volume of the nebular gas. CLOUDY is a rather large piece of code that is designed to simulate any type of emission line region. By specifying the incident radiation and the geometry and chemical composition of the gas CLOUDY carefully produces the emergent spectrum. CLOUDY has the ability to predict the emission intensities of about 10,000 lines. It treats all levels of ionization of metals, charge exchange, radiative recombination,

dielectronic recombination, photoionization from excited states, and collisional ionization. Some of these mechanisms are not accounted for in the abundance determination code such as charge exchange and dielectronic recombination. The impetus for the model correction factor (mcf) is to provide a check for the physical soundness of the approximations made in the abundance code and to also check the validity of the ionization correction factors. The geometry of the gas is also considered in CLOUDY which is fundamental when studying variations in temperature, density, excitation, etc. in angularly large objects.

To determine an mcf for each element in each program object a grid of 75 model PNe were created varying the input parameters of the central star temperature, electron density, and chemical composition of the gas. Forethought went into deciding the range of these three parameters so that the model PNe would be characteristic of our actual program objects. The source spectrum for each model was entered as a blackbody with the stellar temperature and radius specified. The density of the gas is specified by the **hden** command which specifies the number density per unit volume of hydrogen. The third varying input parameter was the metal abundance in the gas. The general abundance of the gas was specified as solar (Grevesse & Anders, 1989) and the metals were shifted together using the **metals** command. The metals command multiplies all elements heavier than He by the scale factor indicated. The values entered for central star temp, density, and metallicity for the grid of model PNe are listed in table 3.2.

Once the CLOUDY spectra were created the line strengths required for the abundance code were extracted from each model PN. These sets of line strengths were then put into ABUN to determine the abundances for each model.

$$\underset{(X/H)_{in}}{CLOUDY\ in} \xrightarrow{\text{----------}} \underset{=ABUN\ in\ (line\ strengths)}{CLOUDY\ out} \xrightarrow{\text{----------}} \underset{(X/H)_{out}}{ABUN\ out}$$

The output from ABUN is compared to the original (X/H) abundances put into CLOUDY. Any difference between the two sets of abundances should be due to the more extensive analytical treatment afforded by the much larger CLOUDY code. Under the umbrella of "more extensive analytical treatment" are the physical processes mentioned earlier (charge exchange, dielectronic recombination) and of course since it's a model nebular spectrum all emission lines due to all ionization stages are available. The model correction factor can then be found for each element of interest and quantified as follows:

$$\xi(X) = (set\ model\ abundance)/(model\ abundance\ as\ seen\ by\ ABUN)$$

$$\xi(X) = (CLOUDY\ X/H\ in)/(ABUN\ X/H\ out)$$

Each of the 75 models has an associated model factor $\xi(X)$ for each element X. Which mcf was applied to each of our program objects was decided by finding the best match between a set of line ratios that were calculated from emission line strengths in both the models and our program objects. The chosen line ratios are diagnostics of physical conditions in the nebulae. The following lists the diagnostic ratios that were used and the physical parameters that they predict.

$log\ (I(O^+) + I(O^{+2}))/I_{H\beta}$	*T_e and metallicity of the gas*
$log\ I(O^+)/I(O^{+2})$	*nebular excitation*
$log\ I(He^+)/I(He^0)$	*nebular degree of excitation*
$log\ I_{4363}/I_{5007}$	*electron temperature*
$log\ I_{6716}/I_{6731}$	*electron density*
$log\ I(He^0)/I_{H\beta}$	*He/H*

$log\ I_{6584}/I_{3727}$	*N/O*
$log\ I_{6724}/I_{3727}$	*S/O*
$log\ I_{3869}/I_{5007}$	*Ne/O*

To find the best match of physical conditions a comparison was made between each program object and all 75 models using these 9 diagnostic line ratios. This comparison was done by summing the absolute values of the differences between each cloudy line ratio and the corresponding line ratio belonging to the program object. Comparing each object to all 75 models, the smallest sum was then taken as the closest match. Once this best match was determined sulfur and argon were corrected for using the appropriate mcf.

This completes our method of abundance determinations from reduced line strengths. At this point we are now in a position to use these relative abundances to analyze the chemical history of our set of PNe and discuss how we can use their chemical properties as tracers of the nucleosynthetic history of the Galactic disk and also as an observational constraint to the chemical yields of massive stars. Appendix A discusses the error associated with our abundance determination methods. In short we found typical uncertainties from 10% to 20% in our measured line strengths which propagates to an error of $\pm$ .2 dex in final abundance.

Table 3.1

Atomic Data Sources

Ion	Atomic Data[1]	Reference
H^0	α_{eff} (λ4861)	Storey & Hummer 1995
He^0	α_{eff} (λ5876)[2]	Pequignot et al. 1991
He^+	α_{eff} (λ4686)	Storey & Hummer 1995
O^+	Ω	Mendoza 1983 McLaughlin & Bell 1993
	A	Weise, Fuhr, & Deters 1996
O^{+2}	Ω	Burke, Lennon, & Seaton 1989 Lennon & Burke 1994
	A	Weise, Fuhr, & Deters 1996
Ne^{+2}	Ω	Butler & Zeippen 1994
	A	Baluja & Zeippen 1988
S^+	Ω	Ramsbottom, Bell, & Stafford 1996
	A	Mendoza 1983
S^{+2}	Ω	Galavís et al. 1995
	A	Mendoza 1983
Ar^{+2}	Ω	Galavís et al. 1995
	A	Mendoza & Zeippen 1983

[1] α_{eff} = effective recombination coefficient; Ω = collision strength; A = transition rate
[2] includes collision effects from the considerably metastable 2 ^{3}S term, from Clegg 1987

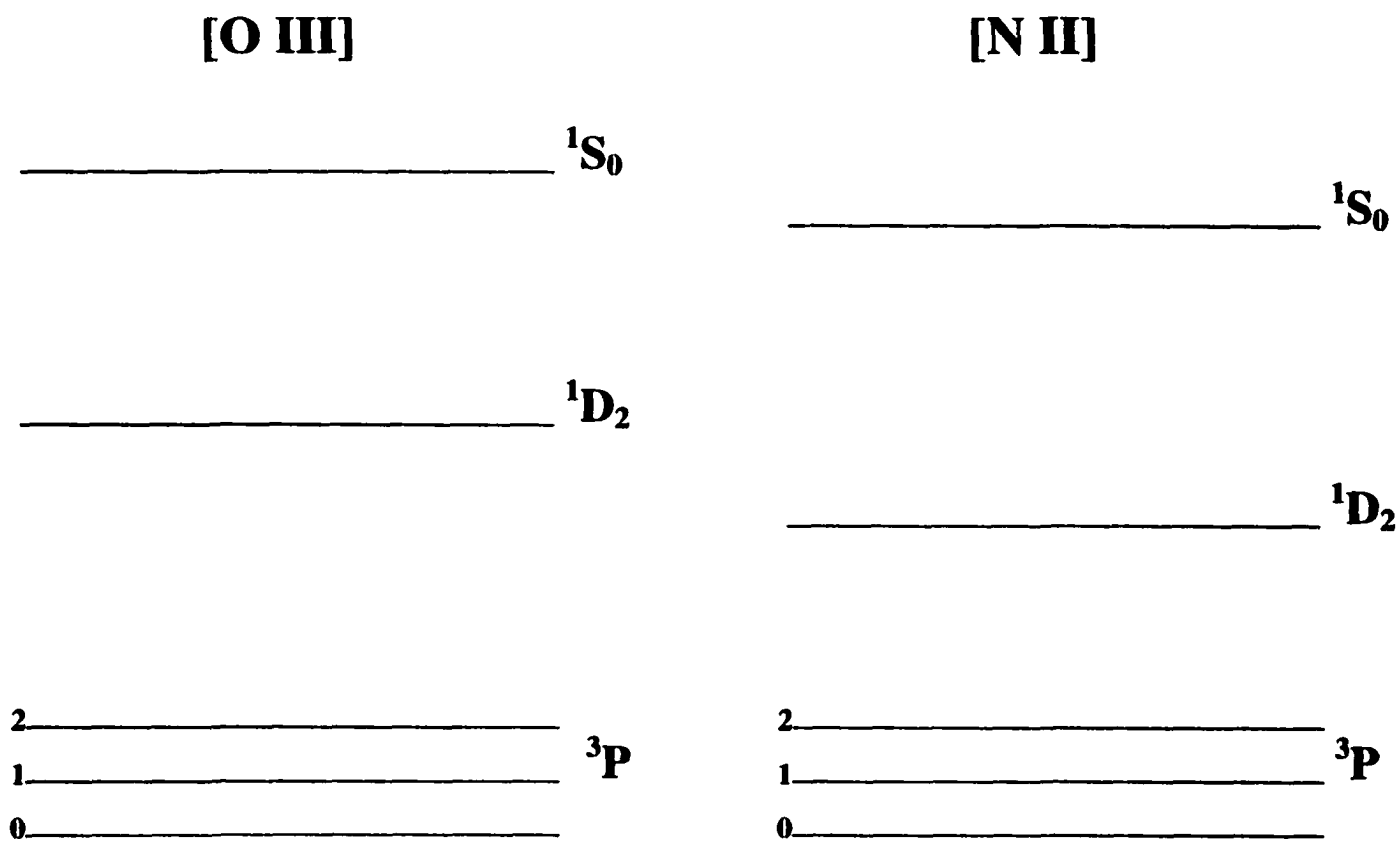

Figure 3.a – The 5 lowest energy levels of the O^{+2} and N^+ ions.

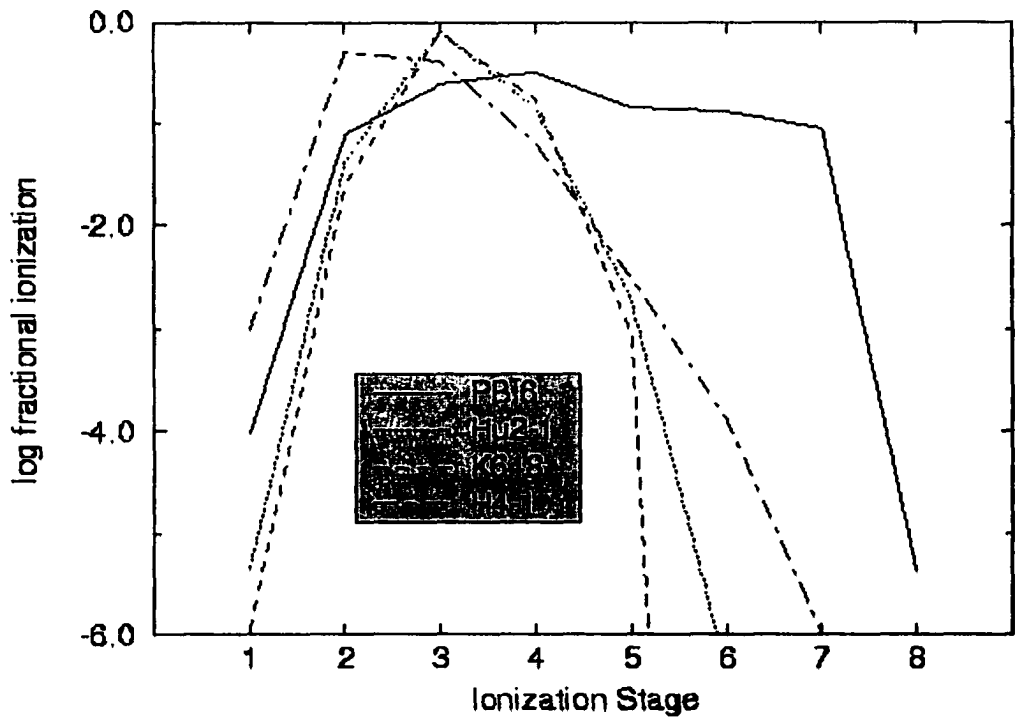

Figure 3.b - Fractional ionization for sulfur versus ionization stage, where 1=neutral, 2=singly ionized, and so on. Figure based on photoionization models for PNe by Henry, Kwitter, & Howard (1996).

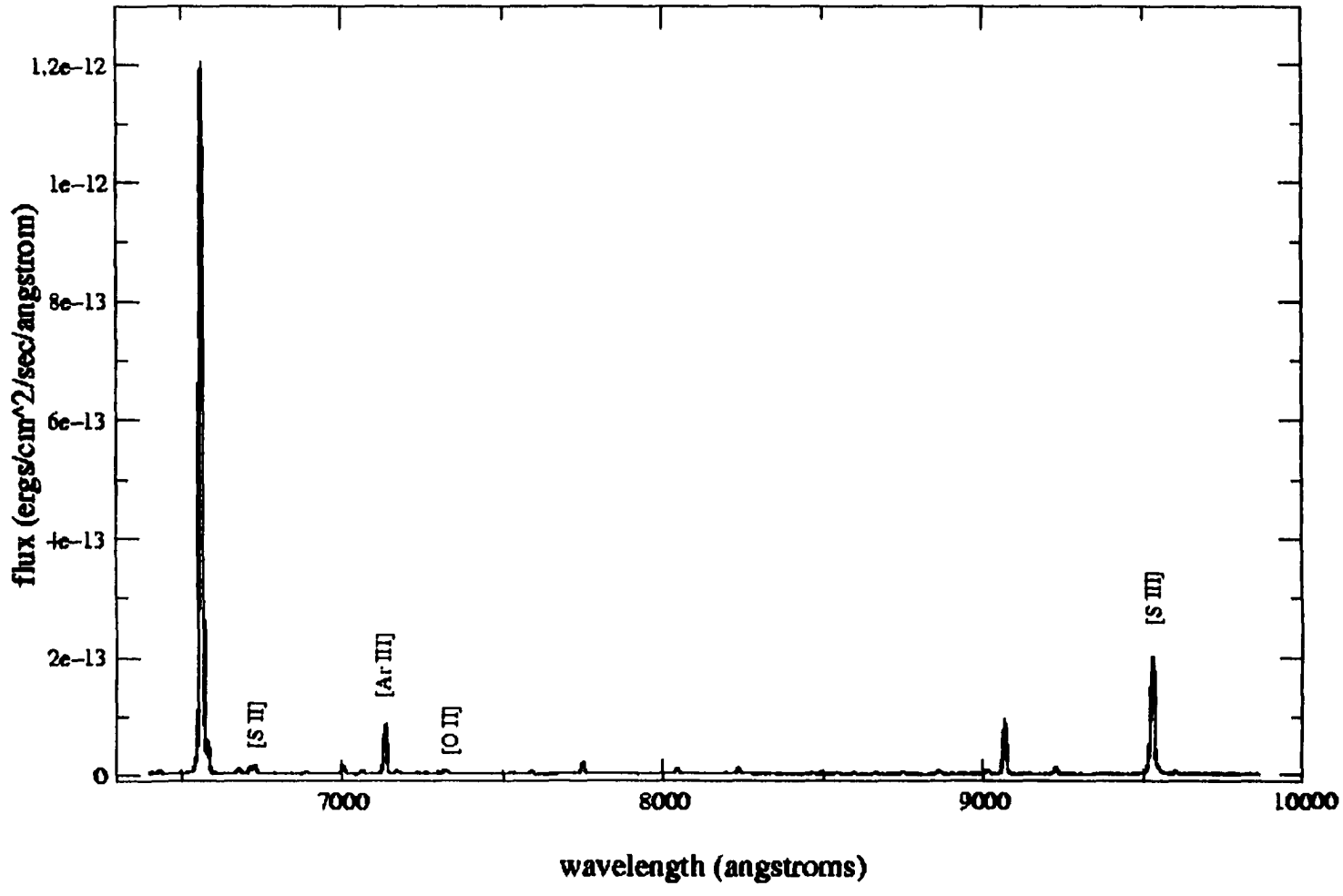

Figure 3.c - Considerably strong near-IR lines of S^{+2} at 9069 and 9532 Å.

Table 3.2
input parameters for mcf grid

ABUN Solar Abundances[1]

he = -1	al = -5.53
c = -3.45	si = -4.45
n = -4.03	s = -4.79
o = -3.13	ar = -5.40
ne = -3.93	ca = -5.64
na = -5.69	fe = -4.49
mg = -4.42	ni = -5.75

Central Star Temps[2]

50,000 K	100,000 K	150,000 K
75,000 K	125,000 K	

Gas Density[3]

hden:	2.5	3	3.7	4	4.2

Metal Scale Factors[4]

low z	solar	high z
metals = .3	metals = 1	metals = 2

[1] Solar abundance values from Grevesse et al. 1989, listed as log of the abundance by number relative to hydrogen.
[2] Blackbody temperatures for central star with $R_* = 10^{10}$ cm.
[3] Density listed as hden which is the log of the number density of hydrogen in the gas in cm^{-3}.
[4] Scale factor that shifts all elements heavier than He.

Chapter 4

Results

4.1 Compiled Abundance Ratios

The results from our abundance determinations are shown in tables 4.1 and 4.2. Table 4.1 lists each object with its determined metal:hydrogen values for oxygen, neon, sulfur, and argon. By convention the metal abundances are given as log(X/H)+12. Table 4.2 lists metal:oxygen values (X/O) for neon, sulfur, and argon. Tables 4.1 and 4.2 also list our program objects with their respective R_g values and distance references, and Log(X/H)+12 and X/O values for the Sun (Grevesse, Noels, & Sauval, 1996) and Orion (Esteban, Peimbert, Torres-Peimbert, & Escalante, 1998).

Keeping in mind the impetus behind this work, our final abundance results are presented in the form of abundance gradients and heavy element ratios. This chapter will present our constructed gradients along with X/O versus O/H plots, and address in some detail how abundance gradients and heavy element ratios can be used in the context of GCE as observational constraints.

4.2 Abundance Gradients

We plot the fraction of metals to hydrogen versus galactocentric distance (radial distance from the center of the Galaxy) to roughly determine the extent of chemical enrichment localized to a given region in the Milky Way. A plot of this nature gives us a gradient that reflects how steeply the metal abundance changes as we move from one radial location in the Galactic disk to another. If the initial mass function (IMF) is assumed to be constant in space and time, a ratio such as X/H will reflect the rate at

which stars convert hydrogen into heavier elements at a particular radial location. Regardless of the IMF, knowing the degree of chemical enrichment as a function of radial location in the Galaxy can provide insight into the history of star formation, which inexorably entwines the IMF and SFR, as a function of space and time. It is important to point out again that our objects are revealing the nature of the ISM at the time of the formation of the progenitor stars which is approximately 4-6 billion years ago for type II PNe. Using objects such as H II regions or type I PNe (which have more massive progenitors) will obviously reflect the nature of the ISM presently or in the more recent past then type II PNe. The time evolution of abundance gradients has the potential to reveal a significant amount of information about the chemical history of a galaxy given that the objects chosen to reveal the gradients are representative of a particular epoch in time. It should be noted that expected theoretical changes in gradients between types I, II, and III PNe and H II regions are rather small and easily lost within observational error (Maciel & Koppen, 1994). Thus PNe play an important role, complementary to HII regions, in revealing abundance patterns due to GCE and stellar evolution. If enough is known about the progenitor star, PNe also make available additional information about low to intermediate mass stellar evolution through signature surface abundance enhancements or depletions.

Figure 4.a is a set of abundance gradient plots for our sample of planetary nebulae. The gradients shown are for O, Ne, S, and Ar and are typical representations of this type of data in that they plot logarithmic X/H abundance against galactocentric distance R_g, where X is the given element and R_g is the distance of the PN from the center of the Milky Way in kpc. The slopes in units of dex/kpc are shown in each panel.

Typical uncertainties for all of the data sets are shown with error bars in the bottom plot. Table 4.3 lists some available abundance gradient results taken from the literature for PNe, H II regions, and B stars. As stated before, abundance gradients have the ability to mark the spatial and temporal changes in metal enrichment within a galaxy. It is not clear exactly how these disk gradients come about initially or evolve in time, but the rate of progression of metal enrichment must be linked to the star formation rate, initial mass function, radial flows of material, infall, and anything else that would affect the enrichment and/or dilution of metals. Within the observational error our results are consistent with those obtained in studies using H II regions, reinforcing our confidence in PN as abundance tracers in galactic disks. The disparate values among sulfur gradients are noteworthy as the uncertainty in sulfur abundances is the impetus of this work. This will be discussed further in Chapter 5.

One of the many questions the rather broad category of GCE tries to address is how theory can analytically reproduce the empirically observed abudance gradients that have been found in spiral disks and other galactic morphologies. If we can carefully determine the value of these abundance gradients then we can provide a reliable observational constraint on theoretically produced gradients that give us insight to both the chemical and dynamic history of the Milky Way and other galaxies.

One additional thought concerning disk gradients; oxygen is the typical metallicity indicator for ionized nebulae because emission lines due its ions are strongly visible and as far as metals go it is highly abundant in the Universe (Pagel 84). In this study we are additionally using sulfur, argon, and neon as metallicity tracers. By doing this we are indeed testing the validity of their use in this context but more specifically we

are attempting to improve observational sulfur abundances so that they alone can be more reliable in tracing the metal enrichment of the Galactic disk and yields of massive stars. The production of S, Ne, and Ar steps along directly with the production of oxygen in massive stars which is why we should be able to use them all as tracers of metallicity in galactic disks. From our knowledge of stellar evolution and the production sites of these elements (discussed in section 4.4) it follows that their gradients should be similar.

4.3 Heavy Element Abundance Ratios

Heavy element abundance ratios were calculated for Ne/O, S/O, and Ar/O. Ratios of metal abundances in this form (X/O) gauge the rate at which both metals, X and O, are synthesized relative to hydrogen and to each other (X/O =(X/H)/(O/H)). If we know what types of stars and what physical environments produce oxygen, neon, sulfur, and argon, then their X/H and X/O abundance ratios should clue us in to the demographics of the previous generations of stars that produced these elements. As was stated in the introduction the progenitor stars of our type II PNe have masses of approximately 1.5 solar masses (Peimbert, 1978). Stars in this mass range do not produce the O, Ne, S, and Ar that we see in their shed envelopes. Tracing the origin of these particular elements and how they may or may not be contaminated (enriched or depleted) by the progenitor star is key in understanding the abundances that we see in all types of planetary nebulae. Understanding the stellar origins of these elements allows us to use their abundances to infer the history of star formation, and observed heavy element ratios to constrain theoretical yields from massive stars which are intimately linked to models of stellar evolution. The following section will discuss the origins of O, Ne, S, and Ar in more detail.

Figure 4.b is a compilation of heavy element ratios plotted against O/H metallicity for different studies of Galactic and extragalactic H II regions and our sample of PN (see caption for references). Three different model predictions for massive star yields are also shown for comparison with the data sets. The horizontal lines depict stellar yield predictions by Nomoto et al. (1997; dashed lines), Woosley & Weaver (1995; dot-dashed lines), and Samland (1998; solid lines) from massive star (10 to about 50 solar masses) yields integrated over a Salpeter IMF. It should be noted that these predicted yields are for type II SNe products only, no contribution from Ia SNe is included in these models. Given the possibly significant contribution that Ia SNe make to S and Ar abundances as indicated in the W7 models of Nomoto et al. (1997), it would be interesting to test how their inclusion affects the model yields.

4.4 Stellar Evolution and the Production of O, Ne, S, and Ar

It is important to consider the origin of the metals we are investigating here if we want to use them to indicate the chemical history of the Galactic disk. The abundance of any given element that is found in a PN (or any object for that matter) will reflect not only the chemical history of the Galaxy previous to its formation but also any chemical enrichment or depletion that has occurred during the lifetime of the progenitor star. This chemical enrichment and depletion occurs via nucleosynthesis in core and shell burning phases and mechanisms such as convective mixing (dredge-up) and hot-bottom burning that can alter abundances seen in the envelope (remember it is the envelope that eventually becomes the PN). With respect to our investigation here I will briefly discuss the origins of oxygen, neon, sulfur, and argon. The following section will discuss self-contamination.

Oxygen is produced via hydrostatic helium burning through the following nuclear reactions:

$$3\alpha \rightarrow {}^{12}C$$
$${}^{12}C(\alpha,\gamma){}^{16}O$$
$$also\ {}^{20}Ne \rightarrow {}^{16}O + {}^{4}He$$

Other isotopes of oxygen can be produced in quiescent and explosive hydrogen burning and He or N burning. The oxygen that we are observing in the abundances of our PNe had to be formed in a physical location that would allow it to be put back into the interstellar medium and swept up in the formation of subsequent generations of stars. Given this and the fact that explosive burning in type II supernovae (SNe) does not significantly modify the fusion products in the outermost layers of massive stars, the oxygen that we see primarily originated via hydrostatic helium burning in massive stars. The ^{12}C + α particle reaction shown above is very sensitive to temperature and density so despite the fact that oxygen is produced in low to intermediate mass stars via this reaction, the products are left behind in the core to be ultimately locked up as a compact remnant.

Neon production has a similar story to oxygen. It can be produced in both the hydrostatic and explosive nucleosynthesis of carbon ${}^{12}C + {}^{12}C \rightarrow {}^{20}Ne + {}^{4}He$. Again the neon that we are seeing in these objects was primarily formed hydrostatically in pre-supernova massive stars. Like oxygen, the abundance of neon is not significantly modified by explosive burning in type II SNe.

The abundances of sulfur and argon have a slightly more exciting story to tell. Hydrostatic nuclear fusion processes that produce sulfur and argon occur in stars much more massive than our type II PNe progenitors. The various isotopes of sulfur and argon

can be produced via both neon and oxygen burning, the s process and explosive nucleosynthesis in supernova events. The rather interesting caveat attached to the abundances of these two elements is that in massive pre-supernova stars the shells that contain oxygen and neon ash exist close enough to the core that during the SN event itself substantial amounts of these quiescent burning products will undergo explosive nuclear burning. So sulfur and argon are drastically modified during SNe events and thus what we see in our PNe abundances is primarily the result of explosive processing. This is very interesting because the yields of these two elements have the potential to describe the physical conditions that formed them. Models of supernova events constructed by Nomoto et al. (1997) indicate that type Ia SNe produce significant amounts of S and Ar. Comparing the theoretical yields of type Ia alone or a mixture of both Ia and II to the observed S and Ar abundances could produce a clearer picture of the contribution that the two types of SNe make to the chemical enrichment of the ISM.

4.5 Self-Contamination

The observed abundances in PN are the results of two basic contributions; previous epochs of galactic chemical enrichment that provided the mix of elements in the natal ISM from which the progenitor star formed, and any products of nucleosynthesis that occur during the lifetime of the star. The nucleosynthetic processes that take place in all stars ultimately modify the original abundances the progenitor star had at the time it was formed. Knowing this the abundances of PNe can be used not only to constrain models of GCE, but also models of stellar evolution and nucleosynthesis. To do this the two basic contributions to PNe abundances must be carefully separated, which requires knowing the sites at which relevant nuclear reactions take place and how the products of

core and shell nucleosynthesis can make their way back to the envelopes of stars ultimately to be shed as PNe.

The process of enhancing or depleting the original surface abundance patterns in PNe is commonly referred to as self-contamination. We have already stated that for the elements of interest in this study (O, Ne, S, and Ar), type II PNe do not self-contaminate allowing us to take the PNe gas abundances of these elements as reflections of those in the ISM from which the original progenitor stars formed. We know this because of the narrow mass range of the progenitor stars for type II PNe. Our knowledge of stellar evolution and nucleosynthesis and how they depend strongly on the initial mass of a star, allows us to roughly determine the degree of self-contamination and which elements are in danger of being modified. Knowing that by definition all stars undergo core nucleosynthesis we need merely to understand the possible means by which nucleosynthetic fuels and products can be mixed between the interior and surface. The opportunities available for stars to mix fusion products and alter surface abundances exist during episodes of convective "dredge up" and "hot-bottom burning." Given that the progenitor stars for type II PNe are thought to reasonably leave their O and Ne abundances unaltered and very safely leave S and Ar unmodified, the following section will just briefly discuss these rather complex processes.

4.6 Dredge-Up and Hot Bottom Burning

Dredge up, as its name implies, is the process of dredging material from the interior of the star and depositing it farther out toward the surface. This can occur in various stages of stellar evolution that give rise to convective regions that penetrate physical sites of nuclear processing.

The first dredge-up stage occurs at the base of the red giant branch (RGB) when the convective envelope reaches down into the core where H fusion has taken place. The products mixed into the envelope are the ashes of H burning, in other words He, C and N (via the CNO bi-cycle). The first dredge up enhances surface abundances of ^{4}He and ^{14}N but depletes surface ^{12}C. All PN progenitor stars ascend the RGB but the extent of contamination of He, C, and N in the envelope depends on the mass of the progenitor. The level of He and N enhancement is actually what divides the various Peimbert "types" of PNe (Peimbert, 1978) and thus dictates the mass of the progenitor star, its nucleosynthetic and kinematic history (Dutra & Maciel, 1990) again why we chose type II PNe.

The second dredge up occurs for stars in the early asymptotic giant branch phase of evolution. At this time the central core is exhausted of its hydrogen and helium and the core and surrounding shell region is mainly comprised of helium and its fusion products. The lower boundary of the convective envelope reaches rather deep into this region (from the surface to the innermost 20% of the stellar mass; Kippenhahn & Weigert 307) dredging up the products of CNO and triple-alpha burning thus enhancing the surface abundances of He and N.

A third dredge up phase occurs during the thermally pulsating stage of the late asymptotic giant branch (AGB). As a reminder, at the tip of the AGB the core is exhausted of its H and He and periodic ignition of the helium and hydrogen shell sources create thermal pulses that ultimately drive away the envelope of the star. At this time the convective envelope dips down into the helium burning shell, which consists primarily of He but contains a significant amount of C, and pulls up both He and C enhancing their

surface abundances. During the interpulse phase, while the hydrogen shell is burning, the base of the convective envelope can become hot enough for CNO reactions to occur. This is what is referred to as hot bottom burning. During this process the outer convective envelope picks up C and He from the helium shell then the hydrogen shell source converts ^{12}C into ^{14}N via the CN bi-cycle. This is yet another means of enhancing surface abundances of ^{4}He and ^{14}N and depleting surface ^{12}C. Hot bottom burning occurs in progenitor stars with initial masses greater than about 5 solar masses.

All of this said, it should be clear that the S, Ar, O, and Ne abundances of our program objects are not subject to self-contamination and thus reflect the abundances of the ISM approximately 4-6 billion years ago (Maciel & Koppen, 1994). The final section of this dissertation will address interpretations of the data, conclusions that can be drawn from this study, possible sources of scatter, and implications for future work.

Table 4.1

object	R_g (kpc)	N/H	O/H	Ne/H	S/H	Ar/H
		----------all values log (X/H) + 12----------				
th2-a	7.30[1]	8.43	8.87	8.29	6.79	6.48
pc 14	4.76	8.08	8.89	8.16	6.94	6.36
n6629	6.93	7.43	8.59	7.72	6.35	6.17
n6578	6.45	8.3	8.81	8.11	7.05	6.43
n6567	7.04[2]	7.92	8.46	7.59	6.4	5.82
n6565	7.01[3]	8.44	8.82	8.18	7.04	6.56
n6439	4.84	8.63	8.8	8.13	7.22	6.71
n6309	6.51	8.48	8.84	8.1	7.17	6.40
n5882	7.22	8.17	8.74	7.97	6.91	6.31
n5307	7.17	7.97	8.6	7.87	6.53	5.86
n3918	7.84[4]	8.29	8.76	7.98	6.69	6.41
n3242a	8.63	7.97	8.67	7.95	6.48	6.06
n3211	8.16	8.36	8.87	7.96	7.01	6.32
n3195	7.76	8.48	8.72	7.91	6.87	6.32
n2867	8.42	8.08	8.73	8.00	6.71	6.34
n2792	8.82	8.20	8.88	8.03	6.67	5.95
m3-6	9.54	8.05	8.87	8.10	7.08	6.40
m3-4	11.46	8.24	8.63	8.06	6.25	6.35
m3-15	6.62[5]	8.48	8.9	8.05	7.07	6.44
m1-57	5.75	8.59	8.80	8.1	7.03	6.55
m1-54	5.51	8.76	8.74	8.19	6.94	6.39
m1-50	4.84	7.97	8.68	8.02	6.82	6.26
m1-5	10.59	7.90	8.0	6.47	6.16	5.72
m1-34	5.02	8.65	8.69	8.1	7.08	6.59
m1-25	4.94	8.36	8.76	7.48	6.99	6.62
j320	12.36	8.09	8.37	7.55	6.30	5.77
ic2621	7.97	8.46	8.77	8.09	6.93	6.72
ic1297	5.71	8.39	8.87	8.15	7.1	6.53
he2-55	8.16	8.43	8.95	8.33	6.93	6.21
he2-48	8.87	8.09	8.62	7.92	6.41	6.3
he2-37	8.62	8.48	8.99	8.23	6.77	6.48
he2-21	10.60	7.64	8.48	7.63	6.39	5.87
he2-158	5.29	7.98	8.58	7.76	6.63	6.12
he2-141	6.40	8.49	8.88	8.10	6.83	6.42
fg1	7.98	8.27	8.6	7.89	6.72	6.24
cn2-1	4.92	8.23	8.88	8.11	6.81	6.25
solar[6]		7.97	8.87	8.08	7.33	6.52
orion[7]		7.78	8.72	7.89	7.17	6.49

[1] this and all other R_g values unless otherwise noted from Maciel 1984
[2] Daub 1982, Sabbadin 1986
[3] Maciel et al. 1986
[4] Gathier et al. 1986
[5] Amnuel et al. 1984
[6] Grevesse, Noels, & Sauval 1996
[7] Esteban et al. 1998

Table 4.2

object	R_g[8] (kpc)	O/H[9]	N/O	Ne/O	S/O	Ar/O
th2-a	7.30	8.87	.396	.286	9.1e-3	4.47e-3
pc 14	4.76	8.89	.167	.202	1.22e-2	3.17e-3
n6629	6.93	8.59	.069	.134	5.72e-3	3.77e-3
n6578	6.45	8.81	.31	.199	1.75e-2	4.17e-3
n6567	7.04	8.46	.293	.135	8.67e-3	2.32e-3
n6565	7.01	8.82	.469	.261	1.88e-2	6.21e-3
n6439	4.84	8.8	.768	.245	3.01e-2	9.31e-3
n6309	6.51	8.84	.48	.198	2.35e-2	4.03e-3
n5882	7.22	8.74	.286	.179	1.58e-2	3.97e-3
n5307	7.17	8.6	.259	.209	9.57e-3	2.02e-3
n3918	7.84	8.76	.379	.186	9.43e-3	5.01e-3
n3242a	8.63	8.67	.22	.213	7.19e-3	2.70e-3
n3211	8.16	8.87	.347	.137	1.53e-2	3.16e-3
n3195	7.76	8.72	.704	.189	1.73e-2	4.93e-3
n2867	8.42	8.73	.248	.21	1.07e-2	4.74e-3
n2792	8.82	8.88	.238	.158	6.91e-3	1.31e-3
m3-6	9.54	8.87	.15	.17	1.61e-2	3.41e-3
m3-4	11.46	8.63	.442	.289	4.54e-3	5.71e-3
m3-15	6.62	8.9	.402	.149	1.58e-2	3.71e-3
m1-57	5.75	8.80	.678	.217	1.86e-2	6.06e-3
m1-54	5.51	8.74	1.04	.282	1.57e-2	4.52e-3
m1-50	4.84	8.68	.218	.246	1.56e-2	4.28e-3
m1-5	10.59	8.0	.78	2.96e-2	1.44e-2	5.3e-3
m1-34	5.02	8.69	.918	.257	2.5e-2	8.1e-3
m1-25	4.94	8.76	.402	5.23e-2	1.71e-2	7.27e-3
j320	12.36	8.37	.546	.159	8.99e-3	2.63e-3
ic2621	7.97	8.77	.546	.232	1.62e-2	1.01e-2
ic1297	5.71	8.87	.385	.221	1.98e-2	5.3e-3
he2-55	8.16	8.95	.334	.264	1.06e-2	2.03e-3
he2-48	8.87	8.62	.323	.218	6.76e-3	5.24e-3
he2-37	8.62	8.99	.338	.187	6.53e-3	3.38e-3
he2-21	10.60	8.48	.16	.158	9.05e-3	2.73e-3
he2-158	5.29	8.58	.252	.151	1.14e-2	3.45e-3
he2-141	6.40	8.88	.451	.185	9.99e-3	3.83e-3
fg1	7.98	8.6	.51	.214	1.45e-2	4.81e-3
cn2-1	4.92	8.88	.237	.18	9.15e-3	2.51e-3
solar[10]		8.87	.13	.16	2.8e-2	4.47e-3
orion[11]		8.72	.11	.15	2.82e-2	5.89e-3

[8] references from table 4.1
[9] values are log (O/H) + 12
[10] Grevesse et al. 1996
[11] Esteban et al. 1998

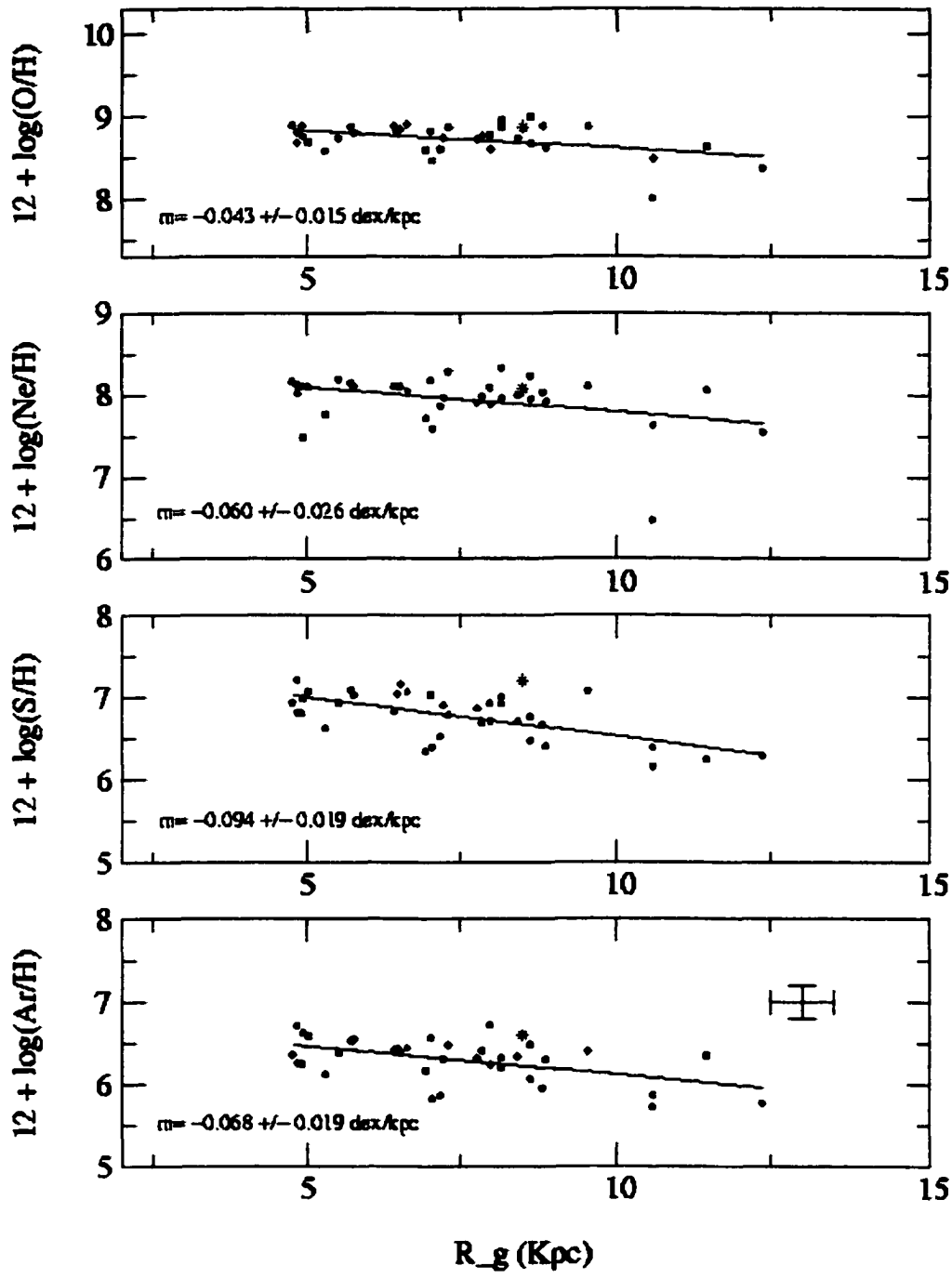

Figure 4.a - Log(X/H)+12 versus galactocentric distance R_g in kpc for oxygen, neon, sulfur, and argon. Data points are from the present sample of Galactic type II PNe. Solid lines are linear fits to the data with slopes shown for each fit. Star symbols represent Solar values for the abundances. Typical uncertainties for all data points are shown with error bars in the bottom plot.

Table 4.3

Gradients (dex/kpc)	log (O/H) + 12	log (Ne/H) + 12	log (S/H) + 12	log (Ar/H) + 12
Henry & Worthey[12]	-0.06 ± 0.01	...	...	...
Shaver et al.[13]	-0.05 ± 0.01	...	-0.01 ± 0.02	-0.06 ± 0.015
Afflerbach et al.[2]	-0.06 ± 0.01	...	-0.063 ± 0.006	...
Simpson et al.[2]	-0.06 ± 0.02	-0.08 ± 0.02	-0.07 ± 0.02	...
Present Study[14]	-0.043 ± 0.015	-0.06 ± 0.026	-0.094 ± 0.019	-0.068 ± 0.019
Smart & Rolleston[15]	-0.07 ± 0.01	...	...	...
Gummersbach et al.[4]	-0.07 ± 0.02	...	...	...
Fesen et al.[16]	-0.04 ± 0.03	...	...	...
Maciel & Koppen[3]	-0.069 ± 0.006	-0.056 ± 0.007	-0.067 ± 0.006	-0.051 ± 0.006

[12] Composite gradient from Shaver, Simpson, Afflerbach, Maciel, and Fesen
[13] H II regions
[14] Type II PNe
[15] B stars
[16] SNR

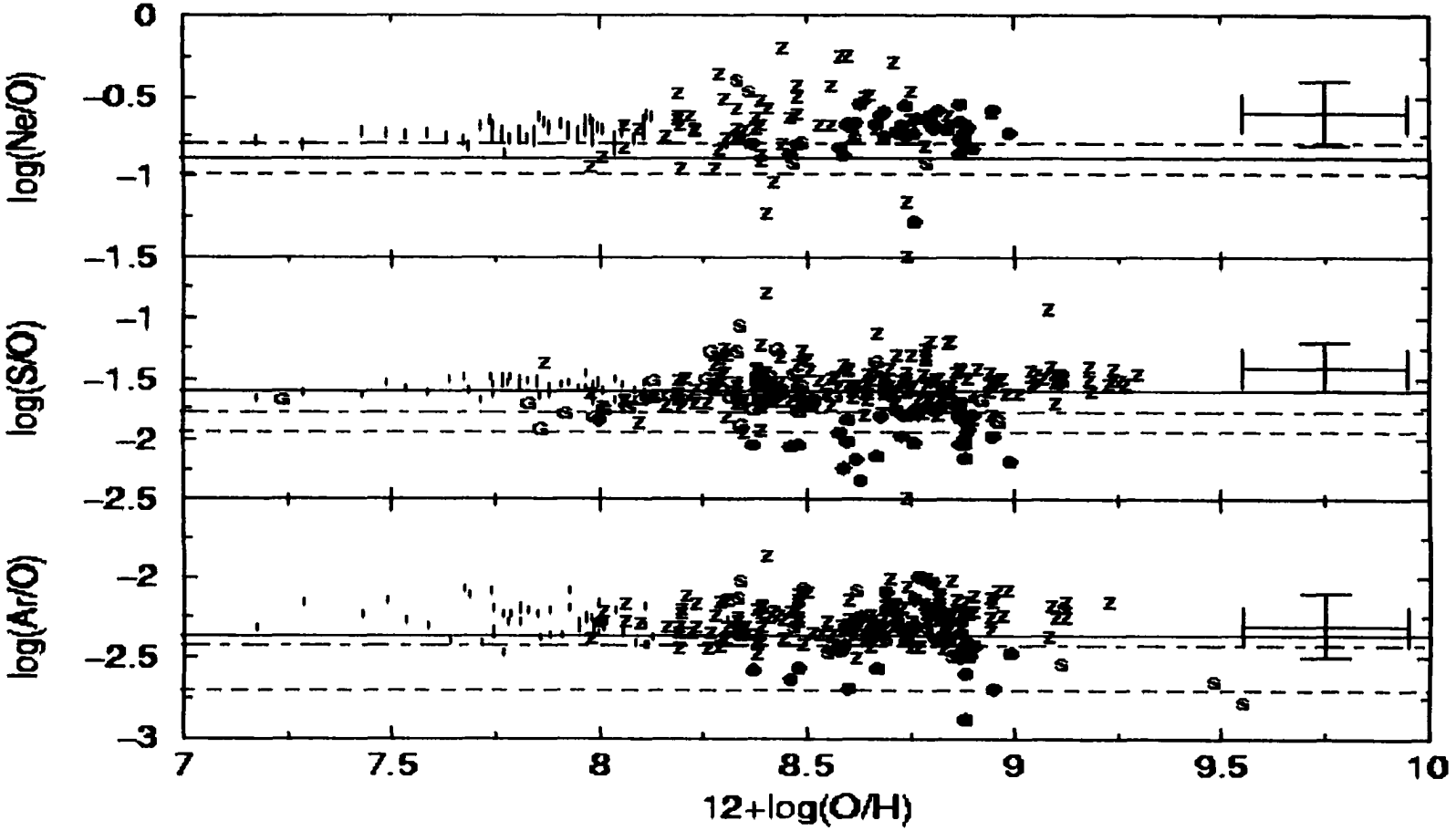

Figure 4.b - Log(X/O) versus log(O/H)+12 for neon, sulfur, and argon. Symbols for data points are as follows; "i", "Z", and "G" are extragalactic H II regions from Izotov & Thuan (1999), van Zee et al. (1998), and Garnett et al. (1995, 1997, 1999) respectively, "S" H II regions from Shaver et al. (1983), and solid dots are Galactic PNe from this study. The horizontal lines sow stellar yield predictions from Nomoto et al. (1997; dashed), Woosley & Weaver (1995; dot-dashed), and Samland (1998; solid) for massive star yields integrated over a Salpeter IMF and corrected to give ratios by number. Typical uncertainties are indicated with error bars.

Chapter 5

Conclusions and Future Work

Recapping the objectives of this dissertation work; we have acquired spectrophotometric observations of 48 southern hemisphere, type II planetary nebulae over an extended ground-based wavelength range of 3500 – 9600 Å. Oxygen, neon, sulfur, and argon abundances were determined for this statistically significant sample of PNe compiling a homogeneous set of chemical information used to construct radial abundance gradients and heavy element ratios. Sulfur abundances have been determined via the under-utilized near-IR lines of the S^{+2} ion at λ9069 and λ9532 Å, thus constituting a collective improvement over previous studies that depend mostly on [S II] lines and the weak [S III] line at λ6312 as the sole prophets of sulfur abundance. The radial abundance gradients and heavy element ratios constructed from our newly acquired observations are consistent with previous studies within the typical uncertainty of ± .2 dex in abundance. Finally the observed heavy element ratios of S/O, Ne/O, and Ar/O are reasonably consistent with predictions of theoretical yields of massive stars.

5.1 The Sulfur Gradient

The sulfur gradient produced by our type II PNe data has a strong slope with scatter that is typical of the uncertainty found in data of this nature, meaning the +/- .2 dex in abundance is due to a combination of errors propagating from observed line strengths to final abundances and intrinsic scatter in the abundances of these objects. To produce a valid gradient a statistically significant and unbiased sample must be observed and reliable distances must be known for each object. Ideally one would hope to do this

with a large homogenous (in physical traits) data set that has been consistently observed, reduced, and analyzed. Abundance gradients have been derived from PNe for decades and there is a large body of work that exists for the entire progenitor mass range of PNe (types I, II, III, and IV). The largest undertakings in this area of work consist of hundreds of PNe that are actually compilations of many separately observed data sets. Among these some simply compile abundances and some re-determine the abundances from gathered line strengths. Our comparatively small sample has the advantage of being physically homogeneous, in other words comprised of type II PNe only (with their narrow range in progenitor mass), and consistent observation, reduction, and analysis technique. It is important to point out that the goal of this work is not to necessarily improve on previously published individual abundances but to reduce any systematic effects that result from compiling a hybrid sample of abundances. Aside from the goal of compiling a homogenous set of abundances, the unique contribution that this work makes is its exploration of S abundances via the strongly representative near-IR lines. To be convinced that using the near-IR lines is a valid means to determine how much sulfur resides in these PNe, further work needs to be done with this data set. In the five-level atom code typically only one emission line is used to determine a particular ionic abundance. It doesn't really matter what that line is as long as it is accounted for in the relationship between the emissivity of that line and the number abundance of the ion that produces it. For S^{+2} the λ9532 Å line was chosen instead of λ9069 Å. In hindsight this may have been an unwise choice given the proximity of the λ9532 Å line to a significantly prominent Paschen feature. The Paschen ε line at λ9542 Å was typically about 1/5 the strength of the [S III] line at λ9532 Å. In extracting the line strengths in

IRAF's SPLOT task it was quite clear that the λ9532 line was being contaminated by another feature so most of the λ9532 line strengths are the result of deblending the two features. The extent to which this deblending created uncertainty in the line strength propagates to an uncertainty in the final S^{+2} abundance that is determined from it. Using the λ9069 line, which doesn't appear to be contaminated by any nearby features, could eliminate that possible source of scatter.

5.2 The Telluric Problem

At the time the observing proposal was written the principle investigators were heavily aware of the problems associated with ground-based observations in the near-IR. This was of course a concern given the location of the λ9069 and λ9532 Å [S III] lines in our spectra. Aside from the blanket attenuation that results from a signal passing through the Earth's atmosphere, strong absorption bands exist in the optical and near-IR regions (4000 – 10,000 Å) due primarily to rotational transitions of water vapor and diatomic oxygen. This absorption is referred to as telluric absorption, telluric meaning of or relating to the Earth as the molecular constituents causing the bands are in the Earth's atmosphere. Given that there was no a priori knowledge of a more appropriate means to remove telluric effects, it was decided that our sulfur emission lines would be corrected using our knowledge of their theoretical atomic ratio.

The λ9069 Å and λ9532 Å lines produced by the S^{+2} ion are due to separate radiative electronic transitions that originate from the same level. The S^{+2} ion is a p^2 system so the energy levels are spaced similarly to the O^{+2} and N^{+} ions (figure 3.a). The λ9069 Å line emits the energy difference between the $^1D_2$ and the $^3P_1$ levels, and the λ9532 Å line results from the $^1D_2$ -> $^3P_2$ transition. In the low matter and radiation

density regime that exists in PNe the ratio of the intensities of these two emission lines is set by the atomic parameters of the parent ion, in other words the ratio of the radiative transition rates. We used this knowledge to correct for any divergence from the theoretical ratio of the line strengths. I refer the reader to Stevenson 1994 for a diagram depicting the behavior of the telluric absorption bands in the region of the [S III] emission lines. The ratio of the Einstein A coefficients gives $I_{\lambda 9532}/I_{\lambda 9069} = 2.48$. If the ratio of the measured line strengths was found to be less than 2.48 the λ9532 line was corrected to achieve the theoretical ratio. If the ratio was greater than 2.48 then the λ9069 line was corrected. Of course this rough correction is only valid when one of the lines is being significantly absorbed compared to the other (Stevenson, 1994), it can not account for the instance of identical absorption at the two line positions, or nearly identical but significant absorption of both lines leaving them highly inconsistent with the rest of the spectrum that is not affected by the telluric bands. This could create distorted abundance ratios considering the hydrogen lines are used to create line strength ratios and number abundance ratios. The intensities of the S^{+2} lines should be considered lower limits to their true values. Distortion from telluric atmosphere effects is not solely a problem seen in astrophysical emission line spectra. Our blessing of an atmosphere can be a curse in many disciplines and considerable work has been done in characterizing the spectral behavior of atmospheric constituents in addition to the blanket attenuation that it generally causes. In the past removing telluric absorption from astrophysical emission line spectra has involved "dividing out" the absorption using a telluric calibration frame. These calibration frames are exposures of telluric reference stars – hot stars with essentially featureless spectra that clearly show the effects of absorption from the Earth's

atmosphere. There are new tasks in v2.11 IRAF, SKYTWEAK and TELLURIC, that exist for the express purpose of removing telluric atmospheric effects, again telluric reference frames are required. Our simple correction to the atomic ratio of the near-IR [S III] lines is sufficient given that there is not considerable absorption or saturation simultaneously in both bands. To carefully and correctly remove telluric effects the correct calibration frames need to be acquired with the observations. The telluric bands that create most of the absorption in the near-IR region are due to water vapor and molecular oxygen, considering the scale height for water vapor is approximately 3 km (Stevenson, 1994) using an observing site at a high altitude would most certainly provide improved conditions for ground based near-IR observations of this nature. Given the relative strength of the telluric absorption features to the [S III] emission lines, it is unlikely that the telluric bands are the sole cause of the systematically low sulfur abundances obtained in this study.

Our exploration into the somewhat novel use of the near-IR [S III] lines as improved prophets of sulfur abundance will not be complete until a judicious comparison is made between results derived from the λ9069, λ9532, and λ6312 Å lines.

5.3 Diffusion of Stellar Orbits

In a study of this nature knowing the galactocentric distances of a PN is tantamount to determining its abundance. Uncertain distances can affect the value of an abundance gradient just as surely as uncertainties in abundance. Utilizing our type II PNe as tracers of the metallicity in their natal ISM, particularly for use in abundance gradients, involves the assumption that the observed PNe have maintained the same radial location since the birth of their respective progenitor stars. So accurate distances

are needed for these objects in addition to a reliable idea of their kinematic history. Given the relatively long lifetimes for the progenitor stars of PNe, it should be noted that the low mass end of PN progenitors have most likely undergone some level of migration from their birthplaces. For a more thorough discussion of the diffusion of stellar orbits I refer the reader to Wielen, Fuchs, & Dettbarn, 1996. In, short given the kinematic history of our PN progenitor stars and the dependence of stellar perturbations on the physical characteristics of the disk, the diffusion of stellar orbits does not significantly affect radial abundance gradients (Wielen et al., 1996). It is important to note however that Wielen et al. do find the dispersion in metallicity at a given galactocentric distance rapidly increases with increasing age, hence longer kinematic history, of the progenitor star. This would increase the scatter about a given determined gradient but diffusion of stellar orbits alone should not affect the value of the gradient (Wielen et al., 1996).

5.4 Heavy Element Ratios

We note the expected independence of our heavy element ratios (X/O) with oxygen abundance. This behavior is required if neon, sulfur, and argon are produced by the same mass range of stars responsible for the production of oxygen, or if these elements are produced in the same ratios by a temporally and spatially invariant IMF. Plotting heavy element ratios in this form against O/H also reveals whether there is a metallicity dependence on the production of these elements or for example if oxygen is being altered by CNO bi-cycles or uncertainty in fusion reaction rates which would have an affect. Again it is noted that in figure 4.c the theoretically predicted yields are for type II SNe products only; no synthesis from Ia SNe was included in these models. Given the

possibly significant contribution that Ia make to S and Ar abundances as indicated in the W7 models of Nomoto et al. (1997), it would be interesting to test how their inclusion affects the model yields. Of course we took great interest in the systematically low S/O values for our type II PNe data. Given that these ratios of Ne/O, S/O, and Ar/O reflect nucleosynthesis and expulsion processes in massive stars, there is no physical reason to expect this disparity in S/O between H II regions and PN. Of course this leads us to consider the uncommon thread that runs throughout our data set. The use of the near-IR lines of [S III] in our abundance calculations is the unique characteristic of our PNe sample. Given the impetus for this project and our primary goal of improving collective sulfur abundances from type II PN, it will be necessary to investigate the dependence of our S/O ratios not only on the [S III] emission lines used as input but also on any possible systematic effects visible in our oxygen abundances.

5.5 Final Comments and Future Work

This particularly valuable data set is far from being exhausted of available information and a number of items remain to be examined. Of the 48 objects that were observed only 36 of them remained after abundance determinations. Each of the 12 objects that are missing from the final analysis was left out primarily due to "missing" emission lines that would allow for temperature, density, or level population calculations. With painfully gained hindsight I am most certain that each of these objects will be regained with a more judicious approach to the measurements performed in SPLOT.

The always interesting sulfur deserves further investigation. For pragmatic reasons it would be quite valuable to be able to gain solid sulfur abundances from ground based observations of either H II regions or PNe. Again in hindsight appropriate telluric

reference frames would have been useful in the removal of the attenuating sky effects in the near-IR. It really should be noted that at the time of the observing run we did not know a priori of the existence of the IRAF TELLURIC package and even with its existence it is not certain that simple division of a telluric reference frame would be appropriate in the removal of effects from such narrow emission line objects such as our low mass progenitor PNe (Stevenson 1994). It is not certain however that even the maximum attenuation afforded by the telluric bands would create the systematically low S/O values that we see in our sample. As was stated before, the final word on sulfur will not be clear until we investigate the dependence of our sulfur abundances on the [S III] emission lines used as input and make internal comparisons between abundances found via the λλ 9532, 9069, and λ 6312 lines.

In closing, this field has undergone decades of investigation and I stand upon the shoulders of giants in confirming that PNe are indeed valuable as representatives of metallicity in spiral galaxies as well as other morphologies. In this specific case our type II PNe have proven themselves useful as tracers of disk metallicity in the Milky Way. To this end they are complimentary to H II regions in producing abundance gradients that are consistent with other studies using gaseous nebulae and B stars. Finally, the rather wide range in progenitor mass for planetaries allows us the opportunity to observationally constrain not only the chemical history previous to the formation of PN progenitor stars, but also the nucleosynthetic and evolutionary processes that occur in this mass range of stars. This study concentrated on just a few specific elements that are primarily synthesized in massive stars but PNe are also useful in exposing the nucleosynthesis and evolution that take place in intermediate mass stars. In this role they

can be strong purveyors of He, N, and C, as abundances of these elements are readily contaminated during the lifetime of progenitor stars in the intermediate mass range.

One final note concerning future work extending from this data set; considerable forethought went into finding an overlap with our sample of PNe and observations that were previously made with the IUE satellite. This was done for the express purpose of compiling carbon abundances for these objects. With no strong representative carbon lines in the optical portion of the spectrum, the consistently re-reduced and compiled IUE Final Archive not only provides extended UV spectral coverage of our sample of type II PNe, but also allows us to keep the homogeneity of our data set intact.

Bibliography

Afflerbach, A., Churchwell, E., Werner, M.W. 1997, ApJ, 478, 190

Amnuel, P.R., Guseinov, O.H., Novruzova, H.I., Rustamov, Y.S. 1984, A&SS, 107, 19

Baluja, K.L. & Zeippen, C.J. 1988, J. Phys. B, 21, 1455

Burke, V.M., Lennon, D.J., & Seaton, M.J. 1989, MNRAS, 236, 353

Butler, K. & Zeippen, C.J. 1994, A&AS, 108, 1

Clegg, R.E.S. 1987, MNRAS, 229, 31

Daub, C.T. 1982, ApJ, 260, 612

Dutra, C.M., Maciel, W.J. 1990, Rev. Mex. Astron. Astrofis. 21, 264

Esteban, C., Peimbert, M., Torres-Peimbert, S., & Escalante, V. 1998, MNRAS, 295, 401

Ferland, G.J. 1990, Ohio State University, Rep. 90-02

Fesen, R.A., Blair, W.P., & Kirshner, R.P. 1985, ApJ, 292, 29

Galavís, M.E., Mendoza, C., Zeippen, C.J. 1995, A&AS, 111, 347

Garnett, D.R., Shields, G.A., Peimbert, M., Torres-Peimbert, S., Skillman, E.D., Dufour, R.J., Terlevich, E., Terlevich, R.J. 1999, ApJ, 513, 168

Garnett, D.R., Skillman, E.D., Dufour, R.J., Peimbert, M., Torres-Peimbert, S., Terlevich, E., Terlevich, R.J., Shields, G.A. 1995, ApJ, 443, 64

Garnett, D.R., Skillman, E.D., Dufour, R.J., Shields, G.A. 1997, ApJ, 481, 174

Gathier, R., Pottasch, S.R., Pel, J.W. 1986b, A&A, 157, 171

Grevesse, N., Anders, E. 1989, in Waddington C.J., ed., AIP Conf. Proc. 183, *Cosmic Abundances of Matter*, Am. Inst. Phys., New York, 1

Grevesse, N., Noels, A., & Sauval, A.J. 1996, in *Cosmic Abundances*, ASP Conf. Ser. 99, S.S. Holt & G. Sonneborn, eds, ASP, p.117

Gummersbach, C.A., Kaufer, A., Schäfer, D.R., Szeifert, T., & Wolf, B. 1998, A&A, 338, 881

Henry, R.B.C., Kwitter, K.B., & Dufour, R.J. 1999, ApJ, 517, 782

Henry, R.B.C., Kwitter, K.B., & Howard, J.W. 1996, ApJ, 458, 215

Henry, R.B.C., Worthey, G. 1999, PASP, 111, 919

Izotov, Y.I., Thuan, T.X. 1999, ApJ, 511, 639

Kingsburgh, R.L., Barlow, M.J. 1994, MNRAS, 271, 257

Kippenhahn, R., Weigert, A. 1990, *Stellar Structure and Evolution*, Springer-Verlag, Germany

Lennon, D.J. & Burke, V.M. 1994, A&AS, 103, 273

Maciel, W.J. 1984, A&AS, 55, 253

Maciel, W.J. 1989, IAU Symp. 131, ed. S. Torres-Peimbert, Kluwer

Maciel, W.J. 1992, *Elements and the Cosmos*, ed. M.G. Edmunds, R.J. Terlevich, Cambridge U. Press, 210

Maciel, W.J., Faúndez-Abans, M., Oliveira, M. 1986, Rev. Mex. Astron. Astrofis., 12, 233

Maciel, W.J., Koppen, J. 1994, A&A, 282, 436

McLaughlin, B.M. & Bell, K.L. 1993, ApJ, 408, 753

Mendoza, C. 1983, in IAU Symp. 103, *Planetary Nebulae*, ed. D.R. Flower, Dordrecht: Reidel, 143

Mendoza, C. & Zeippen, C.J. 1983, MNRAS, 202, 981

Nomoto, K., Iwamoto, K., Nakasato, N., Thielemann F.-K., Brachwitz, F., Tsujimoto, T., Kubo, Y., Kishimoto, N. 1997, Nucl. Phys. A, 621, 467c

Osterbrock, D.E. 1989, *Astrophysics of Gaseous Nebulae and Active Galactic Nuclei*, University Science Books, Mill Valley, CA

Pagel, B.E.J. 1997, *Nucleosynthesis and Chemical Evolution of Galaxies*, Cambridge University Press, Cambridge, UK

Peimbert, M. 1978, IAU Symp. 76, ed. Y. Terzian, Reidel

Péquignot, D., Petitjean, P., Boisson, C. 1991, A&A, 251, 680

Ramsbottom, C.A., Bell, K.L., Stafford, R.P. 1996, Atom Dat Nuc Dat Tab, 63, 57
Sabbadin, F. 1986, A&AS, 64, 579

Samland, M. 1998, ApJ, 496, 155

Shaver, P.A., McGee, R.X., Newton, L.M., Danks, A.C., Pottasch, S.R. 1983, MNRAS, 204, 53

Simpson, J.P., Colgan, S.W.J., Rubin, R.H., Erickson, E.F., Haas, M.R. 1995, ApJ, 444, 721

Smart, S.J. & Rolleston, W.R.J. 1997, ApJ, 481, L47

Stevenson, C.C. 1994, MNRAS, 267, 904

Storey, P.J. & Hummer 1995, MNRAS, 272, 41

Torres-Peimbert, S. Peimbert, M. 1977, Rev. Mex. Astron. Astrofis., 2, 181

van Zee, L., Salzer, J.J., Haynes, M.P., O'Donoghue, A.A., Balonek, T.J. 1998, AJ, 116, 2805
Wielen, R., Fuchs, B., Dettbarn, C. 1996, A&A, 314, 438

Weise, W.L., Fuhr, J.R., Deters, R. 1996, J. Chem. Phys. Ref. Data, Monograph #7

Woosley, S.E., Weaver, T.A. 1995, ApJS, 101, 181

Appendix A:

Error Analysis

The error in final abundances X/H calculated from collisionally excited lines was approximated from a method of propagating the uncertainty in measured line strengths through the equations relating $I_\lambda/I_{H\beta}$ to relative number abundance (Henry, Kwitter, & Dufour 1999). Beginning with our symbolic equation for determining final total element number abundance (relative to H) $N(x) = \sum_i N(x^i) \cdot icf(x) \cdot mcf(x)$ the fractional error in total element abundance can be written as:

$$\frac{\delta_X}{N(X)} = \sqrt{\left(\frac{\delta_{ion}}{\sum_i N(X^i)}\right)^2 + \left(\frac{\delta_{icf}}{icf(X)}\right)^2 + \left(\frac{\delta_{mcf}}{mcf(X)}\right)^2}$$

The contribution from ionization correction factors is estimated at ~10% (Henry, private communication). Any uncertainty associated with the applied model correction factors was not included here but it is not likely to be larger than the error in the ionization correction factors.

Keeping in mind that the first factor in the above sum is $\sum_i N(X^i) = N(X^0) + N(X^1) + N(X^2) + N(X^3) + \ldots$, to formally determine δ_{ion} the uncertainty in each ionic abundance must be determined and added in quadrature. For the collisionally excited lines that are being addressed in this study each contribution to the above sum is related to the measured emission line strengths via:

$$\frac{N(X^i)}{N(H^+)} = \frac{I_\lambda N_e \alpha_{H\beta}^{eff} E_{H\beta}}{I_{H\beta} \chi_{ul}^i A_\lambda E_\lambda}$$

Uncertainty associated with the atomic data is not included in our final estimate of abundance error. This includes the recombination coefficients α_{λ}^{eff}, transition rates A_{λ}, the transition energies E_{λ}, and χ_{ul}^{i} values which depend on T_e, N_e, all collisoinal excitation/de-excitation rates, and radiative de-excitation rates. The electron temperature and density are calculated using ratios of emission line strengths from the [O III], [N II], and [S II] ions. The error associated with these quantities, T_e and N_e, can be propagated from the uncertainty in measured line strength ratios via their relationships in the ABUN subroutines TEMPO3, TEMPN2, and ELECD. Considering the well recognized problems associated with the different temperature dependence of recombination and forbidden lines, the contribution of temperature uncertainty to the error in final abundance should be investigated more carefully in future work.

The measured quantities from which the final error in X/H abundance is propagated are the $I_{\lambda}/I_{H\beta}$ values. This reduced quantity comes from:

$$\frac{I_{\lambda}}{I_{H\beta}} = \frac{F_{\lambda}}{F_{H\beta}} \cdot 10^{cf_{\lambda}} \cdot m$$

where $F_{\lambda}/F_{H\beta}$ is the raw flux ratio measured in SPLOT (IRAF), $10^{cf}{}_{\lambda}$ is the wavelength dependent de-reddening factor, and *m* is a constant merging factor that was applied to the emission lines from 3600 - 6700 Å (a unique *m* for each object). The uncertainty in measured line strengths was not formally approached in this study. Adopted uncertainties for optical line strengths are ± 10% for emission lines stronger than Hβ, ± 20% for those weaker than Hβ, and due to telluric absorption the near-IR lines are uncertain by ±50% (Henry, Kwitter, Dufour 1999).

Appendix B:

Level Balancing

ABUN uses a five-level atom approximation to determine the level populations χ_{ul}^{i} of all relevant ions which are then used in turn to calculate ionic number abundances $N(X^i)$. Shown below is an example of level balancing using a simpler three-level atom. The transitions between levels that contribute here and in ABUN are collisional excitations/de-excitations and radiative de-excitations. This is physically reasonable given the range in electron temperature and density in which PN gas exists. In the equations below the following quantities are represented:

N_e = electron number density (cm^{-3})
N_i = number density of contributing ion with level i populated (cm^{-3})
q_{ij} = collisional excitation rate (cm^3/sec) which depends on collision strength Ω
q_{ji} = collisional de-excitation rate (cm^3/sec), also a function of Ω
A_{ji} = radiative de-excitation rate (sec^{-1})

Transitions into each level are balanced with transitions out of that same level.

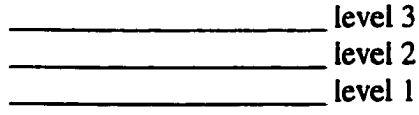

Level 1: $N_1N_eq_{12} + N_1N_eq_{13} = N_3N_eq_{31} + N_3A_{31} + N_2N_eq_{21} + N_2A_{21}$
Level 2: $N_2N_eq_{23} + N_2N_eq_{21} + N_2A_{21} = N_1N_eq_{12} + N_3N_eq_{32} + N_3A_{32}$
Level 3: $N_3N_eq_{32} + N_3N_eq_{31} + N_3A_{32} + N_3A_{31} = N_1N_eq_{13} + N_2N_eq_{23}$

These equations are solved for the N_1, N_2, and N_3 values. Using the constraint $N_1+N_2+N_3=N(X^{i'})$ where $N(X^{i'})$ is the total number density of ion $X^{i'}$ (here i' identifies the ionization stage being considered) the χ_{ul}^{i} values can be determined for each ion:

$$\chi_{ul}^{i'} = {}^{N_i}\!/_{N(X^{i'})} \text{ here } N_i = N(\chi_{ul}^{i'})$$

Appendix C:

ABUN Listing

```
C********THIS PROGRAM CONVERTS LINE STRENGTHS INTO ION ABUNDANCES
C********THE IONS CURRENTLY IN THE PROGRAM ARE:
C********N II, NIII, O II, O III, NE III, NE IV, NE V, C III, C IV,
C******** S II, SIII,& AR III.
      IMPLICIT REAL*8 (A-H,O-Z)
      REAL*8 ICFO,ICFN2,ICFNE3,ICFS23,ICFAR
      DIMENSION CSN2(10),EAN2(10),SWN2(5),ENN2(10)
      DIMENSION CSN3(10),EAN3(10),SWN3(5),ENN3(10)
      DIMENSION CSO2(10),EAO2(10),SWO2(5),ENO2(10)
      DIMENSION CSO3(10),EAO3(10),SWO3(5),ENO3(10)
      DIMENSION CSNE3(10),EANE3(10),SWNE3(5),ENNE3(10)
      DIMENSION CSNE4(10),EANE4(10),SWNE4(5),ENNE4(10)
      DIMENSION CSNE5(10),EANE5(10),SWNE5(5),ENNE5(10)
      DIMENSION CSC3(10),EAC3(10),SWC3(5),ENC3(10)
      DIMENSION CSC4(2),EAC4(2),SWC4(3),ENC4(2)
      DIMENSION CSS2(10),EAS2(10),SWS2(5),ENS2(10)
      DIMENSION CSS3(10),EAS3(10),SWS3(5),ENS3(10)
      DIMENSION CSAR3(10),EAAR3(10),SWAR3(5),ENAR3(10)
C***ATOMIC DATA*****************************************************
C***N II ATOMIC DATA
c***cs from lennon & burke, a&as,103,273 (1994) @ 10,000K: changed
6/5/97
      DATA CSN2/.41,.27,.29,.033,1.12,.88,.098,1.47,.16,.83/
c***ea from NIST #7, JCPRD (1996) 6/18/97
      DATA EAN2/2.07E-6,9.69E-13,5.45E-7,0.,7.40E-6,9.19E-4,3.15E-2,
     1   2.72E-3,1.40E-4,1.17/
      DATA ENN2/9.68E-15,2.6E-14,3.04E-12,6.5E-12,1.63E-14,3.03E-12,
     1   6.49E-12,3.02E-12,6.47E-12,3.45E-12/
      DATA SWN2/1.,3.,5.,5.,1./
C***N III ATOMIC DATA
c***cs fro blum & pradhan apjs, 80, 425, (1992), for 10,000K, changed
on 6/5/97
      DATA CSN3/1.45,.20,.30,.20,.15,.40,.84,1.1,.67,2.04/
c*** ea data from brage, froese, & judge, apj, 445, 457 (1995): changed
6/5/97
c*** 2-1 from NIST #7 JCPRD (1996)
      DATA EAN3/4.79e-5,361.,9.11,0.,372.,65.1,282.,0.,0.,0./
      DATA ENN3/3.47E-14,1.14E-11,1.14E-11,1.14E-11,1.13E-11,1.13E-11,
     1          1.14E-11,1.19E-14,2.8E-14,1.61E-14 /
      DATA SWN3/2.,4.,2.,4.,6./
C***O II ATOMIC DATA
c*** cs & ea updated 6/5/97; consistent w. clouody v90.
c***cs from mclaughlin & bell, apj,408,753 (1993) (2-3 and 4-5 from
mendoza83):
6/5/97
      DATA CSO2/.83,.55,.28,.14,1.17,.83,.41,.55,.27,.28/
c***ea from NIST #7 JCPRD (1996) updated 6/5/97
      DATA EAO2/3.06e-5,1.78e-4,5.22e-2,2.12e-2,1.3e-7,.0991,
     1 5.19e-2,5.34e-2,8.67e-2,1.41e-10/
```

```
      DATA ENO2/5.33E-12,5.33E-12,8.04E-12,8.04E-12,3.88E-15,
     1   2.71E-12,2.71E-12,2.71E-12,2.71E-12,2.19E-16/
      DATA SWO2/4.,6.,4.,4.,2./
C***O III ATOMIC DATA
c***cs and ea updated/checked 6/5/97; consistent w. cloudy v90.
c***cs from lennon & burke, a&as,103,273 (1994) @ 10,000K: 6/5/97
c***except 4-5, which is from burke, lennon,seaton, mn,236,353 (1989).
      DATA CSO3/.55,.27,.25,.033,1.29,.76,.098,1.27,.16,.68/
c***ea from NIST #7 JCPRD (1996) 6/18/97
      DATA EAO3/2.62E-5,3.17E-11,2.41E-6,0.,9.76E-5,6.21E-3,.215,.0181,
     1   6.34E-4,1.71/
      DATA ENO3/2.25E-14,6.09E-14,4.03E-12,8.58E-12,3.84E-14,4.01E-12,
     1   8.56E-12,3.97E-12,8.52E-12,4.55E-12/
      DATA SWO3/1.,3.,5.,5.,1/
C***NE III ATOMIC DATA
c***cs from butler & zeippen, a&as,108,1 (1994): changed 6/5/97
      DATA CSNE3/.77,.21,.75,.084,.24,.45,.05,.15,.017,.27/
c***ea from baluja & zeippen, j.phys.B.,21,1455 (1988); changed 6/16/97
      DATA EANE3/6.01e-3,2.1e-8,.16,3.76e-3,1.16e-3,4.95e-2,2.05,
     1 9.76e-6,0.,2.68/
      DATA ENNE3/1.28E-13,1.83E-13,5.14E-12,1.11E-11,5.52E-14,5.01E-12,
     1   1.1E-11,4.95E-12,1.09E-11,5.95E-12/
      DATA SWNE3/5.,3.,1.,5.,1./
C***NE IV ATOMIC DATA
c***cs and ea from Mendoza83 @10000K
      DATA CSNE4/.838,.559,.156,.313,1.36,.368,.9,.336,.509,.343/
      DATA EANE4/4.84E-4,5.54E-3,.521,1.27,1.48E-6,.115,.4,
     1           .393,.437,2.68E-9/
      DATA ENNE4/8.2E-12,8.21E-12,1.24E-11,1.24E-11,8.93E-15,4.21E-12,
     1           4.22E-12,4.21E-12,4.21E-12,1.33E-15/
      DATA SWNE4/4.,6.,4.,2.,4./
C***NE V ATOMIC DATA
c***cs and ea from Mendoza83 @10000K
      DATA CSNE5/.244,.122,.198,.026,.578,.593,.083,.989,.138,.518/
      DATA EANE5/1.28E-3,5.08E-9,2.37E-5,0.,4.59E-3,.131,4.21,
     1           .365,6.69E-3,2.85/
      DATA ENNE5/8.2E-14,2.21E-13,6.02E-12,6.02E-12,1.39E-13,5.94E-12,
     1           1.26E-11,5.8E-12,1.25E-11,6.68E-12/
      DATA SWNE5/1.,3.,5.,5.,1./
C***C III ATOMIC DATA
c***cs from Berrington et al, AtDat&NucDat Tabs.,33,195; checked
6/16/97
      DATA CSC3/.12,.35,.58,4.,.962,.718,.41,2.78,1.23,2.06/
c***ea from nussbaumer & storey 1978, aa,64,139, except 1909 value of
121.,
c***which comes from kwong et al., apj,411,431 (1993); updated 6/16/97
      DATA EAC3/0.,121.,5.19E-3,1.79E9,2.39E-7,0.,1.45E-3,2.41E-6,
     1   1.09E-3,1.81E-3/
      DATA ENC3/1.04E-11,1.04E-11,1.04E-11,2.03E-11,4.71E-15,1.59E-14,
     1   9.94E-12,1.12E-14,9.93E-12,9.92E-12/
      DATA SWC3/1.,1.,3.,5.,3./
C***C IV ATOMIC DATA
c***cs and ea (@10000 K) from Mendoza83. rechecked 6/17/97
      DATA CSC4/2.96,5.92/
      DATA EAC4/2.63E8,2.65E8/
      DATA ENC4/1.28E-11,1.28E-11/
      DATA SWC4/2.,2.,4./
```

```
C***S II ATOMIC DATA
c***cs from ramsbottom, bell, & stafford, ADNDT,63,57 (1996) updated
6/16/97
      DATA CSS2/2.76,4.14,1.17,2.35,7.47,1.79,3.,2.2,4.99,2.71/
c***ea from mendoza83; rechecked 6/16/97
      DATA EAS2/8.82E-4,2.60E-4,9.06E-2,2.25E-1,3.35E-7,.163,.133,
     1   .0779,.179,1.03E-6/
      DATA ENS2/2.95E-12,2.96E-12,4.87E-12,4.88E-12,6.26E-15,1.92E-12,
     1   1.93E-12,1.92E-12,1.93E-12,9.66E-15/
      DATA SWS2/4.,4.,6.,2.,4./
C***S III ATOMIC DATA
c***cs from galvavis et al., a&as,111,347 (1995); revised 6/17/97
      DATA CSS3/2.33,1.11,.88,.12,5.41,2.65,.37,4.42,.62,1.3/
c***ea fro mendoza83; leave unchanged, 6/17/97
      DATA EAS3/4.72E-4,4.61E-8,5.82E-6,0.,2.07E-3,2.21E-2,.796,
     1          5.76E-2,1.05E-2,2.22/
      DATA ENS3/5.9E-14,1.65E-13,2.25E-12,5.4E-12,1.06E-13,2.19E-12,
     1          5.34E-12,2.08E-12,5.23E-12,3.15E-12/
      DATA SWS3/1.,3.,5.,5.,1./
C***Ar III ATOMIC DATA
c***cs from galvavis et al. a&as,111,347 (1995); revised 6/17/97
      DATA CSAR3/3.087,.67,2.68,.47,1.26,1.61,.28,.54,.093,1.22/
C***ea from Mendoza & Zeippen, MN, 202, 981 (1983). rechecked 6/17/97
      DATA EAAR3/3.08e-2,2.37e-6,.314,.0417,5.17e-3,.0823,3.91,
     1          2.21e-5,0.,2.59/
      DATA ENAR3/2.21e-13,3.12e-13,2.78e-12,6.61e-12,9.1e-14,2.56e-12,
     1          6.39e-12,2.47e-12,6.3e-12,3.82e-12/
      DATA SWAR3/5.,3.,1.,5.,1./
c*************OLD ATOMIC DATA************************
c***cs from Mendoza83 @10000K
c     DATA CSN2/.401,.279,.30,.04,1.13,.89,.13,1.49,.22,.41/
c***cs from Mendoza83 @4000K
c     DATA CSN3/.701,.0952,.139,.08,.0616,.175,.39,.695,.397,1.26/
c***ea from mendoza83 @4000K
c     DATA EAN3/4.77E-5,339.,8.95,0.,364.,59.,251.,0.,0.,0./
c***cs from Mendoza83 @10000K;
c     DATA CSO2/.80,.53,.27,.135,1.20,.73,.29,.41,.28,.29/
c*** ea from zeippen aa 173, 410 (1987)
c     DATA EAO2/3.33E-5,1.68E-4,5.45E-2,2.30E-2,1.30E-7,1.07E-1,
c    1   5.63E-2,5.73E-2,9.36E-2,1.45E-10/
c***cs from Mendoza83 @10000K
c     DATA CSO3/.54,.27,.24,.035,1.29,.72,.10,1.21,.17,.62/
c***cs from Butler and Mendoza,MN,208,17p (1984) @1000K; ea from
Mendoza83
c     DATA CSNE3/1.132,.307,.917,.094,.349,.55,.056,.183,.019,.226/
c     DATA EANE3/5.97E-3,2.18E-8,.17,3.94E-3,1.15E-3,5.42E-2,2.,
c    1   8.51E-6,0.,2.71/
c***cs from Mendoza83 @10000K
c     DATA CSS2/2.79,4.19,.759,1.52,7.59,1.52,3.38,2.56,4.79,2.38/
c***cs from Mendoza83 @10000K
c     DATA CSS3/2.59,1.15,.93,0.,5.81,2.80,.45,4.66,.74,1.88/
c***cs from mendoza & zeippen
C     DATA CSAR3/2.24,.531,2.63,.38,1.18,1.58,.23,.53,0.,.823/
C***cs from Johnson & Kingston, J.Phys.B, 23, 3393 (1990) @ 10000K.
c     DATA CSAR3/3.368,.715,2.93,.451,1.408,1.756,.27,.585,.09,1.159/
C*************************************************************
      PLANCK=6.626E-27
```

```
      C=3.0E10
      TO3=0.
      ED=0.
C***SETS SOLAR ABUNDANCES (GREVESSE & ANDERS 1989, WITH EXTENSIONS BY
C*** GREVESSE & NOELS 1993)  THESE WERE UPDATED 6/27/97 TO BE
CONSISTENT
C*** WITH CLOUDY
      SUNHE=0.1
      SUNC=3.55E-4
      SUNN=9.33E-5
      SUNO=7.41E-4
      SUNNE=1.17E-4
      SUNS=1.62E-5
      SUNAR=3.98E-6
C
C***READS IN EMISSION LINE STRENGTHS
      PRINT*, ' ENTER HE I 5876/HBETA AND HE II 4686/HBETA'
      READ(5,*) R5876,R4686
      PRINT*, 'ENTER C III] 1909/HB, C II 4267, AND CIV 1549/HB'
      READ(5,*) R1909,R4267,R1549
      PRINT*, 'ENTER [N II] 6584/HB AND 5755/HBETA'
      READ(5,*) R6584,R5755
      PRINT*, 'ENTER N III] 1751/HB, N IV] 1485/HB, AND N V 1240/HB'
      READ(5,*) R1751,R1485,R1240
 1010 PRINT*, 'ENTER [O II] 3727/HB, 7325/HB, [O III] 5007/HB
     1AND 4363/HBETA; IF 4363 IS UNOBSERVED, ENTER ZERO AND YOU
     1WILL BE ASKED FOR TO3.'
      READ(5,*) R3727,R7325,R5007,R4363
      IF (R4363.EQ.0.) THEN
         GO TO 1005
      ELSE
         GO TO 1006
      ENDIF
 1005 PRINT*, 'ENTER ELECTRON TEMPERATURE'
      READ(5,*) TO3
 1006 CONTINUE
      PRINT*, 'ENTER [NE III] 3869/HB, [NE IV] 1602/HB,
     1          AND [NE V] 1575/HB'
      READ(5,*) R3869,R1602,R1575
 2000 PRINT*, 'ENTER [S II] 6716/HB, 6731/HB, 6724/HB, AND 4071/HB.
     1 IF THE FIRST TWO ARE UNRESOLVED, ENTER ZEROS;
     1 YOU WILL BE ASKED FOR DENSITY DIRECTLY'
      READ(5,*) R6716,R6731,R6724,R4071
      IF (R6716.EQ.0..OR.R6731.EQ.0.) THEN
         GO TO 1000
      ELSE
         GO TO 1001
      ENDIF
 1000 PRINT*, 'ENTER ELECTRON DENSITY'
      READ(5,*) ED
 1001 CONTINUE
      PRINT*, 'ENTER [S III] 6312, 9532'
      READ(5,*)R6312,R9532
      PRINT*, 'ENTER [Ar III] 7135'
      READ(5,*)R7135
C
C***CONVERTS WAVELENGTHS TO ERGS
```

```
      E4861=PLANCK*C/4861.E-8
      E5876=PLANCK*C/5876.E-8
      E4686=PLANCK*C/4686.E-8
      E6584=PLANCK*C/6584.E-8
      E5755=PLANCK*C/5755.E-8
      E3727=PLANCK*C/3727.E-8
      E5007=PLANCK*C/5007.E-8
      E4363=PLANCK*C/4363.E-8
      E3869=PLANCK*C/3869.E-8
      E1909=PLANCK*C/1909.E-8
      E6716=PLANCK*C/6716.E-8
      E6731=PLANCK*C/6731.E-8
      E6724=PLANCK*C/6724.E-8
      E6312=PLANCK*C/6312.E-8
      E7325=PLANCK*C/7325.E-8
      E1240=PLANCK*C/1240.E-8
      E1485=PLANCK*C/1485.E-8
      E1751=PLANCK*C/1751.E-8
      E1575=PLANCK*C/1575.E-8
      E1602=PLANCK*C/1602.E-8
      E1549=PLANCK*C/1549.E-8
      E9532=PLANCK*C/9532.E-8
      E9069=PLANCK*C/9069.E-8
      E7135=PLANCK*C/7135.E-8
C
C***DETERMINES TO3,TN2,TO2,TS2,&TS3 IF "AURORAL" LINES HAVE BEEN
OBSERVED
C
      IF (TO3.EQ.0.) CALL TEMPO3(R5007,R4363,TO3)
C***DETERMINES S II ELECTRON DENSITY NOW THAT TO3 IS KNOWN
      IF (ED .EQ. 0.) CALL ELECD(R6716,R6731,TO3,ED)
      IF(R5755.GT.0..AND.R6584.GT.0.) THEN
          CALL TEMPN2(R5755,R6584,TN2,ED)
      ELSE
          IF(R4686.EQ.0) THEN
             ALOGTS=4.426+4.827E-4*R5007-1.374E-7*R5007**2
             TN2=14670*ALOGTS-57330
          ELSE
             TN2=10300
          ENDIF
      ENDIF
C     IF(R7325.GT.0..AND.R3727.GT.0.) THEN
C         CALL TEMPO2(R7325,R3727,ED,TO2)
C     ELSE
          TO2=TN2
C     ENDIF
C     IF(R4071.GT.0..AND.R6724.GT.0.) THEN
C         CALL TEMPS2(R4071,R6724,ED,TS2)
C     ELSE
          TS2=TN2
C     ENDIF
C     IF(R9532.GT.0..AND.R6312.GT.0.) THEN
C         CALL TEMPS3(R9532,R6312,ED,TS3)
C     ELSE
          TS3=TN2
C     ENDIF
```

```
C***COMPUTES EFFECTIVE RECOMBINATION COEFFICIENTS.  This section
revised
c***june 27, 1997.
c*** Hbeta effective alpha is a 5th order fit to data from storey &
hummer,
c*** 1995, mn, 272,41.
      ALFHBETA = -12.404592 -0.000347193796*TO3+4.98365006e-08*TO3**2
     1 -3.77545451e-12*TO3**3+1.33944026e-16*TO3**4
     1 -1.75120267e-21*TO3**5
      ALFHBETA = 10**(ALFHBETA)
c*** effective alpha for he2 4686 is a fit to data from storey & hummer
      ALF4686=1.66E-13*(2.E4/TO3)
c***effective alpha for he1 5876. use algorithm from pequignot et al.
1991,
c*** aa,251,680.
      to34=to3*1.e-4
      ALF5876=1.323e-13*((to34**-.696)/(1+1.683*(to34**.667)))
C***COMPUTES COLLISIONAL CORRECTION FACTOR FOR HE0 FROM CLEGG
C***PUT IN NEW RATES FROM KINSTON & FERLAND, APJ, 442, 714.
      T4=TO3*1.E-4
      D=1+(3110.*(T4**-.51)/ED)
      CR=((7.12*(T4**.14)*EXP(-3.776/T4))+(1.47*(T4**-.28)*
     1   EXP(-4.544/T4)))/D
c     ALF5876=2.3E-14*(2.E4/TO3)
C     ALFHBETA=1.62E-14*((2.E4/TO3)**.9)
C***COMPUTES LEVEL POPULATIONS FOR UPPER LEVELS PRODUCING OBSERVED
LINES
      CHIC3=CHI(ENC3,CSC3,EAC3,SWC3,TO3,ED,2)*EAC3(1)+
     1   CHI(ENC3,CSC3,EAC3,SWC3,TO3,ED,3)*EAC3(2)+
     1   CHI(ENC3,CSC3,EAC3,SWC3,TO3,ED,4)*EAC3(3)
      CHIN2=(CHI(ENN2,CSN2,EAN2,SWN2,TN2,ED,4)*EAN2(8))
      CHIN3=(CHI(ENN3,CSN3,EAN3,SWN3,TO3,ED,3)*(EAN3(2)+EAN3(5))+
     1       CHI(ENN3,CSN3,EAN3,SWN3,TO3,ED,4)*(EAN3(3)+EAN3(6))+
     1       CHI(ENN3,CSN3,EAN3,SWN3,TO3,ED,5)*(EAN3(4)+EAN3(7)))
      if(r3727.eq.0) then
      CHIO2=(CHI(ENO2,CSO2,EAO2,SWO2,TN2,ED,4)*(EAO2(6)+EAO2(8)))+
     1  (CHI(ENO2,CSO2,EAO2,SWO2,TN2,ED,5)*(EAO2(7)+EAO2(9)))
      else
      CHIO2=(CHI(ENO2,CSO2,EAO2,SWO2,TN2,ED,3)*EAO2(2))+
     1   (CHI(ENO2,CSO2,EAO2,SWO2,TO3,ED,2)*EAO2(1))
      endif
      CHIO3=(CHI(ENO3,CSO3,EAO3,SWO3,TO3,ED,4)*EAO3(8))
      CHINE3=(CHI(ENNE3,CSNE3,EANE3,SWNE3,TO3,ED,4)*EANE3(3))
      CHINE4=(CHI(ENNE4,CSNE4,EANE4,SWNE4,TO3,ED,4)*EANE4(3)+
     1        CHI(ENNE4,CSNE4,EANE4,SWNE4,TO3,ED,5)*EANE4(4))
      CHINE5=(CHI(ENNE5,CSNE5,EANE5,SWNE5,TO3,ED,5)*(EANE5(4)+
     1        EANE5(7)+EANE5(9)))
      CHIS2=CHI(ENS2,CSS2,EAS2,SWS2,TN2,ED,2)*EAS2(1)+
     1   CHI(ENS2,CSS2,EAS2,SWS2,TN2,ED,3)*EAS2(2)
C     CHI6312=CHI(ENS3,CSS3,EAS3,SWS3,TO3,ED,5)*EAS3(10)
      CHIS3_9532=CHI(ENS3,CSS3,EAS3,SWS3,TO3,ED,4)*EAS3(8)
C     CHIS3_9069=CHI(ENS3,CSS3,EAS3,SWS3,TO3,ED,4)*EAS3(6)
      CHIAR3=CHI(ENAR3,CSAR3,EAAR3,SWAR3,TO3,ED,4)*EAAR3(3)
C***COMPUTES IONIC ABUNDANCES RELATIVE TO H+
      XHE2=R5876*(ALFHBETA/(ALF5876*(1+CR)))*(E4861/E5876)/100.
      XHE3=R4686*(ALFHBETA/ALF4686)*(E4861/E4686)/100.
      XC3=R1909*(E4861/E1909)*(ALFHBETA/CHIC3)*ED/100.
```

```
      XN2=R6584*(E4861/E6584)*(ALFHBETA/CHIN2)*ED/100.
      XN3=R1751*(E4861/E1751)*(ALFHBETA/CHIN3)*ED/100.
      XN4=R1485*(ALFHBETA*6.17E14)/CHIN4(TO3)/100.
      XN5=R1240*(ALFHBETA*6.17E14)/CHIN5(TO3)/100.
      if(r3727.eq.0)then
      XO2=R7325*(E4861/E7325)*(ALFHBETA/CHIO2)*ED/100.
      else
      XO2=R3727*(E4861/E3727)*(ALFHBETA/CHIO2)*ED/100.
      endif
      XO3=R5007*(E4861/E5007)*(ALFHBETA/CHIO3)*ED/100.
      XNE3=R3869*(E4861/E3869)*(ALFHBETA/CHINE3)*ED/100.
      XNE4=R1602*(E4861/E1602)*(ALFHBETA/CHINE4)*ED/100.
      XNE5=R1575*(E4861/E1575)*(ALFHBETA/CHINE5)*ED/100.
      XS2=R6724*(E4861/E6724)*(ALFHBETA/CHIS2)*ED/100.
C     X6312=R6312*(E4861/E6312)*(ALFHBETA/CHI6312)*ED/100.
      XS3=R9532*(E4861/E9532)*(ALFHBETA/CHIS3_9532)*ED/100.
C     XS3=R9069*(E4861/E9069)*(ALFHBETA/CHIS3_9069)*ED/100.
      XAR3=R7135*(E4861/E7135)*(ALFHBETA/CHIAR3)*ED/100.
C***COMPUTES IONIZATION CORRECTION FACTORS
      ICFO=1.0
      IF(XHE2 .GT. 0.)ICFO=(XHE3+XHE2)/XHE2
      ICFN2=1.0
c***11/4/96: changed ICFN2 by adding *ICFO
      IF(XO2 .GT. 0.)ICFN2=((XO3+XO2)/XO2)*ICFO
      ICFNE3=1.0
      IF(XO3 .GT. 0.)ICFNE3=((XO3+XO2)/XO3)*ICFO
      ICFS23=1.0
c      icfs23=(1-(1-icfn2)**3)**(-0.33)
      IF(XO2.GT.0.)ICFS23=1.43+(0.196*(XO3/XO2)**1.29)
C     ICFAR=1.0
C     IF(XO3.GT.0)ICFAR=1.34*((XO2+XO3)/XO3)*ICFO
      ICFAR=1.87
C***COMPUTES ELEMENTAL ABUNDANCES RELATIVE TO H
      XHE=0.
      XN=0.
      XO=0.
      XNE=0.
      XC=0.
      XS=0.
      XAR=0.
      IF((XHE2+XHE3) .GT. 0.) XHE=XHE2+XHE3
      IF(XN2 .GT. 0.) XN=XN2*ICFN2
      IF((XO2+XO3) .GT. 0.) XO=(XO2+XO3)*ICFO
      IF(XNE3 .GT. 0.) XNE=XNE3*ICFNE3
      IF(XC3 .GT. 0.) XC=(XC3/XO3)*(XO2+XO3)*ICFO
      IF(XO3.GT.0) ICFS23=(1-(1-(XO2/XO))**3)**-.33
      IF((XS2+XS3) .GT. 0.) XS=(XS2+XS3)*ICFS23
      IF(XAR3.GT.0)XAR=XAR3*ICFAR
C*** COMPUTES RATIO OF CARBON RECOMB./COLL.  this algorithm is from
c*** pequignot et al. 1991, aa, 251, 680
      z=2
      t4=to3/1.e4
      alpha_4267=(9.6e-14*(z**2.51)*(t4**-.754))/
     1           (1+2.587*(z**-1.44)*t4**.719)
c     rcarbon=(r4267/r1909)*(chic3/alpha_4267)*2.2352/ed
C
C***WRITES OUT ELECTRON TEMPERATURES AND DENSITY
```

```
C      PRINT 9, TO3,TO2,TN2,TS2,TS3,ED
       PRINT 9, TO3,TN2,ED
C***WRITES OUT THE ABUNDANCES
       PRINT 10, XHE2,XHE3
       PRINT 11, XN2,XN3,XN4,XN5
       PRINT 12, XO2,XO3
       PRINT 13, XNE3,XNE4,XNE5
       PRINT 14, XC3
       PRINT 15, XS2,XS3
       PRINT 16, XAR3
       PRINT 22, ICFO,ICFN2,ICFNE3,ICFS23,ICFAR
       PRINT 17, XHE,XC,XN,XO,XNE,XS,XAR
       PRINT 18, XHE/SUNHE,XC/SUNC,XN/SUNN,XO/SUNO,XNE/SUNNE,
     1           XS/SUNS,XAR/SUNAR
       PRINT 19, (XC3/XO3),(XN2/XO2),(XNE3/XO3),(XS/XO),(XAR/XO)
       PRINT 20, (XC3/XO3)/(SUNC/SUNO),(XN2/XO2)/(SUNN/SUNO),
     1           (XNE3/XO3)/(SUNNE/SUNO),(XS/XO)/(SUNS/SUNO),
     1           (XAR/XO)/(SUNAR/SUNO)
c      PRINT 21, RCARBON
    9 FORMAT (///'TO3=',f10.0/,'TN2=',f10.0/,'ED=',f10.0)
C   9 FORMAT (///'TO3=',f10.0/,'TO2=',f10.0/,'TN2=',f10.0/,
C    1         'TS2=',f10.0/,'TS3=',f10.0/,'Ne=',f10.0)
   10 FORMAT (//'He+/H+=',1pg10.3/,'He+2/H+=',1pg10.3)
   11 FORMAT(//'N+/H+=',1pg10.3/,'N+2/H+=',1pg10.3/,
     1       'N+3/H+=',1pg10.3/,'N+4/H+=',1pg10.3)
   12 FORMAT (//'O+/H+=',1pg10.3/,'O+2/H+=',1pg10.3)
   13 FORMAT (//'Ne+2/H+=',1pg10.3/,'Ne+3/H+=',1pg10.3/,
     1        'Ne+4/H+=',1pg10.3)
   14 FORMAT (//'C+2/H+=',1pg10.3)
   15 FORMAT (//'S+/H+=',1pg10.3/,'S+2/H+=',1pg10.3)
   16 FORMAT (//'Ar+2/H+=',1pg10.3)
   17 FORMAT (///'ABUNDANCES (X/H):'/
     1        ' He/H=',1pg10.3/' C/H=',1pg10.3/' N/H=',1pg10.3/
     1        ' O/H=',1pg10.3/' Ne/H=',1pg10.3/' S/H=',1pg10.3/,
     1        ' Ar/H=',1pg10.3)
   18 FORMAT (//'ABUNDANCES RELATIVE (X/H) TO SOLAR:'/
     1        ' He/H=',1pg10.3/' C/H=',1pg10.3/' N/H=',1pg10.3/
     1        ' O/H=',1pg10.3/' Ne/H=',1pg10.3/' S/H=',1pg10.3/,
     1        ' Ar/H= ',1pg10.3)
   19 FORMAT (//'ABUNDANCE RATIOS (X/O):'/
     1          ' C/O=',1pg10.3/' N/O=',1pg10.3/
     1          ' Ne/O=',1pg10.3/,' S/O=',1pg10.3/,' Ar/O=',1pg10.3)
   20 FORMAT (//'ABUNDANCE RATIOS (X/O) RELATIVE TO SOLAR:'/
     1          ' C/O=',1pg10.3/' N/O=',1pg10.3/
     1          ' Ne/O=',1pg10.3/,' S/O=',1pg10.3/,' Ar/O=',1pg10.3)
   21 FORMAT (//'CARBON: RECOMB/COLL. = ',1pg10.3)
   22 FORMAT(//'ICFs (O,N2,NE3,S23,AR)'// 5(1pg10.3))
C
       stop
       END
C
C
C***COMPUTES LEVEL POPULATION OF SPECIFIED LEVEL IXLEVEL
       FUNCTION CHI(EN,CS,EA,SW,T,ED,IXLEVEL)
       IMPLICIT REAL*8 (A-H,O-Z)
       DIMENSION EN(10),CS(10),EA(10),SW(5)
       DIMENSION A(5,5),B(5,1),WKAREA(40)
```

```
      N = 5
      CFAC = ED * 8.63E-6 / SQRT(T)
      BC = 1.38E-16
      DO 100 MM = 1,5
      A(1,MM) = 1.0
 100  B(MM,1) = 0.0
      B(1,1) = 1.0
      A(2,1) = CFAC * CS(1)/(SW(1)*EXP(EN(1)/(BC*T)))
      A(2,2) = -(EA(1)+(CFAC/SW(2))*(CS(1)+CS(5)
     1/EXP(EN(5)/(BC*T))+CS(6)/EXP(EN(6)/(BC*T))+
     2CS(7)/EXP(EN(7)/(BC*T))))
      A(2,3)=EA(5)+(CFAC/SW(3))*CS(5)
      A(2,4)=EA(6)+(CFAC/SW(4))*CS(6)
      A(2,5)=EA(7)+(CFAC/SW(5))*CS(7)
      A(3,1)=(CFAC/SW(1))*CS(2)/EXP(EN(2)/(BC*T))
      A(3,2)=(CFAC/SW(2))*CS(5)/EXP(EN(5)/(BC*T))
      A(3,3)=-(EA(2)+EA(5)+(CFAC/SW(3))*(CS(2)
     1+CS(5)+CS(8)/EXP(EN(8)/(BC*T))+CS(9)/EXP(EN(9)/(BC*T))))
      A(3,4)=EA(8)+(CFAC/SW(4))*CS(8)
      A(3,5)=EA(9)+(CFAC/SW(5))*CS(9)
      A(4,1)=(CFAC/SW(1))*CS(3)/EXP(EN(3)/(BC*T))
      A(4,2)=(CFAC/SW(2))*CS(6)/EXP(EN(6)/(BC*T))
      A(4,3)=(CFAC/SW(3))*CS(8)/EXP(EN(8)/(BC*T))
      A(4,4)=-(EA(3)+EA(6)+EA(8)+(CFAC/SW(4))*(CS(3)
     1+CS(6)+CS(8)+CS(10)/EXP(EN(10)/(BC*T))))
      A(4,5)=EA(10)+(CFAC/SW(5))*CS(10)
      A(5,1)=(CFAC/SW(1))*CS(4)/EXP(EN(4)/(BC*T))
      A(5,2)=(CFAC/SW(2))*CS(7)/EXP(EN(7)/(BC*T))
      A(5,3)=(CFAC/SW(3))*CS(9)/EXP(EN(9)/(BC*T))
      A(5,4)=(CFAC/SW(4))*CS(10)/EXP(EN(10)/(BC*T))
      A(5,5)=-(EA(4)+EA(7)+EA(9)+EA(10)+(CFAC/SW(5))
     1*(CS(4)+CS(7)+CS(9)+CS(10)))
      CALL LEQT2F(A,1,5,5,B,4,WKAREA,IER)
      CHI=B(IXLEVEL,1)
      RETURN
      END
C***COMPUTES O3 TEMPERATURE BASED ON A 5th order poly FIT TO
C*** 6000-20000K RANGE. FIT ACCOUNTS FOR CHANGES IN ATOMIC
C***DATA MADE IN 6/97.
      SUBROUTINE TEMPO3(R5007,R4363,TO3)
      IMPLICIT REAL*8 (A-H,O-Z)
      a0 = 35.9971485
      a1 = -60.8275641
      a2 = 43.8010528
      a3 = -16.1516463
      a4 = 3.00985962
      a5 = -0.225316503
      X=1.34*R5007/R4363
      x=dlog10(x)
c     TO3=112.58-105.51*X+36.26*X**2-4.28*X**3
c     TO3=TO3*1.E3
      tO3=a0+a1*x+a2*x**2+a3*x**3+a4*x**4+a5*x**5
      TO3=TO3*1.E4
      RETURN
      END
C***COMPUTES N2 TEMPERATURE BASED ON A 5th order pply FIT TO
C*** 6000-20000K RANGE. FIT ACCOUNTS FOR CHANGES IN ATOMIC
```

```
C***DATA MADE IN 6/97.  Corrects for effects of electron density.
      SUBROUTINE TEMPN2(R5755,R6584,TN2,ed)
      IMPLICIT REAL*8 (A-H,O-Z)
      a0 = 63.2127097
      a1 = -131.253448
      a2 = 113.525729
      a3 = -49.9022254
      a4 = 11.0512261
      a5 = -0.982077794
      b0 = 64.290029
      b1 = -144.938284
      b2 = 135.873978
      b3 = -64.6479064
      b4 = 15.4808953
      b5 = -1.48636829
      X=1.35*R6584/R5755
      x=dlog10(x)
      z=0
      tn2=a0+a1*x+a2*x**2+a3*x**3+a4*x**4+a5*x**5
      if(ed.gt.1000) then
         tn10000=b0+b1*x+b2*x**2+b3*x**3+b4*x**4+b5*x**5
         z=((ed-1000)/9000)*(tn2-tn10000)
      endif
      tn2=(tn2-z)*1.e4
c     tN2 = 141.2-163.75*X+68.36*X**2-9.75*X**3
c     TN2=TN2*1.E3
      RETURN
      END
C***COMPUTES O2 TEMPERATURE BASED ON A 3RD ORDER POLYFIT
      SUBROUTINE TEMPO2(R7325,R3727,ED,TO2)
      IMPLICIT REAL*8 (A-H,O-Z)
      X=R3727/R7325
      x=dlog10(x)
      IF(LOG10(ED).LE.1.5)
     1      TO2=225.26-301.53*X+141.44*X**2-22.50*X**3
      IF(LOG10(ED).GT.1.5.AND.LOG10(ED).LE.2.5)
     1      TO2=227.61-312.45*X+150.15*X**2-24.46*X**3
      IF(LOG10(ED).GT.2.5.AND.LOG10(ED).LE.3.5)
     1      TO2=212.62-340.34*X+191.11*X**2-36.33*X**3
      IF(LOG10(ED).GT.3.5)
     1      TO2=85.38-203.15*X+180.90*X**2-55.02*X**3
      TO2=TO2*1.E3
      RETURN
      END
C***COMPUTES S2 TEMPERATURE BASED ON A 3RD ORDER POLYFIT
      SUBROUTINE TEMPS2(R4071,R6724,ED,TS2)
      IMPLICIT REAL*8 (A-H,O-Z)
      X=R6724/R4071
      x=dlog10(x)
      IF(LOG10(ED).LE.1.5)
     1      TS2=255.77-478.40*X+311.91*X**2-68.86*X**3
      IF(LOG10(ED).GT.1.5.AND.LOG10(ED).LE.2.5)
     1      TS2=249.18-476.92*X+318.41*X**2-72.01*X**3
      IF(LOG10(ED).GT.2.5.AND.LOG10(ED).LE.3.5)
     1      TS2=228.72-542.48*X+449.33*X**2-125.75*X**3
      IF(LOG10(ED).GT.3.5)
     1      TS2=41.88-198.96*X+397.04*X**2-272.13*X**3
```

```
      TS2=TS2*1.E3
      RETURN
      END
C***COMPUTES S3 TEMPERATURE BASED ON A 3RD ORDER POLYFIT
      SUBROUTINE TEMPS3(R9532,R6312,ED,TS3)
      IMPLICIT REAL*8 (A-H,O-Z)
      X=R9532*1.40/R6312
      x=dlog10(x)
      IF(LOG10(ED).LE.1.5)
     1      TS3=2195.92-1569.34*X+376.18*X**2-30.14*X**3
      IF(LOG10(ED).GT.1.5.AND.LOG10(ED).LE.2.5)
     1      TS3=855.83-811.79*X+251.47*X**2-26.11*X**3
      IF(LOG10(ED).GT.2.5.AND.LOG10(ED).LE.3.5)
     1      TS3=308.40-356.75*X+142.74*X**2-19.28*X**3
      IF(LOG10(ED).GT.3.5)
     1      TS3=167.87-210.33*X+93.77*X**2-14.24*X**3
      TS3=TS3*1.E3
      RETURN
      END
C***COMPUTES ELECTRON DENSITY
c***revised 6/30/97 to account for updated s ii atomic data.
      SUBROUTINE ELECD(R6716,R6731,TO3,ED)
      IMPLICIT REAL*8 (A-H,O-Z)
      A10 = 3316.74018
      A11 = -26871.5458
      A12 = 81745.0749
      A13 = -110497.102
      A14 = 55982.2071
      A20 = 7.88399113
      A21 = -13.4172878
      A22 = 13.8145765
      A23 = -6.17052027
      A24 = 0.640018972
      A30 = -58916.8297
      A31 = 174696.295
      A32 = -194236.78
      A33 = 95983.7251
      A34 = -17787.3484
      A40 = 280263.322
      A41 = -446304.195
      A42 = 105040.481
      A43 = 124563.701
      A44 = -52873.2761
      X=R6716/R6731
      if(x .le. 0.546)
     1      y=a10+a11*x+a12*x**2+a13*x**3+a14*x**4
      if(x .gt. 0.546 .and. x .le. 1.3)
     1      y=a20+a21*x+a22*x**2+a23*x**3+a24*x**4
      if(x .gt. 1.3 .and. x .le. 1.40)
     1      y=a30+a31*x+a32*x**2+a33*x**3+a34*x**4
      if(x .gt. 1.4)
     1      y=a40+a41*x+a42*x**2+a43*x**3+a44*x**4
      ED=(10**Y)*SQRT(TO3/1.E4)
      RETURN
      END
C***COMPUTES THE EXCITATION COEFFICIENT FOR THE N IV 1485 LINE.
C***A TWO-LEVEL ATOM IS ASSUMED.
```

```
C***DATA FROM MENDOZA83 ARE USED.
      FUNCTION CHIN4(TO3)
      IMPLICIT REAL*8 (A-H,O-Z)
      q12=((8.63E-6*.852)/(1.*TO3**.5))/EXP(9.69E4/TO3)
      CHIN4=Q12*2.02E15
      RETURN
      END
C***COMPUTES THE EXCITATION COEFFICIENT FOR THE N V 1240 LINE.
C***A TWO-LEVEL ATOM IS ASSUMED.
C***DATA FROM MENDOZA83 ARE USED.
      FUNCTION CHIN5(TO3)
      IMPLICIT REAL*8 (A-H,O-Z)
      q12=((8.63E-6*2.22)/(2.*TO3**.5))/EXP(1.15E5/TO3)
      q13=((8.63E-6*4.44)/(2.*TO3**.5))/EXP(1.16E5/TO3)
      CHIN5=Q12*2.41E15 + Q13*2.42E15
      RETURN
      END
C
C
C
C
C
C     PRINT*, 'ENTER TO3 AND ED'
C     READ(5,*) TO3,ED
C     PRINT*, ' ENTER TO3'
C     READ(5,*) TO3
C     ED=1.E4
C
C
C     WRITE(8,*) ' HOW MANY OBJECTS?'
C     READ(8,*) N
C     READ(5,10)(PN(I),R3727(I),R3869(I),R4363(I),R4686(I),R5007(I),
C    1   R5755(I),R5876(I),R6584(I),eed(i),I=1,N)
C  10 FORMAT(A6,8F8.1,F8.0)
C     XHEAVE=0.
C     XNAVE=0.
C     XOAVE=0.
C     XNEAVE=0.
C     WRITE(6,40)
C  40 FORMAT(' ','OBJECT',1X,'TO3',5X,'TN2',5X,'ED',5X,'HE+',7X,
C    1   'HE+2',6X,'N+',8X,
C    1   'ICFN+',1X,'O+',8X,'O+2',7X,'IFNO',7X,'NE+2',5X,'ICFNE+2')
C     WRITE(7,50)
C  50 FORMAT(' ','OBJECT    DHE    DN     DO    DNE')
C     DO 100 I=1,N
C     ed=eed(i)
C
C 201 CONTINUE
C     XO1=R6300*(E4861/E6300)*(ALFHBETA/(CHI(ENO1,CSO1,EAO1,SWO1,T,ED,
C    3   4)*6.34E-3))*ED
C     OXRATIO=XO2+XO3
C     OXRATIO=(XO1+XO2+XO3)*ICF
C     XICFN=(XO2+XO3)/XO2
C     XICFNE=(XO2+XO3)/XO3
C 205 CONTINUE
C     WRITE(6,20)PN(I),TO3,TN2,ED,XHE2,XHE3,XN2,ICFN2,XO2,XO3,ICFO,
C    1   XNE3,ICFNE3
```

```
C  20 FORMAT(' ',A6,2X,F7.0,2X,F7.0,2X,F6.0,2X
C    1   3(pe10.2,1x),1x,0pF8.3,1x,2(pe10.2,1x),
C    1   2x,0pF8.3,1x,pE10.2,2x,0pF8.3)
C     DHE=XHE-10.83
C     DN=XN-7.94
C     DO=XO-8.84
C     DNE=XNE-7.98
C     WRITE(7,30)PN(I),XHE,XN,XO,XNE
C     WRITE(7,30)PN(I),DHE,DN,DO,DNE
C  30 FORMAT(' ',A6,2X,4(F5.2,2X))
C     XHEAVE=XHEAVE+(XHE3+XHE2)
C     XNAVE=XNAVE+(XN2*ICFN2)
C     XOAVE=XOAVE+((XO3+XO2)*ICFO)
C     XNEAVE=XNEAVE+(XNE3*ICFNE3)
C 100 CONTINUE
C     XHEAVE=DLOG10(XHEAVE/N)+12.
C     XNAVE=DLOG10(XNAVE/N)+12.
C     XOAVE=DLOG10(XOAVE/N)+12.
C     XNEAVE=DLOG10(XNEAVE/N)+12.
C     WRITE(7,31)XHEAVE,XNAVE,XOAVE,XNEAVE
C  31 FORMAT(' AVERAGE',2X,4(F5.2,2X))
C
C     DIMENSION PN(100),R3727(100),R3869(100),R4363(100),R4686(100)
C     DIMENSION R5007(100),R5876(100),R6584(100),R6716(100),R6731(100)
C     DIMENSION R5755(100),eed(100)
C     r23=(R3727+1.35*R5007)/100.
C     ro2o3=R3727/(1.35*R5007)
C     if(r1602.gt.0.) then
C     eta_ne=(r1602*r3727)/(r3869*(r5007*1.35))
C     eta_ne=log10(eta_ne)
C     else
C     eta_ne=-100.
C     endif
C     PRINT 20, LOG10(r23),LOG10(ro2o3),ETA_NE
C  20 FORMAT (' logR23=',1pg10.3,3x,'log(o2/o3)=',1pg10.3,3x,
C    1         'log(eta_ne)=',1pg10.3)

c   imsl routine name   - leqt2f
le2f0010
c
le2f0020
c-----------------------------------------------------------------------
-le2f0030
c
le2f0040
c   computer            - vax/double
le2f0050
c
le2f0060
c   latest revision     - june 1, 1982
le2f0070
c
le2f0080
c   purpose             - linear equation solution - full storage
le2f0090
c                           mode - high accuracy solution
le2f0100
```

```
c
le2f0110
c   usage               - call leqt2f (a,m,n,ia,b,idgt,wkarea,ier)
le2f0120
c
le2f0130
c   arguments     a     - input matrix of dimension n by n containing
le2f0140
c                           the coefficient matrix of the equation
le2f0150
c                           ax = b.
le2f0160
c                 m     - number of right-hand sides. (input)
le2f0170
c                 n     - order of a and number of rows in b. (input)
le2f0180
c                 ia    - row dimension of a and b exactly as specified
le2f0190
c                           in the dimension statement in the calling
le2f0200
c                           program. (input)
le2f0210
c                 b     - input matrix of dimension n by m containing
le2f0220
c                           the right-hand sides of the equation ax =
b.le2f0230
c                           on output, the n by m matrix of solutions
le2f0240
c                           replaces b.
le2f0250
c                 idgt  - input option.
le2f0260
c                         if idgt is greater than 0, the elements of
le2f0270
c                           a and b are assumed to be correct to idgt
le2f0280
c                           decimal digits and the routine performs
le2f0290
c                           an accuracy test.
le2f0300
c                         if idgt equals 0, the accuracy test is
le2f0310
c                           bypassed.
le2f0320
c                         on output, idgt contains the approximate
le2f0330
c                           number of digits in the answer which
le2f0340
c                           were unchanged after improvement.
le2f0350
c                 wkarea - work area of dimension greater than or equal
le2f0360
c                           to n**2+3n.
le2f0370
c                 ier   - error parameter. (output)
le2f0380
```

```
c                          warning error
le2f0390
c                            ier = 34 indicates that the accuracy test
le2f0400
c                              failed. the computed solution may be in
le2f0410
c                              error by more than can be accounted for
le2f0420
c                              by the uncertainty of the data. this
le2f0430
c                              warning can be produced only if idgt is
le2f0440
c                              greater than 0 on input. (see the
le2f0450
c                              chapter 1 prelude for further
discussion.)le2f0460
c                          terminal error
le2f0470
c                            ier = 129 indicates that the matrix is
le2f0480
c                              algorithmically singular. (see the
le2f0490
c                              chapter 1 prelude).
le2f0500
c                            ier = 131 indicates that the matrix is too
le2f0510
c                              ill-conditioned for iterative improvement
le2f0520
c                              to be effective.
le2f0530
c
le2f0540
c   precision/hardware   - single and double/h32
le2f0550
c                        - single/h36,h48,h60
le2f0560
c
le2f0570
c   reqd. imsl routines - single/ludatn,luelmn,lurefn,uertst,ugetio
le2f0580
c                        - double/ludatn,luelmn,lurefn,uertst,ugetio,
le2f0590
c                          vxadd,vxmul,vxsto
le2f0600
c
le2f0610
c   notation             - information on special notation and
le2f0620
c                          conventions is available in the manual
le2f0630
c                          introduction or through imsl routine uhelp
le2f0640
c
le2f0650
c   copyright            - 1982 by imsl, inc. all rights reserved.
le2f0660
```

```
c
le2f0670
c   warranty            - imsl warrants only that imsl testing has been
le2f0680
c                           applied to this code. no other warranty,
le2f0690
c                           expressed or implied, is applicable.
le2f0700
c
le2f0710
c-----------------------------------------------------------------------
-le2f0720
c
le2f0730
      subroutine leqt2f (a,m,n,ia,b,idgt,wkarea,ier)
le2f0740
c
le2f0750
      dimension          a(ia,1),b(ia,1),wkarea(1)
le2f0760
      double precision   a,b,wkarea,d1,d2,wa
le2f0770
c                                  first executable statement
le2f0780
c                                  initialize ier
le2f0790
      ier=0
le2f0800
      jer=0
le2f0810
      j = n*n+1
le2f0820
      k = j+n
le2f0830
      mm = k+n
le2f0840
      kk = 0
le2f0850
      mm1 = mm-1
le2f0860
      jj=1
le2f0870
      do 5 l=1,n
le2f0880
         do 5 i=1,n
le2f0890
            wkarea(jj)=a(i,l)
le2f0900
            jj=jj+1
le2f0910
    5 continue
le2f0920
c                                  decompose a
le2f0930
      call ludatn (wkarea,n,n,a,ia,idgt,d1,d2,wkarea(j),wkarea(k),
le2f0940
```

```
     *             wa,ier)
le2f0950
      if (ier.gt.128) go to 25
le2f0960
      if (idgt .eq. 0 .or. ier .ne. 0) kk = 1
le2f0970
      do 15 i = 1,m
le2f0980
c                                   performs the elimination part of
le2f0990
c                                   ax = b
le2f1000
         call luelmn (a,ia,n,b(1,i),wkarea(j),wkarea(mm))
le2f1010
c                                   refinement of solution to ax = b
le2f1020
         if (kk .ne. 0)
le2f1030
     *   call lurefn (wkarea,n,n,a,ia,b(1,i),idgt,wkarea(j),wkarea(mm),
le2f1040
     *                wkarea(k),wkarea(k),jer)
le2f1050
         do 10 ii=1,n
le2f1060
            b(ii,i) = wkarea(mm1+ii)
le2f1070
   10    continue
le2f1080
         if (jer.ne.0) go to 20
le2f1090
   15 continue
le2f1100
      go to 25
le2f1110
   20 ier = 131
le2f1120
   25 jj=1
le2f1130
      do 30 j = 1,n
le2f1140
         do 30 i = 1,n
le2f1150
            a(i,j)=wkarea(jj)
le2f1160
            jj=jj+1
le2f1170
   30 continue
le2f1180
      if (ier .eq. 0) go to 9005
le2f1190
 9000 continue
le2f1200
      call uertst (ier,6hleqt2f)
le2f1210
 9005 return
le2f1220
```

```
      end
le2f1230
c   imsl routine name   - ludatn
ludn0010
c
ludn0020
c-----------------------------------------------------------------------
-ludn0030
c
ludn0040
c   computer            - vax/double
ludn0050
c
ludn0060
c   latest revision     - june 1, 1982
ludn0070
c
ludn0080
c   purpose             - nucleus called only by imsl subroutine leqt2f
ludn0090
c
ludn0100
c   precision/hardware  - single and double/h32
ludn0110
c                       - single/h36,h48,h60
ludn0120
c
ludn0130
c   reqd. imsl routines - uertst,ugetio
ludn0140
c
ludn0150
c   notation            - information on special notation and
ludn0160
c                           conventions is available in the manual
ludn0170
c                           introduction or through imsl routine uhelp
ludn0180
c
ludn0190
c   copyright           - 1982 by imsl, inc. all rights reserved.
ludn0200
c
ludn0210
c   warranty            - imsl warrants only that imsl testing has been
ludn0220
c                           applied to this code. no other warranty,
ludn0230
c                           expressed or implied, is applicable.
ludn0240
c
ludn0250
c-----------------------------------------------------------------------
-ludn0260
c
ludn0270
```

```
      subroutine ludatn (a,ia,n,lu,ilu,idgt,d1,d2,apvt,equil,wa,ier)
ludn0280
c
ludn0290
      dimension          a(ia,1),lu(ilu,1),apvt(1),equil(1)
ludn0300
      double precision   a,lu,d1,d2,equil,wa,zero,one,four,sixtn,sixth,
ludn0310
     *                   rn,wrel,biga,big,p,sum,ai,wi,t,test,q,apvt
ludn0320
      data               zero,one,four,sixtn,sixth/0.d0,1.d0,4.d0,
ludn0330
     *                   16.d0,.0625d0/
ludn0340
c                                  first executable statement
ludn0350
c                                  initialization
ludn0360
      ier = 0
ludn0370
      rn = n
ludn0380
      wrel = zero
ludn0390
      d1 = one
ludn0400
      d2 = zero
ludn0410
      biga = zero
ludn0420
      do 10 i=1,n
ludn0430
         big = zero
ludn0440
         do 5 j=1,n
ludn0450
            p = a(i,j)
ludn0460
            lu(i,j) = p
ludn0470
            p = dabs(p)
ludn0480
            if (p .gt. big) big = p
ludn0490
    5    continue
ludn0500
         if (big .gt. biga) biga = big
ludn0510
         if (big .eq. zero) go to 110
ludn0520
         equil(i) = one/big
ludn0530
   10 continue
ludn0540
      do 105 j=1,n
ludn0550
```

```
         jm1 = j-1
ludn0560
         if (jm1 .lt. 1) go to 40
ludn0570
c                                compute u(i,j), i=1,...,j-1
ludn0580
         do 35 i=1,jm1
ludn0590
            sum = lu(i,j)
ludn0600
            im1 = i-1
ludn0610
            if (idgt .eq. 0) go to 25
ludn0620
c                                with accuracy test
ludn0630
            ai = dabs(sum)
ludn0640
            wi = zero
ludn0650
            if (im1 .lt. 1) go to 20
ludn0660
            do 15 k=1,im1
ludn0670
               t = lu(i,k)*lu(k,j)
ludn0680
               sum = sum-t
ludn0690
               wi = wi+dabs(t)
ludn0700
   15       continue
ludn0710
            lu(i,j) = sum
ludn0720
   20       wi = wi+dabs(sum)
ludn0730
            if (ai .eq. zero) ai = biga
ludn0740
            test = wi/ai
ludn0750
            if (test .gt. wrel) wrel = test
ludn0760
            go to 35
ludn0770
c                                without accuracy
ludn0780
   25       if (im1 .lt. 1) go to 35
ludn0790
            do 30 k=1,im1
ludn0800
               sum = sum-lu(i,k)*lu(k,j)
ludn0810
   30       continue
ludn0820
            lu(i,j) = sum
ludn0830
```

```
   35    continue
ludn0840
   40    p = zero
ludn0850
c                                  compute u(j,j) and l(i,j),
i=j+1,...,ludn0860
         do 70 i=j,n
ludn0870
            sum = lu(i,j)
ludn0880
            if (idgt .eq. 0) go to 55
ludn0890
c                                  with accuracy test
ludn0900
            ai = dabs(sum)
ludn0910
            wi = zero
ludn0920
            if (jm1 .lt. 1) go to 50
ludn0930
            do 45 k=1,jm1
ludn0940
               t = lu(i,k)*lu(k,j)
ludn0950
               sum = sum-t
ludn0960
               wi = wi+dabs(t)
ludn0970
   45       continue
ludn0980
            lu(i,j) = sum
ludn0990
   50       wi = wi+dabs(sum)
ludn1000
            if (ai .eq. zero) ai = biga
ludn1010
            test = wi/ai
ludn1020
            if (test .gt. wrel) wrel = test
ludn1030
            go to 65
ludn1040
c                                  without accuracy test
ludn1050
   55       if (jm1 .lt. 1) go to 65
ludn1060
            do 60 k=1,jm1
ludn1070
               sum = sum-lu(i,k)*lu(k,j)
ludn1080
   60       continue
ludn1090
            lu(i,j) = sum
ludn1100
   65       q = equil(i)*dabs(sum)
ludn1110
```

```
            if (p .ge. q) go to 70
ludn1120
            p = q
ludn1130
            imax = i
ludn1140
   70     continue
ludn1150
c                                   test for algorithmic singularity
ludn1160
          if (rn+p .eq. rn) go to 110
ludn1170
          if (j .eq. imax) go to 80
ludn1180
c                                   interchange rows j and imax
ludn1190
          d1 = -d1
ludn1200
          do 75 k=1,n
ludn1210
             p = lu(imax,k)
ludn1220
             lu(imax,k) = lu(j,k)
ludn1230
             lu(j,k) = p
ludn1240
   75     continue
ludn1250
          equil(imax) = equil(j)
ludn1260
   80     apvt(j) = imax
ludn1270
          d1 = d1*lu(j,j)
ludn1280
   85     if (dabs(d1) .le. one) go to 90
ludn1290
          d1 = d1*sixth
ludn1300
          d2 = d2+four
ludn1310
          go to 85
ludn1320
   90     if (dabs(d1) .ge. sixth) go to 95
ludn1330
          d1 = d1*sixtn
ludn1340
          d2 = d2-four
ludn1350
          go to 90
ludn1360
   95     continue
ludn1370
          jp1 = j+1
ludn1380
          if (jp1 .gt. n) go to 105
ludn1390
```

```
c                                     divide by pivot element u(j,j)
ludn1400
         p = lu(j,j)
ludn1410
         do 100 i=jp1,n
ludn1420
            lu(i,j) = lu(i,j)/p
ludn1430
  100    continue
ludn1440
  105 continue
ludn1450
c                                     perform accuracy test
ludn1460
      if (idgt .eq. 0) go to 9005
ludn1470
      p = 3*n+3
ludn1480
      wa = p*wrel
ludn1490
      if (wa+10.d0**(-idgt) .ne. wa) go to 9005
ludn1500
      ier = 34
ludn1510
      go to 9000
ludn1520
c                                     algorithmic singularity
ludn1530
  110 ier = 129
ludn1540
      d1 = zero
ludn1550
      d2 = zero
ludn1560
 9000 continue
ludn1570
c                                     print error
ludn1580
      call uertst(ier,6hludatn)
ludn1590
 9005 return
ludn1600
      end
ludn1610
c   imsl routine name   - luelmn
luen0010
c
luen0020
c-----------------------------------------------------------------------
-luen0030
c
luen0040
c   computer            - vax/double
luen0050
c
luen0060
```

```
c   latest revision      - june 1, 1982
luen0070
c
luen0080
c   purpose              - nucleus called only by imsl subroutine leqt2f
luen0090
c
luen0100
c   reqd. imsl routines - none required
luen0110
c
luen0120
c   notation             - information on special notation and
luen0130
c                            conventions is available in the manual
luen0140
c                            introduction or through imsl routine uhelp
luen0150
c
luen0160
c   copyright            - 1982 by imsl, inc. all rights reserved.
luen0170
c
luen0180
c   warranty             - imsl warrants only that imsl testing has been
luen0190
c                            applied to this code. no other warranty,
luen0200
c                            expressed or implied, is applicable.
luen0210
c
luen0220
c-----------------------------------------------------------------------
-luen0230
c
luen0240
      subroutine luelmn (a,ia,n,b,apvt,x)
luen0250
c
luen0260
      dimension          a(ia,1),b(1),apvt(1),x(1)
luen0270
      double precision   a,b,x,sum,apvt
luen0280
c                                  first executable statement
luen0290
c                                  solve ly = b for y
luen0300
      do 5 i=1,n
luen0310
    5 x(i) = b(i)
luen0320
      iw = 0
luen0330
      do 20 i=1,n
luen0340
```

```
         ip = apvt(i)
luen0350
         sum = x(ip)
luen0360
         x(ip) = x(i)
luen0370
         if (iw .eq. 0) go to 15
luen0380
         im1 = i-1
luen0390
         do 10 j=iw,im1
luen0400
            sum = sum-a(i,j)*x(j)
luen0410
   10    continue
luen0420
         go to 20
luen0430
   15    if (sum .ne. 0.d0) iw = i
luen0440
   20 x(i) = sum
luen0450
c                                    solve ux = y for x
luen0460
      do 30 ib=1,n
luen0470
         i = n+1-ib
luen0480
         ip1 = i+1
luen0490
         sum = x(i)
luen0500
         if (ip1 .gt. n) go to 30
luen0510
         do 25 j=ip1,n
luen0520
            sum = sum-a(i,j)*x(j)
luen0530
   25   continue
luen0540
   30 x(i) = sum/a(i,i)
luen0550
      return
luen0560
      end
luen0570
c   imsl routine name   - lurefn
lurn0010
c
lurn0020
c------------------------------------------------------------------------
-lurn0030
c
lurn0040
c   computer            - vax/double
lurn0050
```

```
c
lurn0060
c   latest revision     - june 1, 1982
lurn0070
c
lurn0080
c   purpose             - nucleus called only by imsl subroutine leqt2f
lurn0090
c
lurn0100
c   precision/hardware  - single and double/h32
lurn0110
c                       - single/h36,h48,h60
lurn0120
c
lurn0130
c   reqd. imsl routines - single/luelmn,uertst,ugetio
lurn0140
c                       - double/luelmn,uertst,ugetio,vxadd,vxmul,
lurn0150
c                           vxsto
lurn0160
c
lurn0170
c   notation            - information on special notation and
lurn0180
c                           conventions is available in the manual
lurn0190
c                           introduction or through imsl routine uhelp
lurn0200
c
lurn0210
c   copyright           - 1982 by imsl, inc. all rights reserved.
lurn0220
c
lurn0230
c   warranty            - imsl warrants only that imsl testing has been
lurn0240
c                           applied to this code. no other warranty,
lurn0250
c                           expressed or implied, is applicable.
lurn0260
c
lurn0270
c-----------------------------------------------------------------------
-lurn0280
c
lurn0290
      subroutine lurefn (a,ia,n,ul,iul,b,idgt,apvt,x,res,dx,ier)
lurn0300
c
lurn0310
      dimension          a(ia,1),ul(iul,1),b(1),x(1),res(1),dx(1)
lurn0320
      dimension          apvt(1)
lurn0330
```

```
      dimension          accxt(2)
lurn0340
      double precision   a,accxt,b,ul,x,res,dx,zero,xnorm,dxnorm,apvt
lurn0350
      data               itmax/75/,zero/0.d0/
lurn0360
c                                      first executable statement
lurn0370
      ier=0
lurn0380
      xnorm = zero
lurn0390
      do 10 i=1,n
lurn0400
         xnorm = dmax1(xnorm,dabs(x(i)))
lurn0410
   10 continue
lurn0420
      if (xnorm .ne. zero) go to 20
lurn0430
      idgt = 50
lurn0440
      go to 9005
lurn0450
   20 do 45 iter=1,itmax
lurn0460
         do 30 i=1,n
lurn0470
      accxt(1) = 0.0d0
lurn0480
      accxt(2) = 0.0d0
lurn0490
            call vxadd(b(i),accxt)
lurn0500
            do 25 j=1,n
lurn0510
               call vxmul(-a(i,j),x(j),accxt)
lurn0520
   25       continue
lurn0530
            call vxsto(accxt,res(i))
lurn0540
   30    continue
lurn0550
         call luelmn (ul,iul,n,res,apvt,dx)
lurn0560
         dxnorm = zero
lurn0570
         xnorm = zero
lurn0580
         do 35 i=1,n
lurn0590
            x(i) = x(i) + dx(i)
lurn0600
            dxnorm = dmax1(dxnorm,dabs(dx(i)))
lurn0610
```

```
            xnorm = dmax1(xnorm,dabs(x(i)))
lurn0620
   35     continue
lurn0630
          if (iter .ne. 1) go to 40
lurn0640
          idgt = 50
lurn0650
          if (dxnorm .ne. zero) idgt = -dlog10(dxnorm/xnorm)
lurn0660
   40     if (xnorm+dxnorm .eq. xnorm) go to 9005
lurn0670
   45 continue
lurn0680
c                                    iteration did not converge
lurn0690
      ier = 129
lurn0700
 9000 continue
lurn0710
      call uertst(ier,6hlurefn)
lurn0720
 9005 return
lurn0730
      end
lurn0740
c-----------------------------------------------------------------------
-
c
c   computer            - vax/single
c
c   latest revision     - june 1, 1982
c
c   purpose             - print a message reflecting an error condition
c
c   usage               - call uertst (ier,name)
c
c   arguments    ier    - error parameter. (input)
c                            ier = i+j where
c                              i = 128 implies terminal error message,
c                              i =  64 implies warning with fix message,
c                              i =  32 implies warning message.
c                              j = error code relevant to calling
c                                  routine.
c                name   - a character string of length six providing
c                            the name of the calling routine. (input)
c
c   precision/hardware  - single/all
c
c   reqd. imsl routines - ugetio,uspkd
c
c   notation            - information on special notation and
c                            conventions is available in the manual
c                            introduction or through imsl routine uhelp
c
c   remarks      the error message produced by uertst is written
c                to the standard output unit. the output unit
```

```
c                number can be determined by calling ugetio as
c                follows..   call ugetio(1,nin,nout).
c                the output unit number can be changed by calling
c                ugetio as follows..
c                              nin = 0
c                              nout = new output unit number
c                              call ugetio(3,nin,nout)
c                see the ugetio document for more details.
c
c   copyright           - 1982 by imsl, inc. all rights reserved.
c
c   warranty            - imsl warrants only that imsl testing has been
c                         applied to this code. no other warranty,
c                         expressed or implied, is applicable.
c
c-----------------------------------------------------------------------
-
c
      subroutine uertst (ier,name)
c                                     specifications for arguments
      integer             ier
c     integer             name(1)
c                                     specifications for local variables
c     integer             i,ieq,ieqdf,iounit,level,levold,nameq(6),
c    *                    namset(6),namupk(6),nin,nmtb
      integer             i,ieqdf,iounit,level,levold,
     .                    nin
      character*6         namset,name,nameq
      character*1         ieq
c     data                namset/1hu,1he,1hr,1hs,1he,1ht/
      data                namset/'uerset'/
c     data                nameq/6*1h /
      data                nameq/'      '/
c     data                level/4/,ieqdf/0/,ieq/1h=/
      data                level/4/,ieqdf/0/,ieq/'='/
c                                     unpack name into namupk
c                                     first executable statement
c     call uspkd (name,6,namupk,nmtb)
c                                     get output unit number
      call ugetio(1,nin,iounit)
c                                     check ier
      if (ier.gt.999) go to 25
      if (ier.lt.-32) go to 55
      if (ier.le.128) go to 5
      if (level.lt.1) go to 30
c                                     print terminal message
c     if (ieqdf.eq.1) write(iounit,35) ier,nameq,ieq,namupk
      if (ieqdf.eq.1) write(iounit,35) ier,nameq,ieq,name
c     if (ieqdf.eq.0) write(iounit,35) ier,namupk
      if (ieqdf.eq.0) write(iounit,35) ier,name
      go to 30
    5 if (ier.le.64) go to 10
      if (level.lt.2) go to 30
c                                     print warning with fix message
c     if (ieqdf.eq.1) write(iounit,40) ier,nameq,ieq,namupk
      if (ieqdf.eq.1) write(iounit,40) ier,nameq,ieq,name
c     if (ieqdf.eq.0) write(iounit,40) ier,namupk
```

```
      if (ieqdf.eq.0) write(iounit,40) ier,name
      go to 30
   10 if (ier.le.32) go to 15
c                                     print warning message
      if (level.lt.3) go to 30
c     if (ieqdf.eq.1) write(iounit,45) ier,nameq,ieq,namupk
      if (ieqdf.eq.1) write(iounit,45) ier,nameq,ieq,name
c     if (ieqdf.eq.0) write(iounit,45) ier,namupk
      if (ieqdf.eq.0) write(iounit,45) ier,name
      go to 30
   15 continue
c                                     check for uerset call
c     do 20 i=1,6
c        if (namupk(i).ne.namset(i)) go to 25
c        if (name.ne.namset) go to 25
c  20 continue
      levold = level
      level = ier
      ier = levold
      if (level.lt.0) level = 4
      if (level.gt.4) level = 4
      go to 30
   25 continue
      if (level.lt.4) go to 30
c                                     print non-defined message
c     if (ieqdf.eq.1) write(iounit,50) ier,nameq,ieq,namupk
      if (ieqdf.eq.1) write(iounit,50) ier,nameq,ieq,name
c     if (ieqdf.eq.0) write(iounit,50) ier,namupk
      if (ieqdf.eq.0) write(iounit,50) ier,name
   30 ieqdf = 0
      return
   35 format(19h *** terminal error,10x,7h(ier = ,i3,
c    1       20h) from imsl routine ,6a1,a1,6a1)
     1       20h) from imsl routine ,a6,a1,a6)
   40 format(27h *** warning with fix error,2x,7h(ier = ,i3,
c    1       20h) from imsl routine ,6a1,a1,6a1)
     1       20h) from imsl routine ,a6,a1,a6)
   45 format(18h *** warning error,11x,7h(ier = ,i3,
c    1       20h) from imsl routine ,6a1,a1,6a1)
     1       20h) from imsl routine ,a6,a1,a6)
   50 format(20h *** undefined error,9x,7h(ier = ,i5,
c    1       20h) from imsl routine ,6a1,a1,6a1)
     1       20h) from imsl routine ,a6,a1,a6)
c
c                                     save p for p = r case
c                                       p is the page namupk
c                                       r is the routine namupk
   55 ieqdf = 1
c     do 60 i=1,6
c  60 nameq(i) = namupk(i)
   60 nameq = name
   65 return
      end
c
c-----------------------------------------------------------------------
-
c
```

```
c   computer            - vax/single
c
c   latest revision     - june 1, 1981
c
c   purpose             - to retrieve current values and to set new
c                           values for input and output unit
c                           identifiers.
c
c   usage               - call ugetio(iopt,nin,nout)
c
c   arguments    iopt   - option parameter. (input)
c                           if iopt=1, the current input and output
c                           unit identifier values are returned in nin
c                           and nout, respectively.
c                           if iopt=2, the internal value of nin is
c                           reset for subsequent use.
c                           if iopt=3, the internal value of nout is
c                           reset for subsequent use.
c                nin    - input unit identifier.
c                           output if iopt=1, input if iopt=2.
c                nout   - output unit identifier.
c                           output if iopt=1, input if iopt=3.
c
c   precision/hardware  - single/all
c
c   reqd. imsl routines - none required
c
c   notation            - information on special notation and
c                           conventions is available in the manual
c                           introduction or through imsl routine uhelp
c
c   remarks      each imsl routine that performs input and/or output
c                operations calls ugetio to obtain the current unit
c                identifier values. if ugetio is called with iopt=2 or
c                iopt=3, new unit identifier values are established.
c                subsequent input/output is performed on the new units.
c
c   copyright           - 1978 by imsl, inc. all rights reserved.
c
c   warranty            - imsl warrants only that imsl testing has been
c                           applied to this code. no other warranty,
c                           expressed or implied, is applicable.
c
c-----------------------------------------------------------------------
-
c
      subroutine ugetio(iopt,nin,nout)
c                                     specifications for arguments
      integer             iopt,nin,nout
c                                     specifications for local variables
      integer             nind,noutd
      data                nind/1/,noutd/2/
c                                     first executable statement
      if (iopt.eq.3) go to 10
      if (iopt.eq.2) go to 5
      if (iopt.ne.1) go to 9005
      nin = nind
```

```
      nout = noutd
      go to 9005
    5 nind = nin
      go to 9005
   10 noutd = nout
 9005 return
      end
c   imsl routine name   - vxadd                                        vxad0010
c                                                                      vxad0020
c------------------------------------------------------------------vxad0030
c                                                                      vxad0040
c   computer            - vax/double                                   vxad0050
c                                                                      vxad0060
c   latest revision     - january 1, 1978                              vxad0070
c                                                                      vxad0080
c   purpose             - extended precision add                       vxad0090
c                                                                      vxad0100
c   usage               - call vxadd (a,acc)                           vxad0110
c                                                                      vxad0120
c   arguments a - double precision number to be added to the           vxad0130
c                           accumulator. (input)                       vxad0140
c                 acc   - accumulator. (input and output)              vxad0150
c                   acc is a double precision vector of length         vxad0160
c                   2. on output, acc contains the sum of              vxad0170
c                   input acc and a.                                   vxad0180
c                                                                      vxad0190
c   precision/hardware  - double/h32                                   vxad0200
c                       - not available/h36,h48,h60                    vxad0210
c                                                                      vxad0220
c   reqd. imsl routines - none required                                vxad0230
c                                                                      vxad0240
c   notation    - information on special notation and                  vxad0250
c                   conventions is available in the manual             vxad0260
c                   introduction or through imsl routine uhelp         vxad0270
c                                                                      vxad0280
c   remarks  vxadd adds the double precision number a to the           vxad0290
c      extended precision accumulator, acc. the subroutine             vxad0300
c     assumes that an extended precision number is already in          vxad0310
c       the accumulator. therefore, before the first call to           vxad0320
c       vxadd, acc(1) and acc(2) must be set to zero.                  vxad0330
c                                                                      vxad0340
c   copyright  - 1978 by imsl, inc. all rights reserved.               vxad0350
c                                                                      vxad0360
c   warranty  - imsl warrants only that imsl testing has been          vxad0370
c                   applied to this code. no other warranty,           vxad0380
c                   expressed or implied, is applicable.               vxad0390
c                                                                      vxad0400
c------------------------------------------------------------------vxad0410
c                                                                      vxad0420
      subroutine vxadd(a,acc)                                          vxad0430
c                                                                      vxad0440
c                          specifications for arguments                vxad0450
      double precision   a,acc(2)                                      vxad0460
c                          specifications for local variables          vxad0470
      double precision   x,y,z,zz                                      vxad0480
c                          first executable statement                  vxad0490
      x = acc(1)                                                       vxad0500
```

```
      y = a                                                          vxad0510
      if (dabs(acc(1)).ge.dabs(a)) go to 1                           vxad0520
      x = a                                                          vxad0530
      y = acc(1)                                                     vxad0540
c                          compute z+zz = acc(1)+a exactly           vxad0550
    1 z = x+y                                                        vxad0560
      if (dsign(1.0d0,x).ne.dsign(1.0d0,y)) go to 5                  vxad0570
      zz = (0.46d0*z-z)+z                                            vxad0580
      zz = ((x-zz)-(z-zz))+y                                         vxad0590
      go to 10                                                       vxad0600
    5 continue                                                       vxad0610
      zz = (x-z)+y                                                   vxad0620
c                          compute zz+acc(2) using double            vxad0630
c                            precision arithmetic                    vxad0640
   10 continue                                                       vxad0650
      zz = zz+acc(2)                                                 vxad0660
c                     compute acc(1)+acc(2) = z+zz exactly           vxad0670
      acc(1) = z+zz                                                  vxad0680
      if (dsign(1.0d0,z).ne.dsign(1.0d0,zz)) go to 15                vxad0690
      x = (0.46d0*acc(1)-acc(1))+acc(1)                              vxad0700
      acc(2) = ((z-x)-(acc(1)-x))+zz                                 vxad0710
      go to 20                                                       vxad0720
   15 continue                                                       vxad0730
      acc(2) = (z-acc(1))+zz                                         vxad0740
   20 continue                                                       vxad0750
      return                                                         vxad0760
      end                                                            vxad0770
c   imsl routine name   - vxmul                                      vxmu0010
c                                                                    vxmu0020
c-----------------------------------------------------------------   vxmu0030
c                                                                    vxmu0040
c   computer            - vax/double                                 vxmu0050
c                                                                    vxmu0060
c   latest revision     - july 1, 1983                               vxmu0070
c                                                                    vxmu0080
c   purpose             - extended precision multiply                vxmu0090
c                                                                    vxmu0100
c   usage               - call vxmul (a,b,acc)                       vxmu0110
c                                                                    vxmu0120
c   arguments    a      - input double precision number              vxmu0130
c                b      - input double precision number              vxmu0140
c                acc    - accumulator. (input and output)            vxmu0150
c                  acc is a double precision vector of length        vxmu0160
c                  2.  on output, acc contains the sum of            vxmu0170
c                  input acc and a*b.                                vxmu0180
c                                                                    vxmu0190
c   precision/hardware  - double/h32                                 vxmu0200
c                       - not available/h36,h48,h60                  vxmu0210
c                                                                    vxmu0220
c   reqd. imsl routines - vxadd                                      vxmu0230
c                                                                    vxmu0240
c   notation   - information on special notation and                  vxmu0250
c                conventions is available in the manual              vxmu0260
c                introduction or through imsl routine uhelp          vxmu0270
c                                                                    vxmu0280
c remarks vxmul adds the product a*b to the extended precision       vxmu0290
c       accumulator, acc. the subroutine assumes that an             vxmu0300
```

```
c       extended precision number is already in the                    vxmu0310
c       accumulator.  therefore, before the first call to              vxmu0320
c       vxmul, acc(1) and acc(2) must be set to zero.                  vxmu0330
c                                                                      vxmu0340
c   copyright  - 1978 by imsl, inc. all rights reserved.               vxmu0350
c                                                                      vxmu0360
c   warranty   - imsl warrants only that imsl testing has been         vxmu0370
c                applied to this code. no other warranty,              vxmu0380
c                expressed or implied, is applicable.                  vxmu0390
c                                                                      vxmu0400
c----------------------------------------------------------------------vxmu0410
c                                                                      vxmu0420
      subroutine vxmul (a,b,acc)                                       vxmu0430
c                          specifications for arguments                vxmu0440
      double precision   a,b,acc(2)                                    vxmu0450
c                          specifications for local variables          vxmu0460
      double precision   x,ha,ta,hb,tb                                 vxmu0470
      integer            ix(2)                                         vxmu0480
      equivalence        (x,ix(1))                                     vxmu0490
      data               i/0/                                          vxmu0500
c                          split a = ha+ta                             vxmu0510
c                                b = hb+tb                             vxmu0520
c                          first executable statement                  vxmu0530
      x = a                                                            vxmu0540
      ix(2) = ix(2).and.(61440)                                        vxmu0550
      ha=x                                                             vxmu0560
      ta=a-ha                                                          vxmu0570
      x = b                                                            vxmu0580
      ix(2) = ix(2).and.(61440)                                        vxmu0590
      hb = x                                                           vxmu0600
      tb = b-hb                                                        vxmu0610
c                    compute ha*hb,ha*tb,ta*hb, and ta*tb              vxmu0620
c                            and call vxadd to accumulate the          vxmu0630
c                            sum                                       vxmu0640
      x = ta*tb                                                        vxmu0650
      call vxadd(x,acc)                                                vxmu0660
      x = ha*tb                                                        vxmu0670
      call vxadd(x,acc)                                                vxmu0680
      x = ta*hb                                                        vxmu0690
      call vxadd(x,acc)                                                vxmu0700
      x = ha*hb                                                        vxmu0710
      call vxadd(x,acc)                                                vxmu0720
      return                                                           vxmu0730
      end                                                              vxmu0740
c   imsl routine name   - vxsto                                        vxst0010
c                                                                      vxst0020
c----------------------------------------------------------------------vxst0030
c                                                                      vxst0040
c   computer            - vax/double                                   vxst0050
c                                                                      vxst0060
c   latest revision     - january 1, 1978                              vxst0070
c                                                                      vxst0080
c   purpose             - double precision store.                      vxst0090
c                                                                      vxst0100
c   usage               - call vxsto(acc,d)                            vxst0110
c                                                                      vxst0120
c   arguments    acc    - accumulator. (input)                         vxst0130
```

```
c                  acc is a double precision vector of length  vxst0140
c                  2. acc is assumed to be the result of       vxst0150
c                  calling vxadd or vxmul to perform extended  vxst0160
c                  precision operations.                       vxst0170
c       d       - double precision scalar. (output)            vxst0180
c                  on output, d contains a double precision    vxst0190
c                  approximation to the value of the extended  vxst0200
c                  precision accumulator.                      vxst0210
c                                                              vxst0220
c   precision/hardware  - double/h32                           vxst0230
c              - not available/h36,h48,h60                     vxst0240
c                                                              vxst0250
c   reqd. imsl routines - none required                        vxst0260
c                                                              vxst0270
c   notation     - information on special notation and         vxst0280
c                  conventions is available in the manual      vxst0290
c                  introduction or through imsl routine uhelp  vxst0300
c                                                              vxst0310
c   copyright    - 1978 by imsl, inc. all rights reserved.     vxst0320
c                                                              vxst0330
c   warranty     - imsl warrants only that imsl testing has been vxst0340
c                  applied to this code. no other warranty,    vxst0350
c                    expressed or implied, is applicable.      vxst0360
c                                                              vxst0370
c-------------------------------------------------------------vxst0380
c                                                              vxst0390
      subroutine vxsto (acc,d)                                 vxst0400
c                          specifications for arguments        vxst0410
      double precision   acc(2),d                              vxst0420
c                                  first executable statement  vxst0430
      d = acc(1)+acc(2)                                        vxst0440
      return                                                   vxst0450
      end                                                      vxst0460
```